PALACKÝ UNIVERSITY OLOMOUC
Faculty of Science
Department of Experimental physics

MASTER THESIS

Properties of the nanoparticles prepared by seeded-growth method and their interaction with a protein

Author:	Bc. Iveta Vilímová
Study programme:	N1701 Physics
Study branch:	Nanotechnology
Form of study:	Full-time
Supervisor:	Doc. RNDr. Karolína Machalová Šišková, Ph.D.
Year:	2019

I hereby declare that I have written this thesis solely by myself and all the sources used in the thesis are properly cited and listed.

In Olomouc ……. ...…….....

I would like to express my thanks and deep gratitude

to my supervisor, Doc. RNDr. Karolína Machalová Šišková, Ph.D., for her endless patience, advice, guidance and for always being open to questions and discussion,

to my family, for their unwavering support during my studies and to my friends for always being there to lend me an ear.

Furthermore, I would like to acknowledge Mgr. Lukáš Nosek, Ph.D. for his help with measurement of TEM images, Mgr. Pavlína Andrýsková for instruction in measurement with Malvern Zetasizer instrument, and RNDr. Josef Kapitán, Ph.D. for allowing and helping us use his optical Raman instrument for SERS measurements.

Bibliografická identifikace:

Jméno a příjmení autora	Iveta Vilímová
Název práce	Vlastnosti nanočástic připravených růstem ze zárodků a jejich interakce s bílkovinou
Typ práce	Diplomová
Pracoviště	Katedra experimentální fyziky
Vedoucí práce	Doc. RNDr. Karolína Machalová Šišková, Ph.D.
Rok obhajoby práce	2019
Abstrakt	Tato práce je zaměřena na dvou-krokovou syntézu kovových nanočástic typu jádro-slupka využívající čerstvých či předem připravených zárodků. Připravené koloidní systémy nanočástic jsou charakterizovány pomocí UV-Vis spektroskopie, transmisní elektronové mikroskopie (TEM), dynamického rozptylu světla (DLS) a měřením zeta potenciálů. Je demonstrován přímý vliv parametrů a podmínek syntéz na charakteristické vlastnosti nanočástic složených ze stejného (Ag-Ag NČ) a odlišného plasmonického kovu (Au-Ag NČ). Povrchem-zesílenou Ramanovou spektroskopií (SERS) je otestována schopnost připravených Ag-Ag a Au-Ag nanočástic zesílit Ramanův rozptyl pro zvolenou bílkovinu, albumin hovězího séra, využitím dvou excitačních vlnových délek (532 nm a 785 nm).
Klíčová slova	Ag NČ, Ag-Ag NČ, Au NČ, Au-Ag NČ, nanočástice jádro-slupka, syntézy nanočástic, koloid, protein, povrchem zesílená Ramanova spektroskopie, SERS, rezonance povrchového plasmonu, SPR, růst ze zárodků
Počet stran	91
Počet příloh	2
Jazyk	Anglický

Bibliographical identification:

Autor's first name and surname	Iveta Vilímová
Title	Properties of the nanoparticles prepared by seeded-growth method and their interaction with a protein
Type of thesis	Master
Department	Department of Experimental Physics
Supervisor	Doc. RNDr. Karolína Machalová Šišková, Ph.D.
The year of presentation	2019

Abstract

This work is focused on two-step synthesis of metal core-shell NPs prepared via seeded-growth method exploiting freshly or previously prepared seeds. The as-prepared colloidal systems of NPs are characterized using UV-Vis spectroscopy, transmission electron microscopy (TEM), dynamic light scattering (DLS), and measurement of zeta-potential values. The direct influence of synthetic parameters and conditions on the characteristic properties of core-shell NPs consisting of the same (Ag-Ag NPs) or different (Au-Ag) plasmonic metal is demonstrated. The ability of the selected colloidal systems to enhance Raman scattering after the interaction with the selected protein, bovine serum, is tested out with surface-enhanced Raman spectroscopy (SERS) at two different excitation laser lines (532 and 785 nm).

Keywords

Ag NPs, Ag-Ag NPs, Au NPs, Au-Ag NPs, borohydride, citrate, colloid, core-shell, dynamic light scattering (DLS), formation of NPs, nanoparticles, protein, surface-enhanced Raman spectroscopy (SERS), surface plasmon resonance, seeded-growth, transmission electron microscopy (TEM), two-step synthesis, UV-Vis spectroscopy, zeta-potential

Number of pages	91
Number of appendices	2
Language	English

Table of content

1 Introduction

Nanoparticles (NPs), along with nanoparticle-composed materials, have offered unrestricted space for research and innovation for last few decades. Syntheses and characterization of NPs were put at the forefront of scientific interest due to the vast area of NPs applications, either implemented or potential.

Colloidal noble-metal NPs, more specifically gold (Au) and silver (Ag) NPs are well-known for their many applications through the human history, with a steady rise in popularity in the last few decades. Their unique properties are possible to be successfully adjusted with specific morphology and surface-modification, resulting in their effective applications in various scientific fields and measurement techniques.

While NPs can be synthesized with various approaches, this work is focused on two-step synthesis of metal core-shell Ag-Ag and Au-Ag NPs prepared via seeded-growth method. The main goal is to demonstrate the direct influence of synthetic parameters on characteristic properties of core-shell NPs consisting of the same (Ag-Ag NPs) or different (Au-Ag) plasmonic metal.

The prepared colloidal core-shell NPs and their properties are characterized with complementary techniques, such as UV-Vis spectroscopy, transmission electron microscopy (TEM), dynamic light scattering (DLS), and measurement of zeta-potential values.

Lastly, the change of these properties and the ability of the prepared NPs to enhance Raman scattering after the interaction with the bovine serum albumin (the protein) is tested out with surface-enhanced Raman spectroscopy (SERS) at two different excitation laser lines.

The structure of this work is as follows: in chapter 2, the theoretical background is given on the formation and synthesis of colloidal NPs, with short description of techniques used for characterization. In chapter 3, aims of the work are summarized. In the experimental part in chapter 4, the nomenclature used for the colloidal systems in this work is established, followed by experimental details of the syntheses and subsequent characterization of prepared NPs. Results are discussed in chapter 5, with conclusion drawn in chapter 6.

2 Theoretical part

Types and classification of NPs are based on their origin, dimensions and composition. In this work, focus is put on colloidal NPs. Their chemical, electrical, magnetic and optical properties provide variety of applications as nanoscale materials in fields of biotechnology, nanomedicine, etc. [1–3]

2. 1 Colloids

The utilization of metal NPs can be dated deep into the human history. One of the earliest example of practical application of metallic NPs synthesized through chemical methods can be considered the process of using metals to manufacture glass, in region of Egypt and Mesopotamia in 14th and 13th century BC. [4]

Similarly, the Lycurgus Cup from Roman Empire in 4th century is another example how ancient civilizations used metal NPs. A dichroic glass of the Lycurgus Cup contains Ag-Au NPs in the alloy form, causing a display of a green colour when the light passes from the front of the Cup and of a red colour when the light passes from behind. [4, 5]

In Mesopotamia during the 9th century a metallic polish containing Ag and Cu NPs was used to decorate the ceramics, giving it iridescent shine of blue and green colour under certain conditions. The ceramics revealed two layers of larger and smaller Ag NPs, allowing interference of scattered light.

Colloidal Ag and Au NPs were found in yellow and red coloured stained glass in churches from the medieval period. [2, 4]

The first scientific report of preparation of NPs can be attributed to Michael Faraday, who in 1857 described his experiments with Au colloidal solutions. Faraday discovered optical properties of Au colloid differ from bulk gold, which was the early observation of quantum size effects of NPs. [1, 2]

Description of NPs behaviour was accomplished at the end of 19th century by Wilhelm Ostwald, who introduced his theory of particle gold induced by Ostwald ripening. [6] His son Wolfgang Ostwald, the founder of the German Colloid society, also had a great influence in the area of colloidal chemistry.

In the year 1925, the Nobel Prize was given to Richard Zsigmondy for his invention of the ultra microscope and subsequent observation of colloidal particles. [1]

2.1.1 Colloidal systems

A Colloid is composed of a medium of dispersion (i.e. the continuous phase) and the suspended particles (i.e. the dispersed phase). The size of particles in a dispersed phase is in the range between 1 nm and 1000 nm, but all dimensions do not have to fit under 1μm necessarily.

Colloids can be described and divided by a variety of approaches. The most common division is based on whether the phases are in gas, liquid, or solid state and whether it is possible to clearly distinguish between them. [7]

The lyophilic colloids are strongly attracted to their medium of dispersion, the lyophobic group have no such attraction (e.g. hydrophilic and hydrophobic colloids).

Monodisperse colloids have narrow size distribution and contain particles of approximately the same size, whereas in polydisperse colloids particle sizes vary in somewhat broad range. [8]

Properties of colloidal NPs can be controlled by the parameters such as: their crystalline structure, composition, size and shape. It requires understanding of the mechanism of NPs formation process. [1]

2. 2 Formation of NPs

2.2.1 Nucleation

Historically, the explanation of colloidal formation was first given by the classical nucleation theory (CNT) developed by Döring and Becket in 1930. Nucleation is thermodynamic concept explaining the emergence of a new phase, the nucleus, from metastable homogenous phase. CNT describes that a thermodynamic system strives to maximize its entropy and the description of vapour condensating to liquid was extended to other phase transitions, along with growth processes of NPs. [1, 9]

Further advancement of nucleation is described in Figure 1, where the nucleation mechanism around a metastable critical point is shown. Figure 1a shows the nucleation and particle growth in the original fluid due to a large thermodynamic driving force, Figure 1b shows a two-step mechanism occurring around the metastable critical point, offering perspective that the dynamic of nucleation is more affected by metastable states and growth dynamics, rather than thermodynamic driving force. [1, 10]

Another pivotal distinction is between homogeneous and heterogeneous nucleation, used in seeded-growth syntheses.

The homogenous nucleation is a spontaneous process occurring randomly but requiring the supercritical state (e.g. supersaturation).

The heterogeneous nucleation occurs on solid surfaces at preferential sites (e.g. phase boundaries, impurities), where the lower effective surface energy decreases the activation energy of nucleation. Subsequently, the heterogeneous nucleation is more frequent than the homogeneous one, but it is presumed that both processes occur during NP synthesis either simultaneously, or consecutively.

In thermodynamic models of the nucleation and particle growth, there is a persisting problem of not including the chemical aspect of creating monomers (e.g. via reduction) and alterations occurring due to inconsistency of synthesis parameters (i.e. temperature, pH, concentrations, stabilizers).

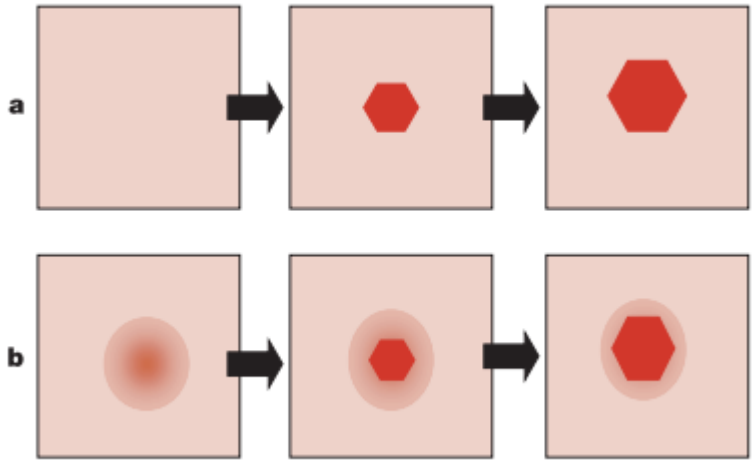

Figure 1 Nucleation mechanism around metastable critical point. (a) Nucleation and particle growth in the original fluid due to a large thermodynamic driving force. (b) Two-step mechanism occurring around the metastable critical point, where a fluid droplet forms first through the phase separation or presence of critical fluctuations. The nucleation rate is increased by the high density of the droplet and covering film provides a barrier between growing particle and original fluid. This protective layer ensures monomers (i.e. molecules) are accessible during next growth steps and that there is time for proper orientation and bonding of monomers. The dynamic of nucleation is more affected by metastable states and growth dynamics, rather than thermodynamic driving force. [10]

Recent research in the formation process of NPs (led by J. Polte [1]) disregards the nucleation as the driving force of particle growth and its description via CNT. The research shows that the particle growth is directed by a colloidal stability and occurs only because of aggregation and coalescence.

Colloidal stability, aggregation barrier and formation process of NPs are further discussed in the following parts.

2.2.2 Stability of NPs

Research on chemical synthesis of colloidal NPs systems (i.e. via wet chemical reduction) shows that the growth mechanism of NPs is not determined by thermodynamic forces, as is stipulated by CNT. The stability of NPs plays a more significant role, which is possible to observe with new data from the experiments focused on monitoring the sizes and concentration of NPs during syntheses.

Generally, NPs are unstable with tendency a to aggregate due to electrostatic, magnetic and van der Waals forces. Repulsive forces discouraging the aggregation, agglomeration, and coalescence can be realized through electrostatic and steric stabilization or their combination. [1, 11]

Electrostatic stabilization is achieved by an electrical double layer (EDL), where the surface charge of the NP is surrounded by solvated ions of a different charge (Figure 2a). Surface charge of a particle provides an opposing force to the van der Waals

attraction force. In the EDL, the inner layer (Stern layer) is compact while the outer layer is diffuse, which is described by Stern-Gouy-Chapman theory where the surface potential declines within the EDL of the NP. This is established by solving Poisson equation with Debye-Hückel linearization of exponential function, thus providing a description of the electric surface potential $\psi(x)$ distribution. The width of the EDL is called Debye length λ (Figure 2b).

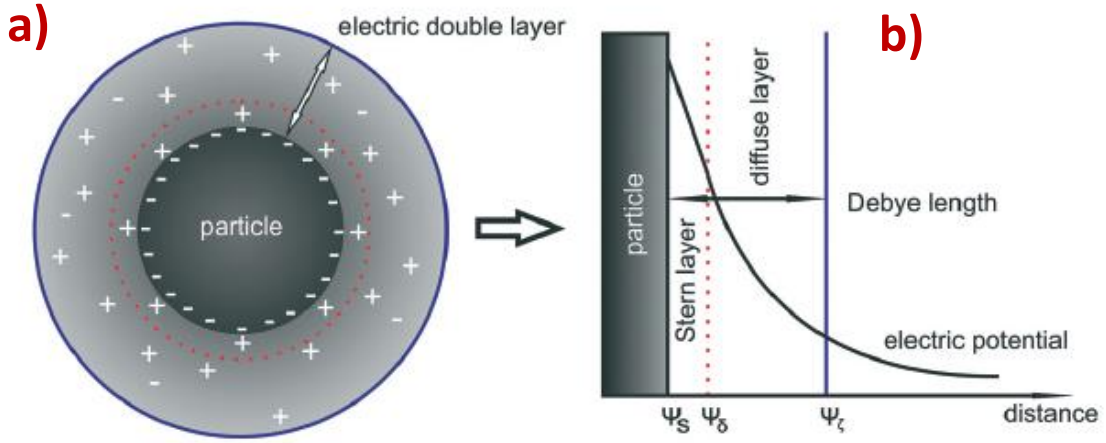

Figure 2 **Electric double layer EDL.**(a) EDL of opposing charges formed around NP, (b) consisting of outer diffuse layer and inner (Stern) compact layer.[1]

However, to explain colloidal stability a description of interaction between at least two EDLs (i.e. two NPs) is needed. In that case, the electric potential distribution and ion concentration of two (or more) particles overlap and are grounds for EDL interaction forces, which can be further determined for different instances (by e.g. the properties of EDL and geometry of particles). EDL repulsive forces also decrease exponentially with the mutual distance of NPs and change considerably with the difference in parameters of surface charge, constant surface potential, thickness of EDL, etc.

Colloidal stability is further described by the DLVO theory developed by Derjaguin, Landau (Russian scientists), Vervey and Overbeek (Dutch scientists). The DLVO theory states the adding together of EDL repulsive forces and van der Waals attractive forces results in the total force between colloidal NPs, i.e. the total interaction potential $W_{total}(D)$ (Figure 3). The aggregation barrier, represented by a maximum of the total interaction potential curve, generates the activation energy for aggregation that has to be overcome by the two NPs in order to aggregate.

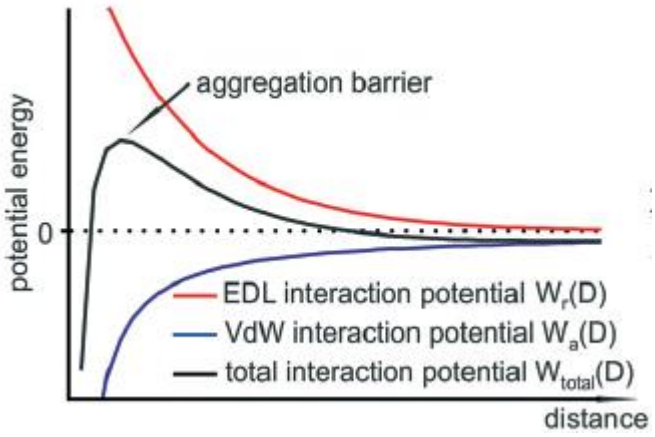

Figure 3 **Interaction potentials and aggregation barrier of two NPs.** The sum of the EDL interaction potential and the van der Waals interaction potential provides the curve of the total interaction potential, the maximum of the curve corresponds to the aggregation barrier of NPs. [1]

The stability of the system and of the aggregation barrier is affected by the particle size, value of the surface potential and ion concentration. The EDL forces are strongly dependent on ion concentration due to ions present in the compact and diffuse layers of EDL. Since the ion concentration directly corresponds to Debye length, the surface potential is decreased exponentially, i.e. the EDL reduces with growing ion concentration (Figure 4a).

Additionally, both attractive and repulsive forces are proportional to the particle size, making the total interaction potential proportional to the radius of the NPs. Accordingly, the aggregation barrier increases with the growing size of the NPs, evoking better colloidal stability. Therefore, the larger NPs are predominantly more stable than smaller NPs (Figure 4b).

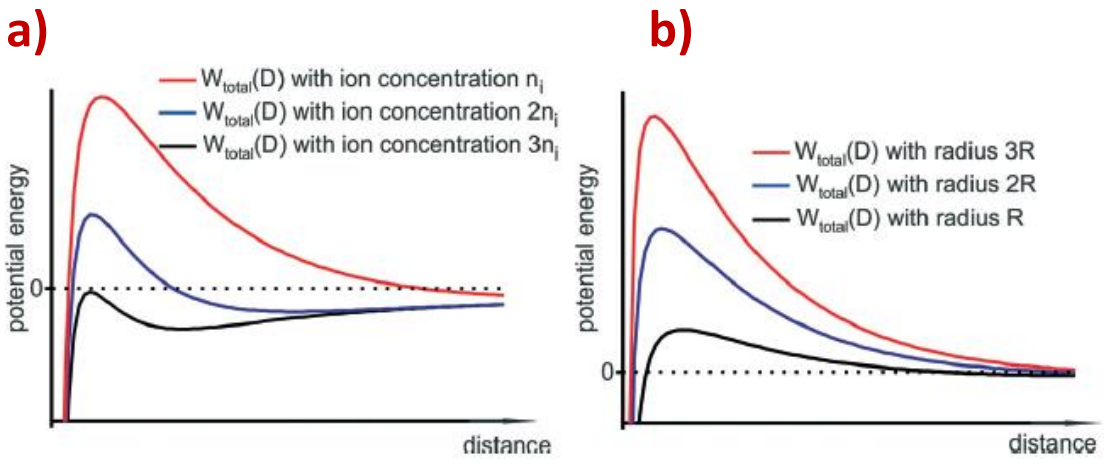

Figure 4 **Parameters influencing the colloidal stability.** (a) Effect of ion concentration on the total interaction potential $W_{total}(D)$, (b) Effect of particle size on the total interaction potential $W_{total}(D)$ and on the maximum of the curve (i.e. the aggregation barrier). [1]

Another way to reach better colloidal stability is the process of steric stabilization, Adsorption of large molecules (e.g. surfactants, polymers) on the surface of the NP prevents the aggregation of NPs by providing the protective layer between the two NPs. The space between the aggregating NPs would become denser, leading to a decrease of entropy, which is not a thermodynamically beneficial prospect. The repulsive forces from the steric stabilization are added to the total interaction potential $W_{total}(D)$. Steric stabilization forces have a short range of interaction and depend mostly on temperature, polymer solubility and concentration.

A disruption of both the steric and electrostatic stabilization leads to aggregation and coalescence on the macroscopic scale and to the destruction of the NPs. Similar effect can be achieved by dissolving the NPs with specific chemical compounds. [1]

2. 3 Synthesis of NPs

Generally, NPs can be prepared by various approaches - physical, chemical, or their combination. Physical methods (e.g. mechanical techniques such as milling and grinding, photolithography, laser ablation, etc.) are based on "top-down" approach by obtaining NPs from larger bulk of a material.

On the other hand, chemical "bottom-up" methods (e.g. colloidal aggregation, organic synthesis, self-assembly, etc.) depend on interaction and aggregation of atoms and molecules, prompted by a chemical reaction. "Bottom-up" approach typically offers uniformity and smaller size distribution of NPs. In recent years, the effort was focused on the development of more environmentally friendly alternatives to physical and chemical methods, thus introducing so called "green syntheses". [12–15]

Chemical syntheses can be divided by a state of a phase in which they are prepared, by the temperature of the chemical reaction and by number of steps in the synthesis. In case of metal and colloidal NPs the process of wet chemical reduction via "two-step seeded growth method" is the most common synthetic procedure. [1]

2.3.1 Synthesis of colloidal NPs

Colloidal NPs are often prepared by the reduction of dissolved metal precursor (e.g. a metal salt) with a reducing agent (e.g. sodium borohydride, ascorbic acid, citrates, etc.) in aqueous (or non-aqueous) solutions. The addition of stabilizing agents (e.g. citrate ions, polymers) provides the electrostatic stabilization (via repulsive forces) and steric stabilization, further influencing the aggregation and coalescence of NPs.

Size distribution of colloidal NPs is typically controlled by a "seeded-growth" method where the particle growth is induced by a process of fast reduction for generating small seeds, with subsequent adding of a weak reducing agent. The seeds have a crucial influence on the size, shape and structure of the final NPs, and on the reaction kinetics. The age of the seeds and their subsequent stability is also the key parameter of NP synthesis.

Size distribution control of NPs is influenced by mixing conditions and thus the synthetic process might not always consistently yield the same result.

2.3.2 Synthesis of Ag NPs

The synthesis of Ag NPs discussed in this work is based on the reduction of silver nitrate ($AgNO_3$) with sodium borohydride ($NaBH_4$). The growth mechanism consists of four steps (Figure 5), starting with a quick reduction of silver salt. Reducing agent $NaBH_4$ induces the fast reduction, shortening its span into few milliseconds. As the actual particle growth occurs at much slower rate, it is evidently separated from the reduction process.

The second step is the first stage of coalescence (a merging of particles). The coalescence would not be possible without aggregation, which is caused by an insufficient colloidal stability. Therefore, colloidal stability is an essential principle of actual particle growth.

The third step is a metastable state, occurring between two steps of coalescence. The metastable state is thought to be connected to the hydrolysis of residual BH_4^- into $B(OH)_4^-$, which also affects the surface chemistry of Ag NPs (hydrolysis is further accelerated in the presence of metal NPs). The metastable state clearly separates two steps of coalescence and is not present in the growth mechanism of Au NPs.

The hydrolysis of borohydride is most likely related to a change of electrostatic stability and its decrease. This initiates the final step of a synthesis and the second coalescent step. The process of coalescence is stopped when the size of NPs reaches a point of adequate colloidal stability, preventing further aggregation and coalescence.
[1, 16, 17]

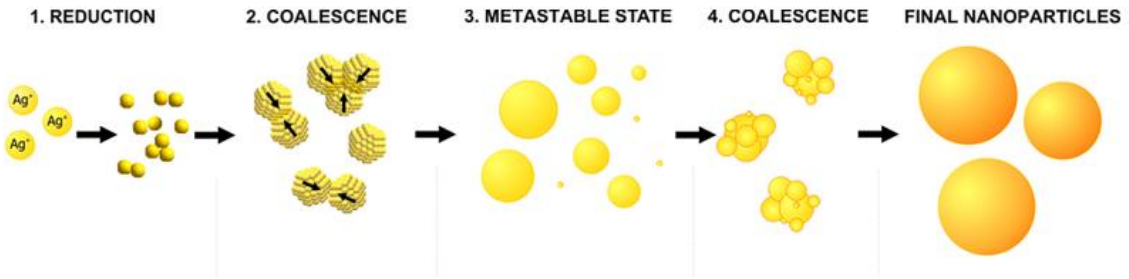

Figure 5 **Ag NPs growth mechanism.** (1) Reduction of metal salt to monomers, (2) coalescence of primary particles, (3) the metastable state between two steps of coalescence, (4) the second step of coalescence and the last step of the synthesis, the forming of final NPs. (Modified from [16])

The addition of a stabilizing agent and thus providing further colloidal stability influences the length of metastable state, particle size in each step and long-term stability of final NPs, but the growth mechanism in itself is not altered. [1, 16, 17]

2.3.3 Synthesis of Au NPs

The most commons syntheses of colloidal Au NPs are reductions with sodium borohydride ($NaBH_4$) and sodium citrate.

Synthesis of Au NPs with$NaBH_4$ is based on the same principles as the synthesis of Ag NPs with the only exception: absence of metastable state (chapter 2.3.2). In the first step, the metal precursor, tetrachloroauric acid ($HAuCl_4$), is reduced by $NaBH_4$. After the formation of first clusters in the second step, the coalescence and aggregation start in the third step. The process of coalescence is stopped when the size of NPs reaches a point of adequate colloidal stability (Figure 6). [1]

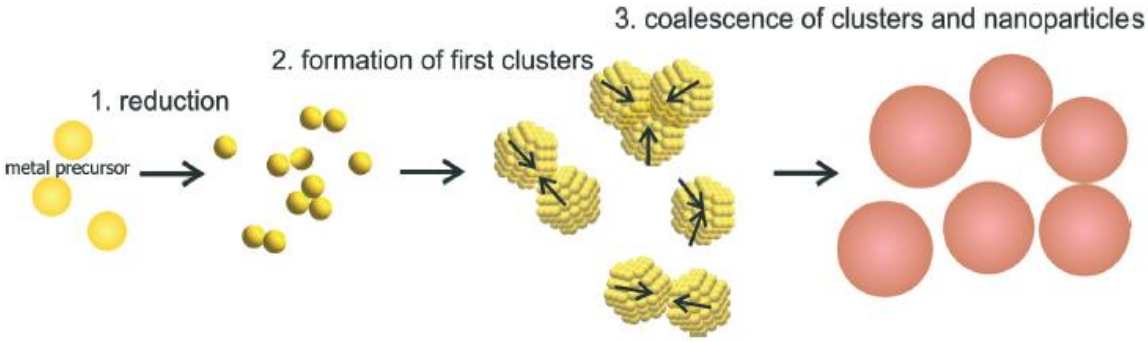

Figure 6 Au NPs growth mechanism via reduction of $NaBH_4$. (1) Reduction of metal precursor to monomers, (2) formation of first clusters, (3) coalescence and the last step of the synthesis, the formation of final NPs. [1]

Another way to obtain relatively monodisperse Au NPs is through the reduction of $HAuCl_4$ with sodium citrate at the elevated temperature, the process known as Turkevich synthesis.

In the first step, small clusters are formed by a partial reduction of the precursor, followed by the coalescence into small seed particles in the second step. In the third step, a further growth of reduced Au monomers on seed particles proceeds due to existing EDL of the seed particles. The fast growth of final particles in the fourth step of the synthesis stops when the precursor is completely consumed (Figure 7). [1, 18]

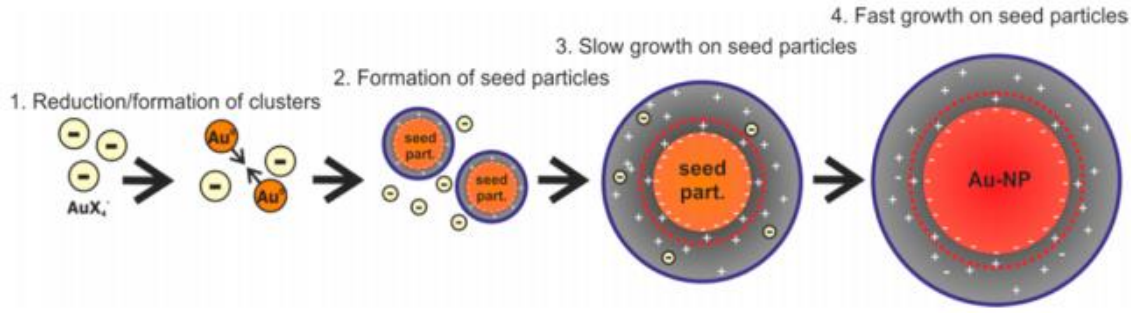

Figure 7 **Au NPs growth mechanism via reduction of sodium citrate.** (1) Reduction of metal precursor, formation of clusters, (2) the formation of seed particles via coalescence, (3) growth on seed particles, (4) the formation of final NPs due to faster growth. [18]

The mechanism of Turkevich synthesis is a seed-mediated growth. As the final NPs grow from particles formed at the beginning of the synthesis, the total number of particles does not change after the formation of seed particles.

The size of the final NPs is set by the total number of NPs and is determined by the time seed particles are formed. That occurs during a very short interval immediately after the metal precursor and reducing agent are mixed together, i.e. usually within the first 30 seconds of the synthesis. The number of the seed particles is determined by the size of the seed particles and amount of Au monomers available for seed formation. [1, 18, 19]

2.3.4 Synthesis of core-shell Ag-Ag and Au-Ag NPs

The seeded growth method is used for syntheses of core-shell NPs in particular, due to the clear separation of the whole process into two distinct steps: (i) the preparation of the seeds (core) and subsequent (ii) formation of the final NPs (shell) respectively. [20, 21]

The colloidal systems prepared via syntheses mentioned in the previous chapters (2.3.2 and 2.3.3) are used as a seed solution and their particles represent "cores". The "shell" of either the same or different metal is added by the deposition of ions on the surface of the seed through an additional reduction of the metal salt by a mild reducing agent.

The core-shell NPs discussed in this work are monometallic Ag-Ag NPs and bimetallic Au-Ag NPs.

Bimetallic NPs have more intriguing properties than monometallic ones consisting of the corresponding metal. Consequently, unique optical (thermal, electronic, etc.) sized dependent effects are obtained. [22]

For instance, bimetallic NPs are used as signal enhancers in Surface Enhanced Raman Spectroscopy with better results than their monometallic counterparts due to their material composition and the amendable core-shell ratio. [23]

2. 4 Characterization of NPs

With a rapid increase of research on NPs and their subsequent applications, a precise characterization of their properties became necessary. For proper characterization of NPs it is always important to combine several complementary techniques, either for studying specific property, or their combination. [24]

In this work, properties on NPs are characterized by UV-Vis spectroscopy, transmission electron microscopy, dynamic light scattering, measurement of zeta-potential and surface-enhanced Raman spectroscopy.

2.4.1 UV-Vis spectroscopy

Ultraviolet-visible spectroscopy is a technique based on the absorption of ultraviolet (UV) and visible (Vis) light radiation (i.e. the wavelengths in the interval between200 nm - 800 nm). The absorption of specific amount of energy form the absorbed light causes excitation of electrons from the full ground state orbital (i.e. energy level) with low energy to unoccupied orbital with a higher energy. The larger the size of the gap between orbitals, the greater amount of the energy is needed, which results in the absorption of shorter wavelengths with higher frequency. [25]

The colour of the absorbed light can be predicted by a colour of the illuminated substance. A particular portion a of wavelengths is absorbed when white light (containing all wavelengths from visible spectrum) passes through a substance, resulting in appearance of reflected colour (demonstrated by the colour wheel in Figure 8). [26]

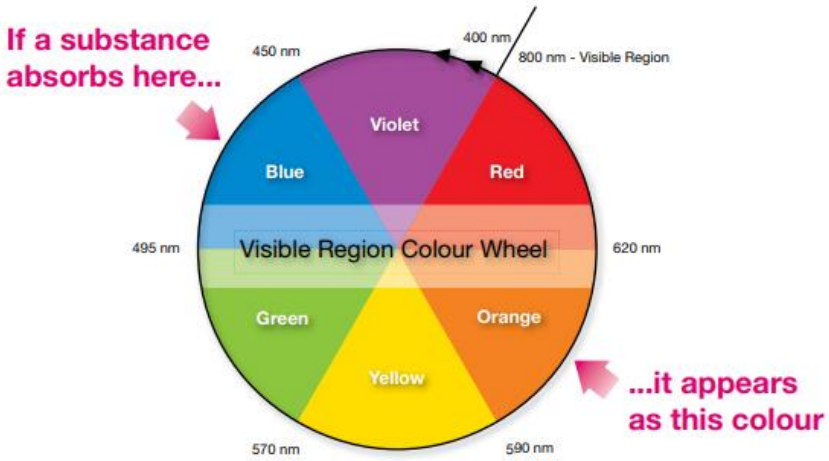

Figure 8 The colour wheel of the wavelengths in the visible region. Corresponding colours are on the opposite of each other, showing the relation between appearance and absorption of a substance. [26]

The absorbance of UV and visible light is measured by UV-Vis spectrometer. The spectrometer is composed from a light source (its type can vary depending on the region of a measurement), a monochromator (i.e. a prism, splitting the light into separate wavelengths), a sample, a reference, detector and a data output. The sample and the reference are contained in glass or quartz cuvettes for the measurement.

The measurement can be performed either at a single wavelength or through a predetermined spectral range. The intensity of a light passing through the cuvette with the sample is compared to the intensity of light that passes through the reference cuvette. The amount of the absorbed light is called the absorbance. From the collected data, UV-Vis spectrum of a sample is obtained by showing specific peaks of the highest absorbance for the sample, signifying the absorption of a specific wavelength.

UV-Vis spectroscopy is a method used for the characterization of shape and size properties of NPs. The unique optical properties of noble metal NPs are due to their surface plasmon resonance, which is the collective excitation of free conductive electrons excited by electromagnetic radiation (Figure 9). [27]

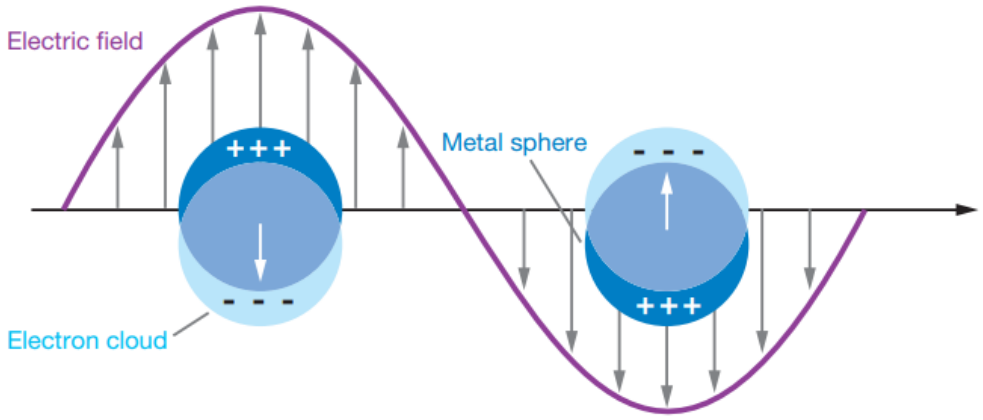

Figure 9 **Localized surface plasmon.** The particle is significantly smaller than the wavelength of incident light, leading to local oscillation of a plasmon around the particle. The oscillation frequency is called localized surface plasmon resonance. [27]

Surface plasmon resonance (SPR) absorption peak depends on the size, shape and aggregation of NPs, enabling UV-Vis spectroscopy to determine the aggregation level, size and concentration of NPs, especially in colloidal systems. It is a non-destructive technique, leaving the sample without alteration. [28–30] The short time of measurement together with its relative simplicity and accessibility allows its applications in various industrial and scientific fields. [31–35]

2.4.2 Transmission electron microscopy (TEM)

Transmission Electron Microscopy (TEM) is a technique base on similar principles as the light microscopy. However, instead of the white light, a beam of electrons is used

for analysing the sample, resulting in images of a greater resolution and a better magnitude than the images obtained by the light microscopy. [36]

An electron emission source (i.e. electron gun) emits the high energy beam of electrons into the vacuum. The system of condenser lens focuses the beam into a required size as it passes through the sample. Parts of the beam are transmitted and focused by an objective aperture of several types of lens into fluorescent screen and subsequently into CCD camera. [37, 38]

TEM is commonly used technique [39–44] offering information about the size of NPs and their morphology, thought the analysis of NPs size does not occur rapidly and in real-time. In case of NPs, the preparation of the sample is essential. The sample is prepared by placing a small amount of colloidal system upon circular TEM grid with a supporting mesh. During the drying process, aggregation and alteration of the size distribution and morphology may occur. [28]

2.4.3 Dynamic light scattering (DLS)

Dynamic Light Scattering (DLS), also known as Photon Correlation Spectroscopy or Quasi-Elastic Light Scattering, is another available method for NPs characterization and size distribution. [45–49] The size of NPs is determined from the intensity of fluctuations of the scattered light passing through the sample of NPs in colloidal suspension. [50]

A laser beam as a light source illuminates the sample in a cuvvete and the scattered light is measured by the detector at the angle 173° or 90° (depending on a particular setup). As the particles are suspended in a liquid, the fluctuations of a scattering intensity caused by the speed of the Brownian motion (i.e. the random motion of particles induced by the motion of surrounding molecules in a liquid) are measured at the stable temperature and known viscosity of the surrounding liquid. These fluctuations are analysed by the auto-correlation function. [51]

The acquired size distribution data shows the intensity of scattered light from particles of various sizes. This intensity based size distribution can be converted to number base size distribution, representing a number of particles that scatter light with the varying amount of intensity that was measured. [52]

In the case of non-spherical NPs, the measured size of the NP is a hydrodynamic diameter of a theoretical sphere with the same translational diffusion (with the same speed) as the NP. This can pose a problem, when, for instance, rod-like shape NPs are measured. The measured size is also affected by all substances adsorbed on the surface of NPs (e.g. polymers, stabilizers, etc.) and the thickness of the Debye length of EDL.

Furthermore, the accuracy of DLS technique is based on the monodispersity of the sample. If the colloidal system is polydisperse, the smaller particles can be concealed by the larger ones and be left out of measured data. [28]

2.4.4 Zeta-potential

Zeta-potential is the electrostatic potential at the EDL of NPs in colloidal suspensions. In colloids, zeta-potential determines the degree of electrostatic interaction among NPs, indicates the stability or instability of a colloidal system and can reveal its inclination to aggregation. [53]

The colloidal system with the zeta-potential of ±30 mV is considered to be stable; while the colloid with a value of zeta-potential close to 0 mV (i.e. in the interval between +5 mV and -5 mV) tends to aggregate.[54]

The measurement of zeta-potential is a relatively simple and common technique [55–58], usually it can be performed with the same instrument as the measurement of DLS.

2.4.4 Surface-enhanced Raman spectroscopy (SERS)

Surface-enhanced Raman spectroscopy (SERS), also called surface-enhanced Raman scattering is a technique derived from Raman spectroscopy (Raman scattering, Raman Effect). Raman scattering is the inelastic light scattering of the photons incident on the molecules of a material. The majority of photons is scattered elastically, their energy is unchanged. Nevertheless, some photons change their energy after coming into the contact with a material, which can provide an insight into the chemical and vibrational structure of molecules. [59–61]

SERS technique magnifies (enhances) Raman signals form molecules positioned near the surface (or at the surface) of metal materials (usually metal NPs). The signal is enhanced by electromagnetic and chemical enhancement. The electromagnetic enhancement occurs due to the excitation of surface plasmon resonances in metal NPs, induced by the laser light with a specific excitation line. Plasmonic properties of metal NPs (e.g. resonance frequency, surface electromagnetic field) are strongly dependent on the type, size, shape and structure of NPs. [23, 62]

In the chemical enhancement, a molecule is chemically adsorbed on the surface of the metal NPs, providing the transfer of the charge. In practical applications, both mechanisms of enhancement can be combined; with the electromagnetic enhancement being the stronger component of the two. Moreover, the enhancement is influenced by the distance between molecule and the surface of the substrate, type of substrate (e.g. solid substrate, colloids) and the aggregation state. [23, 62]

The preparation of colloidal NPs is relatively uncomplicated, making colloidal NPs commonly used for SERS enhancement. Their plasmonic resonance can be modified by the change of the type, size, shape and structure of NPs.

The distance between a molecule and the surface of the substrate is dependent on chemical bonds and surface charges of NPs. When the charge of the molecule is the opposite of the surface charge of the NPs, attractive forces arise along with the aggregation and decrease of zeta potential of NPs. With the aggregation of NPs, SERS activity is increased provided that the excitation laser line falls within the surface plasmon resonance region. Surface plasmon resonance of aggregated NPs shifts to a longer wavelength with

a broad spectrum adjustable for different excitation line of lasers. However, the aggregation process is quite random, leading to varying SERS enhancement through the sample. The experimental conditions are difficult to be optimized and lack a sufficient reproducibility. [23, 62–64]

SERS is widely used in bioanalytical applications, namely in detections and quantification of small molecules, DNA, proteins, etc., with measurement optimized for the molecular specificity and high enhancement factors. [44, 65–71]

SERS detection of proteins (and other biologically relevant structures and molecules) allows a greater specificity with the spectra of narrow and unique peaks. The influence of water on the SERS signal is mostly negligible, allowing the detection in aqueous solutions with a small amount of a biological sample.

Specific detection of proteins often employs targeting agents for specific proteins. The detection of a protein discussed in this work is non-specific, using the inherent spectrum of a protein. This label-free detection is induced by the aggregation of colloidal NPs with an added protein. [23, 62]

3 Aims of the work

- Two-step synthesis of core-shell Ag-Ag NPs and Au-Ag NPs via seeded-growth method.

- Characterization of prepared Ag-Ag NPs and Au-Ag NPs with following methods:

    - UV-Vis spectroscopy (UV-Vis),

    - Transmission electron microscopy (TEM),

    - Dynamic light scattering (DLS),

    - Measurement of zeta-potential values.

- Testing out the ability of prepared NPs to enhance Raman scattering of the particular protein (Bovine Serum Albumin) by using different excitation laser lines (532 and 785 nm).

4 Experimental part

In case of core-shell noble metal NPs preparation, seeded-growth method is used in general, which utilizes a process of a fast reduction for generating small seeds, with subsequent adding of a weak reducing agent.

Metal core-shell Ag-Ag and Au-Ag NPs are prepared in an aqueous solution by the reduction of a dissolved metal precursor (metal salt, e.g. silver nitrate) with reducing agent such as sodium borohydride, ascorbic acid, etc. Access to larger NPs with a narrow size distribution can be granted via seeded-growth method.

Size distribution control of NPs is influenced by mixing conditions and thus the synthetic process does not always reliably yield the same result.

Additionally, the final size of NPs is influenced by mixing conditions as well as by other experimental parameters, particularly in case of Ag-systems, where mixing conditions represent an important factor in the growth of NPs and their final size. Nevertheless, growth mechanism itself is not altered.

4. 1 Chemicals

Silver nitrate ($AgNO_3$, 99,9999 % purity, abbreviated as "Ag+"), sodium borohydride ($NaBH_4$, > 98 % purity, abbreviated as "Bh") and tetrachloroauric acid ($HAuCl_4$, > 99 % purity), L-ascorbic acid (≥ 99,0 % purity, abbreviated as "Asc"), L-aspartic acid (≥ 98 % purity, abbreviated as "Asp") and Bovine Serum Albumin (BSA, ≥ 96 % purity) were acquired from Sigma-Aldrich. No additional purification was performed. Solutions were prepared with deionized water (purification system Milli-Q). All glassware was cleaned with acid (aqua regia, a mixture of nitric acid and hydrochloric acid, optimally in a molar ratio of 1:3) and copious amounts of deionized water prior to its usage.

4. 2 Nomenclature

For easier comprehension and better orientation, naming convention was developed for seed solutions and colloidal NP systems.

Seed solutions are either prepared immediately, i.e. preceding the synthesis of a colloidal system, or aged, more stable seed solution is used.

The recently prepared seed solution is named by the following order:

'Type of metal' NP- 'Type of reducing agent'-'Age',

i.e. AgNP-Bh-5min-(1) means that they are seeds of silver NP prepared by using sodium borohydride as the reducing gent, and the solution was stirred for five minutes before its usage as seeds in the next step of a colloidal NP system preparation. The Arabic numerals

'(1), (2)' in brackets indicate repetition of the synthesis, while Roman numerals '(I), (II)' signify same synthesis with a later stage hydrolysis of sodium borohydride

Names of the final colloidal systems prepared from seed solutions are changed by removing the first hyphen between 'NP' and 'Type of reducing agent', and adding the abbreviations of further reactants in the order of their subsequent introduction into a particular system. Either the metal salt silver nitrate, $AgNO_3$, was added as the first reactant, followed by the reducing agent L-ascorbic acid (_Ag+_Asc), or the order was reversed (_Asc_Ag+). Ergo, the naming sequence is as follows:

'Type of metal' NP 'Type of reducing agent'_'Progress of synthesis'-'Age',

i.e. AgNPBh_Ag+_Asc-(1) means that this colloidal system was prepared from seed solution where sodium borohydride was used as a reducing agent, and first silver nitrate was added, followed by L-ascorbic acid. The numerals in the bracket symbolize stage of hydrolysis of sodium borohydride as discussed above.

The prepared seed solutions and final colloidal systems derived from them are summarized in Table 1.

Table 1 Prepared seed solutions and final colloidal systems.

Metal	Seed solution	Final colloidal system
Ag	AgNP-Bh-5min-(1)	AgNPBh_Ag+_Asc-(1)
	AgNP-Bh-5min-(I)	AgNPBh_Ag+_Asc-(I)
	AgNP-Bh-5min-(2)	AgNPBh_Ag+_Asc-(2)
	AgNP-Bh-5min-(II)	AgNPBh_Ag+_Asc-(II)
Au	AuNP-Bh-5min-(1)	AuNPBh_Ag+_Asc-(1)
	AuNP-Bh-5min-(I)	AuNPBh_Ag+_Asc-(I)

Correspondingly, the name of an aged seed solution follows the same notation, with the only exception: the reducing agent abbreviation is put before 'NP' label. The seed solution should be more stable in this case, because more time elapsed and enabled a better stabilization of seeds:

'Type of metal' 'Type of reducing agent' NP -'Age',

i.e. AuCtrNP-7m means that they are seeds of gold NPs prepared by using sodium citrate as a reducing gent, and at the time of usage they are 7 months aged.

The final colloidal systems are labelled similarly, except the name of the aged seed solution is left unchanged, and only the progress of synthesis is added:

'Type of metal' 'Type of reducing agent' NP-'Age'_'Progress of synthesis',

i.e. AuCtrNP-7m_Asc_Ag+-(1) means that this colloidal system was prepared from the seed solution AuCtrNP-7m and first L-ascorbic acid was added, followed by silver nitrate. Colloidal systems prepared from stable seed solutions are summarized in Table 2.

Table 2 Final colloidal systems from stable seed solutions.

Metal	Seed solution	Final colloidal system
Ag	AgBhNP-7m	AgBhNP-7m_Ag+_Asc
		AgBhNP-7m_Ctr-Ag+_Asc
		AgBhNP-7m_Asc_Ag+
Au	AuBhNP-7m	AuBhNP-7m_Ag+_Asc-(1)
		AuBhNP-7m_Asc_Ag+-(1)
		AuBhNP-7m_Ag+_Asc-(2)
		AuBhNP-7m_Asc_Ag+-(2)
	AuCtrNP-7m	AuCtrNP-7m_Ag+_Asc-(1)
		AuCtrNP-7m_Asc_Ag+-(1)
		AuCtrNP-7m_Ag+_Asc-(2)
		AuCtrNP-7m_Asc_Ag+-(2)

4. 3 Formation of Ag-Ag NPs

The synthesis of core-shell Ag-Ag NPs is separated into two steps: synthesis of seed solution and subsequent synthesis of the final colloidal system. The seed solution is prepared by the reduction of dissolved metal precursor silver nitrate $AgNO_3$ with sodium borohydride $NaBH_4$. The final colloidal system is prepared from a seed solution with an additional reduction of metal salt $AgNO_3$ by L-ascorbic acid.

There were 4 types of synthesis performed, differing in the age of the seed solution, sequence of steps and in the introduction of an additional surface-modifier of the seeds.

Table 3 Syntheses types of the final core-shell Ag-Ag NP colloidal systems

Name	Description
Type 1 Ag-Ag NP synthesis	The seed solution is freshly prepared prior to the synthesis of the final colloidal system which can be labelled as (AgNPBh_Ag+_Asc) according to our nomenclature.
Type 2 Ag-Ag NP synthesis	The seed solution is 7 months aged at the time of the synthesis of the final colloidal system, labelled as (AgBhNP-7m_Ag+_Asc).
Type 3 Ag-Ag NP synthesis	The seed solution is 7 months aged at the time of synthesis of the final colloidal system (so far, the same as Type 2 Ag-Ag NP systems), however, the addition of the other reactants is performed in a reverse order than in Type 2 Ag-Ag NP synthesis. It is thus labelled as (AgBhNP-7m_Asc_Ag+).
Type 4 Ag-Ag NP synthesis	The seed solution is 7 months aged at the time of the synthesis of the final colloidal system (so far, the same as Type 2 Ag-Ag NP systems); the addition of sodium citrate (as another surface-modifier) simultaneously with $AgNO_3$ is included in the synthesis. It is then labelled as (AgBhNP-7m_Ctr-Ag+_Asc).

4.3.1 Type 1 Ag-Ag NPs synthesis

The seed solution (AgNP-Bh-5min) was prepared by mixing together 5 mL of 0.8 mM $AgNO_3$ aqueous solution, 5 mL of 4.48 mM NaBH4, and 10 mL of deionized water. Seed solution (AgNP-Bh-5min) was then stirred at the rate of 1150 rpm for 5 minutes.

Subsequently, 0.5 mL of the seed solution (AgNP-Bh-5min) was added to 12.5 mL of 0.2 mM $AgNO_3$ aqueous solution, followed by 250 μL of 10 mM ascorbic acid aqueous

solution. The final colloidal system (AgNPBh_Ag+_Asc) was stirred at the rate of 1350 rpm for 10 seconds, then at the rate of 850 rpm for additional 25 minutes.

Sodium borohydride used during the preparation of the seed solution (AgNP-Bh-5min) was stored in an ice bath, due to its inclination to quickly and unpredictably oxidize at temperatures exceeding 8 °C. The stage of the hydrolysis and simultaneous oxidation of sodium borohydride has a strong influence on the formation process of the seeds, as will be further demonstrated in the following chapters.

After finishing the synthesis of seed solution AgNP-Bh-5min-(1) and colloidal system AgNPBh_Ag+_Asc-(1), the procedure of this synthesis was repeated. However, this time by using a more hydrolysed (and thus oxidized) sodium borohydride solution stored in an ice bath. It resulted in seed solution AgNP-Bh-5min-(I) and colloidal system AgNPBh_Ag+_Asc-(I).

Each step of the whole processes was replicated, thus resulting in seed solution AgNP-Bh-5min-(2), colloidal system AgNPBh_Ag+_Asc-(2), seed solution AgNP-Bh-5min-(II) and colloidal system AgNPBh_Ag+_Asc-(II).

4.3.2 Type 2 Ag-Ag NPs synthesis

Colloidal solutions (systems) which reveal a good stability in time are considered as stable. The formation process of NPs in these systems is completed, leading to steady-state surface chemistry and possible decrease of reactivity.

Seed solution AgNP-7m was prepared dissolving 3.42 mg $NaBH_4$ in 75 mL of deionized water submerged in an ice bath. The mixture was stirred at the rate of 1000 rpm while drop-wise adding of 7.5 mL of 2.2 mM $AgNO_3$ in the middle of the stirring vortex. The mixture was withdrawn from the ice bath after 3 minutes and subsequently stirred for 1 hour until reaching the room temperature.

At the time of the preparation of the final colloidal system, seed solution AgBhNP-7m was 7 months aged.

The final colloidal system was prepared by adding 0.5 mL of the seed solution (AgBhNP-7m) to 12.5 mL of 0.2 mM $AgNO_3$ aqueous solution, followed by the addition of 250 μL of 10 mM ascorbic acid aqueous solution. The final colloidal system (AgBhNP-7m_Ag+_Asc) was stirred at the rate of 1350 rpm for 10 seconds, then at the rate of 850 rpm for additional 25 minutes.

4.3.3 Type 3 Ag-Ag NPs synthesis

The final colloidal system AgBhNP-7m_Asc_Ag+ was prepared from seed solution AgBhNP-7m, but the further steps of the synthesis were reversed than in Type 2 Ag-Ag NP systems, i.e. 0.5 mL of the seed solution (AgBhNP-7m) was added to 250 μL of 10 mM ascorbic acid aqueous solution, followed by the addition 12.5 mL of 0.2 mM $AgNO_3$ aqueous solution. The solution (AgBhNP-7m_Asc_Ag+) was stirred at the rate of 1350 rpm for 10 seconds, then at the rate of 850 rpm for additional 25 minutes.

4.3.4 Type 4 Ag-Ag NPs synthesis

Sodium citrate is included in this type of synthesis as a surface-modifier (it provides an additional electrostatic stabilization) and another mild reducing agent.

In the previous syntheses 0.2 mM $AgNO_3$ aqueous solution, 2.03 mg of $AgNO_3$ in 60 mL of distilled water, was used to prepare colloidal systems. In this type of synthesis, 2.03 mg of $AgNO_3$ was dissolved in 60 mL of 1 mM sodium citrate solution. The final colloidal system was then prepared by adding 0.5 mL of the seed solution (AgBhNP-7m) to 12.5 mL of 0.2 mM $AgNO_3$ in 1 mM sodium citrate solution, followed by the addition of 250 μL of 10 mM ascorbic acid aqueous solution. The final colloidal system (AgBhNP-7m_Ctr -Ag+_Asc) was stirred at the rate of 1350 rpm for 10 seconds, then at the rate of 850 rpm for additional 25 minutes.

4. 4 Formation of Au-Ag NPs

The synthesis of core-shell Au-Ag NPs is separated into two steps: synthesis of seed solution and subsequent synthesis of the final colloidal system. The seed solution is prepared by the reduction of the metal precursor, tetrachloroauric acid $HAuCl_4$, employing the strong reducing agent, sodium borohydride $NaBH_4$, or the mild reducing agent, sodium citrate. The final colloidal system is then prepared from a particular seed solution using the subsequent reduction of the added metal salt $AgNO_3$ by L-ascorbic acid (weak reducing agent).

There were 5 types of synthesis performed, differing in the age of the seed solution, reducing agent and sequence of steps.

Table 4 Syntheses types of the final core-shell Au-Ag NP colloidal systems

Name	Description
Type 1 Au-Ag NP synthesis	The seed solution is freshly prepared prior to the synthesis of the final colloidal system which can be labelled as (AuNPBh_Ag+_Asc) according to our nomenclature.
Type 2 Au-Ag NP synthesis	The seed solution (AuBhNP-7m) is 7 months aged at the time of the synthesis of the final colloidal system, labelled as (AuBhNP-7m_Ag+_Asc).
Type 3 Au-Ag NP synthesis	The seed solution is 7 months aged at the time of synthesis of the final colloidal system (so far, the same as Type 2 Ag-Ag NP systems), however, the addition of the other reactants is performed in a reverse order than in Type 2 Ag-Ag NP synthesis. It is thus labelled as (AuBhNP-7m_Asc_Ag+).
Type 4 Au-Ag NP synthesis	The seed solution is (AuCtrNP-7m) 7 months aged at the time of the synthesis of the final colloidal system; It is then labelled as (AuCtrNP-7m_Ag+_Asc).
Type 5 Au-Ag NP synthesis	The seed solution is 7 months aged at the time of synthesis of the final colloidal system (so far, the same as Type 2 Ag-Ag NP systems), however, the addition of the other reactants is performed in a reverse order than in Type 4 Au-Ag NP synthesis. It is thus labelled as (AuCtrNP-7m_Asc_Ag+).

4.4.1 Type 1 Au-Ag NPs synthesis

The Au seeds (AuNP-Bh-5min) were prepared by mixing together 5 ml of 0.94 mM $HAuCl_4$ aqueous solution, 5 mL of 4.48 mM $NaBH_4$ aqueous solution, and 10 mL of deionized water. The seed solution (AuNP-Bh-5min) was then stirred at the rate of 1150 rpm for 5 minutes.

Subsequently, 0.5 mL of the seed solution (AuNP-Bh-5min) was added to 12.5 mL of 0.2 mM $AgNO_3$ aqueous solution, followed by 250 μL of 10 mM ascorbic acid aqueous solution. The final colloidal system (AuNPBh_Ag+_Asc) was stirred at the rate of 1350 rpm for 10 seconds, then at the rate of 850 rpm for additional 25 minutes.

After finishing the synthesis of the seed solution AuNP-Bh-5min-(1) and final colloidal system AuNPBh_Ag+_Asc-(1), the synthesis was repeated using more hydrolyzed sodium borohydride stored in an ice bath, resulting in seed solution AuNP-Bh-5min-(I) and final colloidal system AuNPBh_Ag+_Asc-(I).

4.4.2 Type 2 Au-Ag NPs synthesis

Seed solution AuBhNP-7m was prepared by dissolving 3.43 mg $NaBH_4$ in 75 mL of deionized water submerged in an ice bath. The mixture was stirred at the rate of 1000 rpm while adding drop-wise 9 mL of 2.2 mM $HAuCl_4$ in the middle of the stirring vortex. The mixture was withdrawn from an ice bath after 6 minutes and subsequently stirred for 1 hour until reaching the room temperature.

At the time of preparation of the final colloidal system, the seed solution AuBhNP-7m was 7 months aged.

The final colloidal system was prepared by adding 0.5 mL of the seed solution (AuBhNP-7m) to 12.5 mL of 0.2 mM $AgNO_3$ aqueous solution, followed by the addition of 250 μL of 10 mM ascorbic acid aqueous solution. The final colloidal system (AuBhNP-7m_Ag+_Asc-(1)) was stirred at the rate of 1350 rpm for 10 seconds, then at the rate of 850 rpm for additional 25 minutes.

The process was replicated to obtain the final colloidal system AuBhNP-7m_Ag+_Asc-(2).

4.4.3 Type 3 Au-Ag NP synthesis

The final colloidal system AuBhNP-7m_Asc_Ag+-(1) was prepared from seed solution AuBhNP-7m, thus the same seed solution as in Type 2 Au-Ag NP synthesis, but the further steps of the synthesis were reversed, i.e. 0.5 mL of the seed solution (AuBhNP-7m) was added to 250 μL of 10 mM ascorbic acid aqueous solution, followed by the addition of 12.5 mL of 0.2 mM $AgNO_3$ aqueous solution. The solution AgBhNP-7m_Asc_Ag+-(1) was stirred at the rate of 1350 rpm for 10 seconds, then at the rate of 850 rpm for additional 25 minutes.

The process was replicated to acquire colloidal system AuBhNP-7m_Asc_Ag+-(2).

4.4.4 Type 4 Au-Ag NP synthesis

Seed solution AuCtrNP-7m was obtained by bringing 200 mL of 0.2 % sodium citrate solution to a boiling point in 500-mL Erlenmeyer flask and adding $HAuCl_4$ aqueous solution prepared by mixing 20,52 g of $HAuCl_4$ in 10.26 mL of deionized water. The mixture was kept at boiling point by IKA C-MAG HS7 magnetic stirrer with ceramic heating plate for 1 hour. Afterwards, the mixture was stirred for additional one hour until reaching the room temperature.

At the time of preparation of the final colloidal system, the seed solution AuCtrNP-7m was 7 months aged.

The final colloidal system was prepared by adding 0.5 mL of the seed solution AuCtrNP-7m to 12.5 mL of 0.2 mM $AgNO_3$ aqueous solution, followed by the addition of 250 μL of 10 mM ascorbic acid aqueous solution. The final colloidal system AuCtrNP-7m_Ag+_Asc-(1) was stirred at the rate of 1350 rpm for 10 seconds, then at the rate of 850 rpm for additional 25 minutes.

The process was replicated to acquire the final colloidal system AuCtrNP-7m_Ag+_Asc-(2).

4.4.5 Type 5 Au-Ag NP synthesis

The final colloidal system AuCtrNP-7m_Asc_Ag+-(1) was prepared from seed solution AuCtrNP-7m, thus the same seed solution as in Type 2 Au-Ag NP synthesis, but the further steps of the synthesis were reversed, i.e. 0.5 mL of the seed solution (AuCtrNP-7m) was added to 250 μL of 10 mM ascorbic acid aqueous solution, followed by the addition of12.5 mL of 0.2 mM $AgNO_3$ aqueous solution. The solution AuCtrNP-7m_Asc_Ag+-(1) was stirred at the rate of 1350 rpm for 10 seconds, then at the rate of 850 rpm for additional 25 minutes.

The process was replicated to acquire colloidal system AuCtrNP-7m_Asc_Ag+-(2).

4. 5 Characterization of Ag-Ag and Au-Ag NPs

The as-prepared core-shell Ag-Ag and Au-Ag NPs were characterized by UV-Vis spectroscopy, transmission electron microscopy (TEM), dynamic light scattering (DLS), measurement of zeta-potential values and surface-enhanced Raman spectroscopy (SERS).

4.5.1 UV-Vis

UV-Vis spectra of freshly prepared and aged (1 week, 9 months) colloidal Ag-Ag and Au-Ag NPs were recorded on the spectrometer Specord PLUS 250 (ChromSpec), in the range between 190 nm − 1100 nm. Quartz cuvettes with 2.5 mL of the colloidal sample were used for the measurements. Deionized water in the quartz cuvette served as a reference.

4.5.2 TEM

The size and shape of Ag-Ag and Au-Ag NPs were evaluated by Jeol 2010F transmission electron microscope, equipped with a LaB_6 cathode (accelerating voltage 80 kV - 200 kV; CCD camera Keenview G2). A drop (3 μL) of a particular colloidal sample was deposited onto a carbon-coated copper grid. Grids were allowed to dry at room temperature in a Petri dish covered by its lid for at least one day before performing TEM measurement.

4.5.3 DLS, Zeta-potential

The size distribution of colloidal Ag-Ag and Au-Ag NPs (aged for approx. 9 months) was measured with Zetasizer Nano Series (Malvern Instruments). A scattering angle is set by the manufacturer at 173°, the laser wavelength is 633 nm, and the measurement was performed at 25°C in a disposable polystyrene cuvette filled with 1 mL of a particular colloidal sample, which was diluted with deionized water at 1:10 v/v ratio. The measurement was set at "multiple narrow mode" resolution and automated number of "runs" during the measurement. A mean result of three measurements was recorded.

The same instrument was used for measuring zeta-potential of colloidal Ag-Ag and Au-Ag NPs (aged for approx. 9 months). The 0.75 mL of a particular sample (no dilution) was placed into a disposable zeta-potential cell and a mean result of three measurements was recorded.

4.5.4 SERS

The final colloidal systems of core-shell Ag-Ag and Au-Ag NPs were 9 months aged at the time of the SERS measurements. L-aspartic acid and sodium chloride (NaCl) were used as a surface modifier prior to the addition of BSA to a particular final colloidal system in order to induce NPs aggregation due to the changes of zeta-potential values.

250 μL of 10 mM aspartic acid aqueous solution was added to 1 mL of the final colloidal system (diluted in 1:1 v/v ratio with deionized water), followed by 100 μL of BSA aqueous solution (1 mg/mL concentration).

22 μL of 5 mM NaCl aqueous solution (to achieve the final concentration of 1.1 x 10^{-1} M NaCl in the sample) was added to 1 mL of the final colloidal system (diluted in 1:1 v/v ratio with deionized water), followed by 100 μL of BSA aqueous solution (1 mg/mL concentration).

The UV-Vis and SERS spectra of samples were recorded both prior and after the addition of BSA solution, to determine whether the process of aggregation shifts the SPR peak close to the regions of available excitation wavelengths (532 nm and 785 nm).

The first round of SERS measurements was performed with a home-made Raman optical instrument (the author of this ROA instrument is dr. Josef Kapitán) using the 90° geometry, excitation laser line of 532 nm with a 13 mW power and acquisition time 120 s. The measurement was carried out with a capped micro-cuvette filled with 87 μL of a particular sample.

The second round of SERS measurements was performed with ProRaman-L Raman Spectrometer (purchased from RMI) using the excitation laser line of 785 nm with a 100 mW power and acquisition time 120 s. The measurement was carried out with a quartz cuvette filled with the whole amount (1.35 mL) of a particular sample.

5 Results and discussion

5. 1 UV-Vis spectra and TEM imaging

UV-Vis spectra of Ag and Au NPs seed solutions and Ag-Ag and Au-Ag final colloidal systems were measured shortly after the synthesis (further determined by the time signature at the end of the designated name).

TEM images were obtained from copper TEM grid with dried samples of the seed solutions or final colloidal systems, therefore, only size and shape of nanoparticles are investigated; the aggregation state might be influenced by the process of drying.

5.1.1 Ag-Ag NPs

5.1.1.1 Freshly prepared seeds - the effect of the stage of borohydride hydrolysis

Preparation of the seed solution is the first step of the synthesis of core-shell NPs. UV-Vis spectra of seed solutions AgNP-Bh-5min-(I) and AgNP-Bh-5min-(2) are shown in Figure 10. These seed solutions differ in the stage of borohydride hydrolysis: freshly prepared borohydride was used in case AgNP-Bh-5min-(2), while hydrolysed borohydride (for half an hour, but kept in ice-bath in a refrigerator) was employed in case AgNP-Bh-5min-(I).

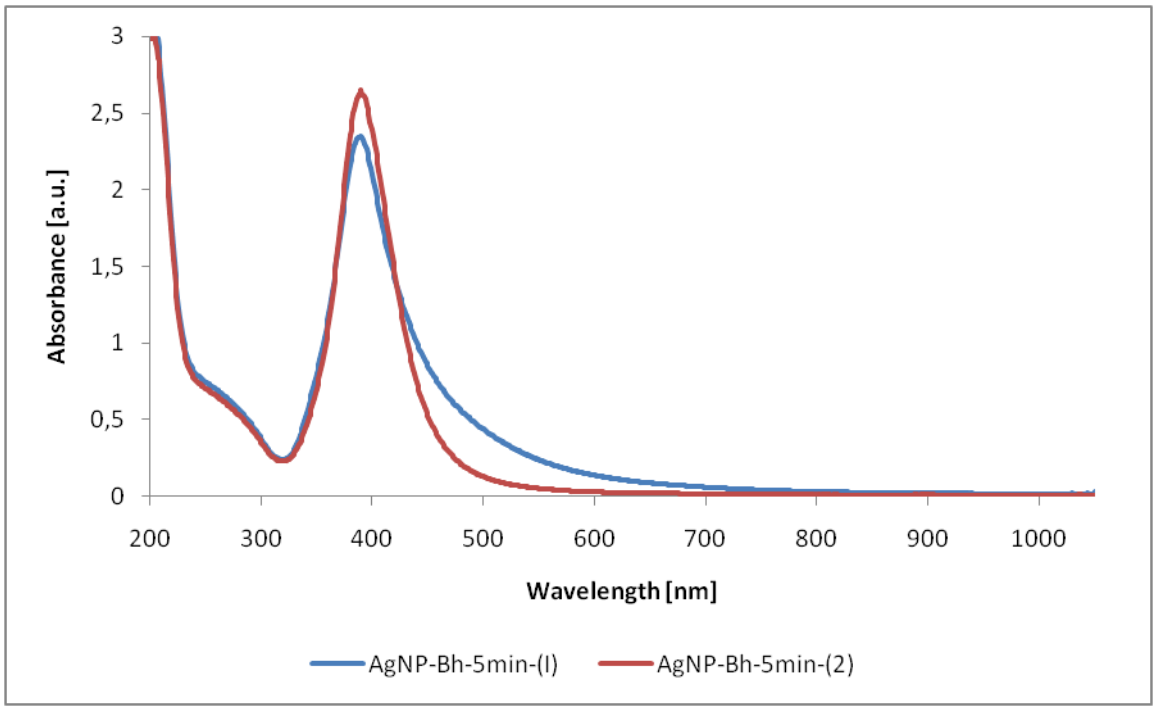

Figure 10 UV-Vis spectra of seed solutions AgNP-Bh-5min-(I) and AgNP-Bh-5min-(2). Absorption peaks at around 400 nm indicate surface plasmon resonance of anisotropic NPs, different broadness of peaks is attributed to a different stage of $NaBH_4$ hydrolysis.

In Figure 10, the sharp absorption peaks at around 400 nm are attributed to the surface plasmon resonance (SPR) of nearly spherical Ag NPs. The degree of dispersion of NPs (of the same type and consisting of the same material) is given by the shape of the absorption peak; narrow shape indicates a smaller degree of dispersion. Seed solution AgNP-Bh-5min-(I) (blue line), shows a possible beginning of aggregation (recognized according to its broader and asymmetric shape of SPR peak). This fact can be associated with a later stage of hydrolysis of reducing agent $NaBH_4$ used for the preparation of AgNP-Bh-5min-(I) (blue line).

The example of the shape of Ag seeds is demonstrated via TEM imaging in Figure 11.

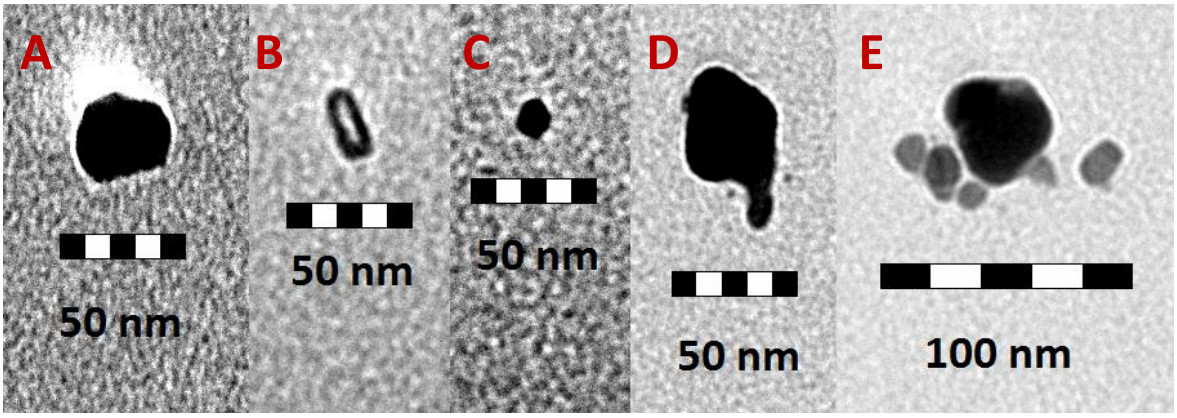

Figure 11 TEM images of seed solutions AgNP-Bh-5min-(I) (A, B, C) and AgNP-Bh-5min-(2) (D, E). A) – E) Ag seeds.

Final colloidal systems AgNPBh_Ag+_Asc-(I) and AgNPBh_Ag+_Asc-(2) are prepared from seed solutions AgNP-Bh-5min-(I) and AgNP-Bh-5min-(2) which differ in the stage of $NaBH_4$ hydrolysis (a later in (I) and an early in (2), respectively). UV-Vis spectra of these final colloidal systems are shown in Figure 12.

In Figure 12, the absorption peak at around 265 nm is evident due to an incomplete disintegration of ascorbic acid (its double bond between carbon and oxygen is responsible for this absorption maximum).

Absorption peaks located at around 400 nm in Figure 12 are markedly broader and more asymmetric compared to the absorption peaks around the same wavelength in Figure 10. The relatively smaller intensity of absorption peaks in Figure 12 is most probably due to a lower number of the final NPs, compared to that of the seed solution. The broadening of the SPR peak and its slight shift toward the red part of the spectrum (higher wavelengths) point to a larger size distribution, the presence of aggregates and elongated rod-like nanoparticles. The latter can be derived from the presence of a shoulder at around 356 nm which can be attributed to a transversal mode of SPR characteristic for non-symmetrical particles (such as rods, triangles, etc.)

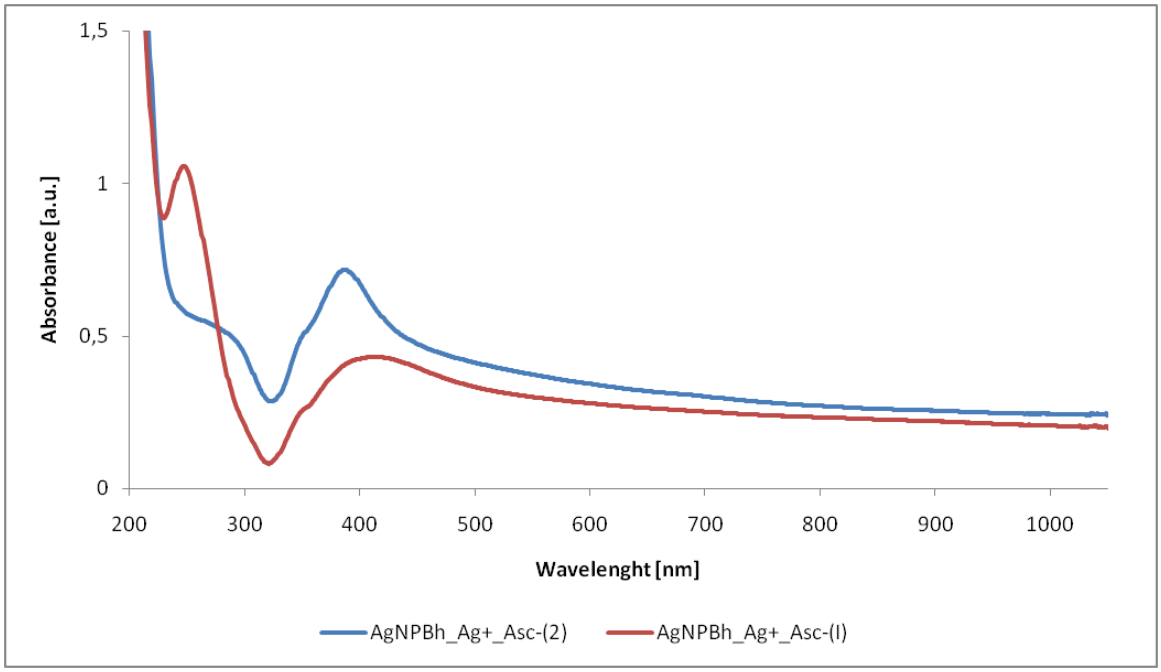

Figure 12 UV-Vis spectra of colloidal systems AgNPBh_Ag+_Asc-(I) (red) and AgNPBh_Ag+_Asc-(2) (blue). The absorption peak at around 250 nm due to an incomplete disintegration of ascorbic acid (red line), broader absorption peaks at around 400 nm with a slight shoulder visible at the point of 356 nm (red and blue line).

TEM images of colloidal systems AgNPBh_Ag+_Asc-(I) and AgNPBh_Ag+_Asc-(2) are shown in Figure 13. Larger aggregates and non-symmetrical rod-like NPs are both present in the final colloidal systems.

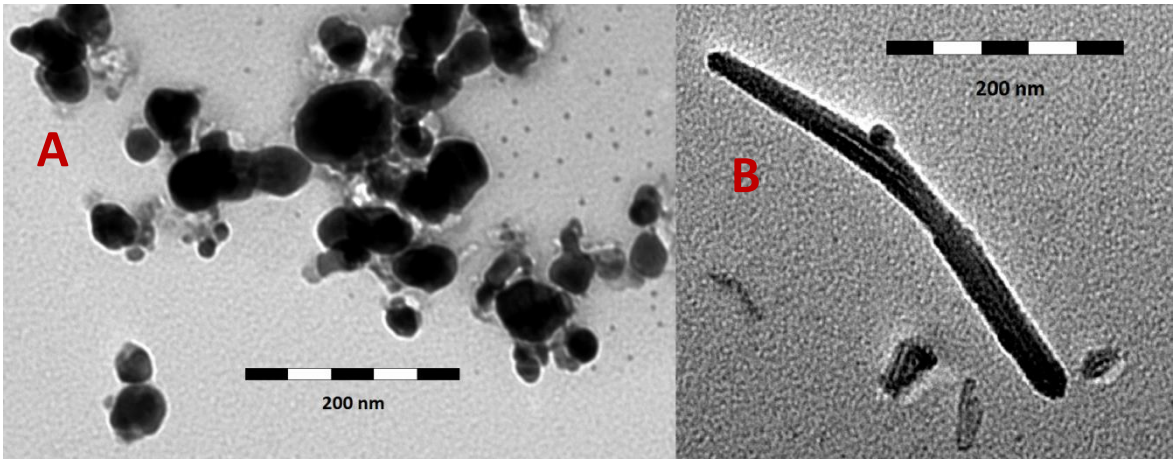

Figure 13 TEM images of colloidal systems AgNPBh_Ag+_Asc-(2) (A) and AgNPBh_Ag+_Asc-(I) (B). A) Aggregates of Ag-Ag NPs of final colloidal system AgNPBh_Ag+_Asc-(2) also with rod-like NPs present, similar to B) non-symmetrical Ag-Ag NP with rod-like shape in final colloidal system AgNPBh_Ag+_Asc-(I) (no aggregates present).

5.1.1.2 Usage of stable seeds

Another approach to prepare a final colloidal system by employing seed-mediated growth is to use older more stable seed solutions as discussed in [64]. Therefore, seed solution AgBhNP-7m was used to prepare colloidal system AgBhNP-7m_Ag+_Asc.

The prominent discrepancy among the UV-Vis spectra of the final colloidal systems prepared from seed solutions of a different type is shown in Figure 14.

Apparently, the non-uniformity of characteristic absorption peaks at around 400 nm (sharper in the case of AgNPBh_Ag+_Asc-(2); while broader in the case of the other two) with further shoulders and/or enhanced absorption in the region above 450 nm can be directly connected with the stage of borohydride hydrolysis because the other synthetic parameters are hold the same. Based solely on UV-Vis spectra, it can be thus concluded that the less hydrolysed $NaBH_4$, the narrower NP size distribution obtained.

The maximum of the absorption peak of the colloidal system AgBhNP-7m_Ag+_Asc (Figure 14, red line) even shifted to the value of 450 nm, most likely due to the aggregation of the NPs in the colloidal system. Simultaneously, there is a second maximum in this spectrum with a broad maximum centred at around 900 nm, as well as, a clear shoulder at 350 nm. They can represent longitudinal and transversal modes of rod-like (and/or triangular) nanoparticles, respectively.

The comparison of these colloidal systems thus demonstrates the difference in their electrostatic stabilization and displays the influence of EDL on the process of NPs formation.

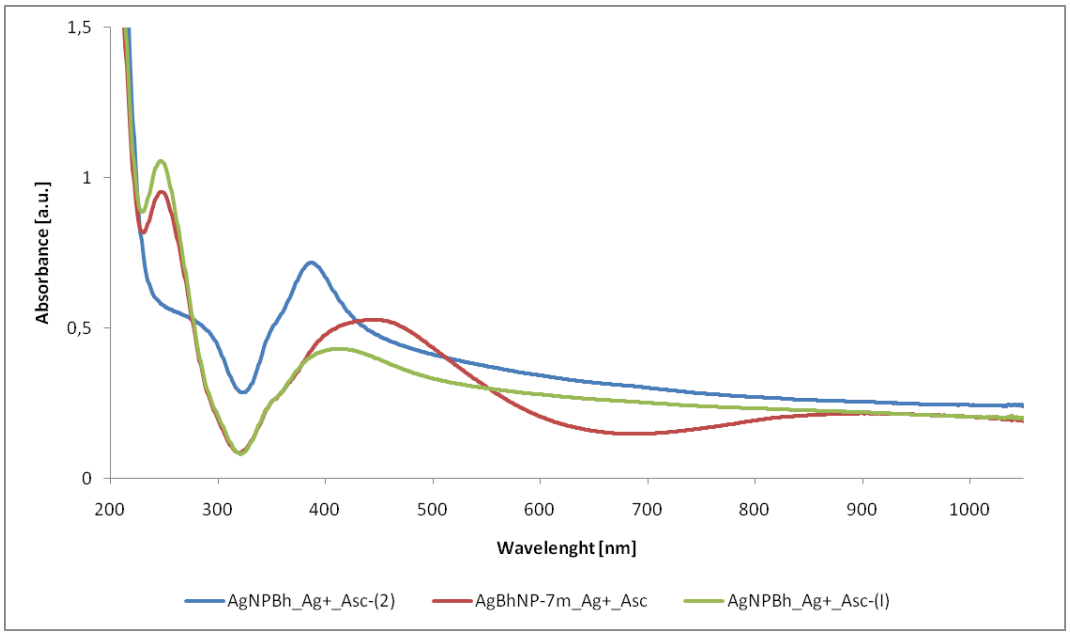

Figure 14 UV-Vis spectra of colloidal systems AgBhNP-7m_Ag+_Asc (red), AgNPBh_Ag+_Asc-(I) (green), AgNPBh_Ag+_Asc-(2) (blue). The absorption peak at around 400 nm of the colloidal system AgNPBh_Ag+_Asc-(2) (blue line) is sharper than the absorption peaks of the colloidal systems AgNPBh_Ag+_Asc-(I) (green line) and AgBhNP-7m_Ag+_Asc (red line), which shifted to the value of 450 nm due to aggregation of the system.

Unfortunately, TEM images could not be obtained owing to continuous layer on TEM copper grid. The final colloidal system formed aggregates that were impossible to be evaluated with TEM imaging.

5.1.1.3 Effect of citrate and/or ascorbate on the final colloidal systems

The citrate is used as a surface modifier in the synthesis to obtain smaller and more homogenous size distribution. Similarly, by reversing the order of the synthesis (by starting with weak reducing agent ascorbic acid) it was tried to determine, whether the formation process of NPs is altered.

The seed solution AgBhNP-7m was used to prepare colloidal systems AgBhNP-7m_Ctr-Ag+_Asc and AgBhNP-7m_Asc_Ag+. UV-Vis spectra of these final colloidal systems are shown in Figure 15.

In Figure 15, the absorption peak at around 265 nm stemming from the residual ascorbic acid is evident for system AgBhNP-7m_Ctr-Ag+_Asc (blue line). The addition of sodium citrate during the synthesis functions as a stabilizing agent, providing an additional electrostatic stabilization of EDL.

Absorption peak in the spectrum of AgBhNP-7m_Ctr-Ag+_Asc positioned at around 400 nm (blue line in Figure 15) is comparatively narrow as that of the starting AgBhNP-7m, indicating a relatively smaller size distribution of NPs. Sodium citrate slows down the rapid particle growth, and the point of colloidal stability is reached more quickly. The second broad maximum in the spectrum of AgBhNP-7m_Ctr-Ag+_Asc (blue line in Figure 15) together with the shoulder around 340 nm may be attributed to the rod-like and/or triangular NPs.

The colloidal system labelled as AgBhNP-7m_Asc_Ag+ (red line) was prepared with reversed steps of the synthesis. The metal salt $AgNO_3$ to be reduced is added after the reducing agent ascorbic acid. While this approach provides ascorbic acid with a sufficient time to disintegrate, as is evidenced by the absence of the absorption peak at around 265 nm; it also encourages the aggregation, coalescence and larger size distribution is observed (represented by a red-shift of the SPR maximum). The absorption peak at around 400 nm shifted toward the value of 450 nm and is notably broad. Simultaneously, a shoulder at round 350 nm on the left part of the SPR peak is present, pointing to the existence of non-symmetrical particles of rod-like and/or triangular shape.

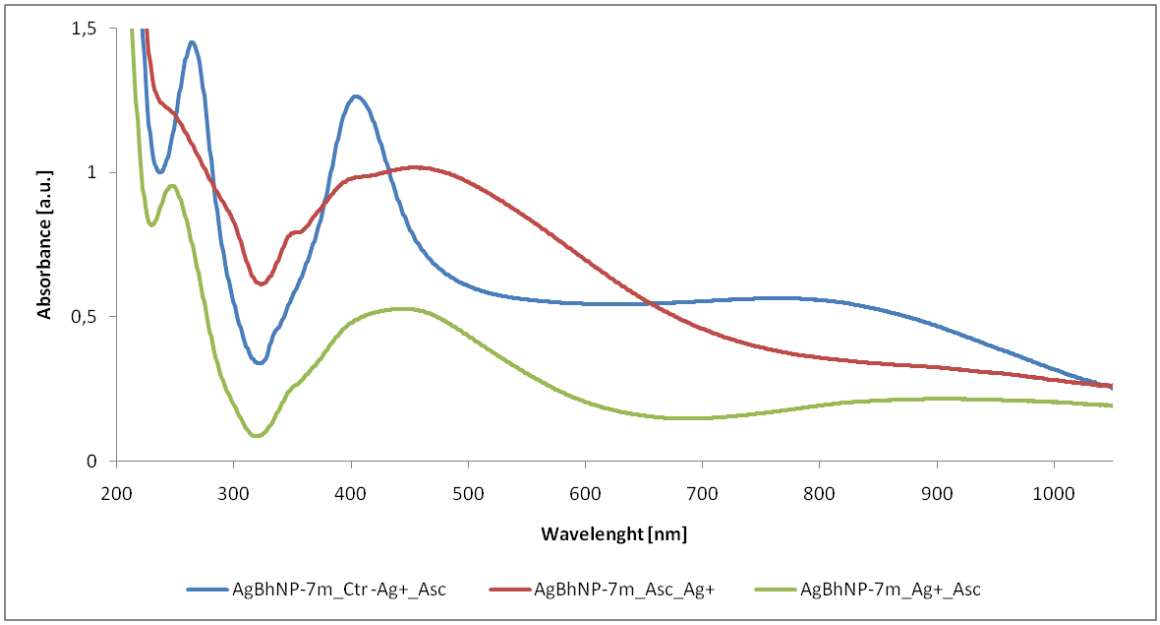

Figure 15 UV-Vis spectra of colloidal systems AgBhNP-7m_Ctr-Ag+_Asc (blue), AgBhNP-7m_Asc_Ag+ (red), AgBhNP-7m_Ag+_Asc (green). The absorption peak at around 250 nm due to incomplete disintegration of ascorbic acid (blue line), broad absorption peaks at around 400 nm with slight "shoulder" visible at the point of 350 nm (red line).

TEM images of colloidal system AgBhNP-7m_Ctr-Ag+_Asc are shown in Figure 16. The addition of sodium citrate resulted in relatively narrow size distribution, smaller final NP sizes (than those generated during the synthesis without the presence of citrate), rod-like and /or irregularly triangular NP shapes.

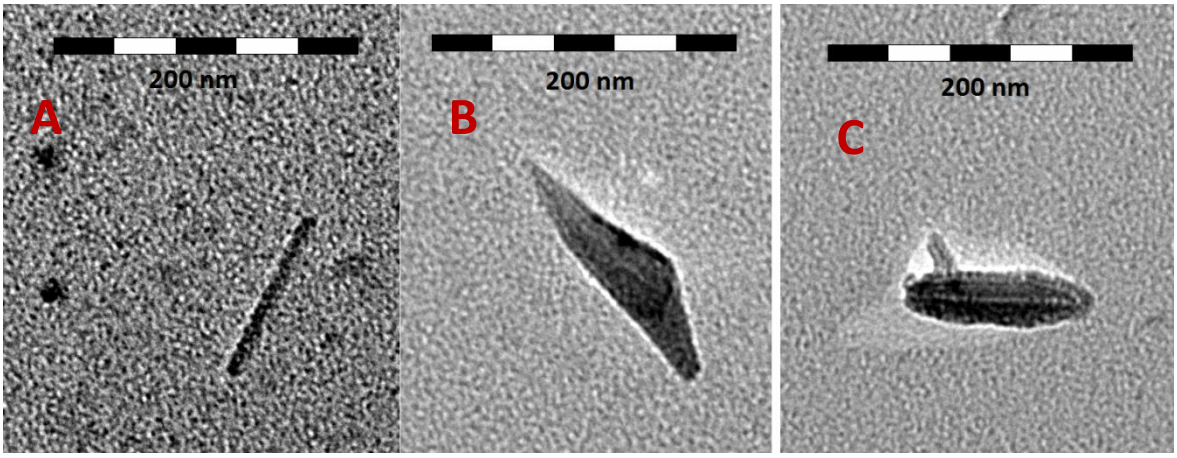

Figure 16 TEM images of colloidal system AgBhNP-7m_Ctr-Ag+_Asc. A) – C) rod-like and irregularly triangular NPs together with spherical ones.

TEM images of colloidal system AgBhNP-7m_Asc_Ag+ are shown in Figure 17. In the contrast to TEM images of colloidal system with sodium citrate (Figure 16), TEM images shown in Figure 17 revealed larger size distribution and polydispersity. In

correspondence with UV-Vis spectra of the same colloidal system (Figure 15, red line), both non-symmetrical and rod-like NPs are present together with almost spherical ones.

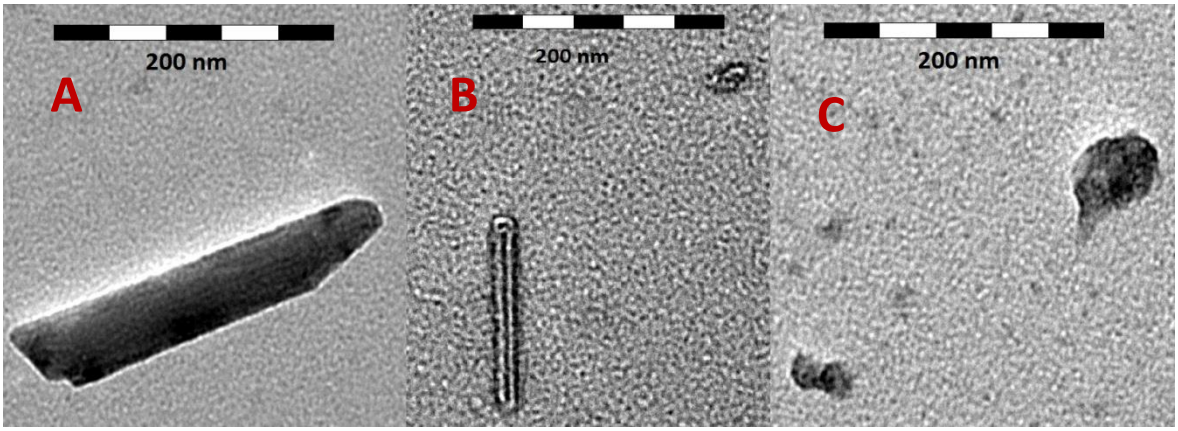

Figure 17 TEM images of colloidal system AgBhNP-7m_Asc_Ag+. A) – B) rod-like NPs, C) non-symmetrical NPs

5.1.2 Au-Ag NPs

5.1.2.1 Freshly prepared seeds – the effect of the stage of borohydride hydrolysis

Since the seeds of Ag NPs proved to be quite reactive, polydisperse and, consequently, the final colloidal Ag-Ag NP systems were not easily prepared reproducibly, an effort was put into the synthesis of Au-Ag NPs. Main idea of producing the core-shell NPs with Au core and Ag shell was to improve the reproducibility of synthesis and NP dispersity owing to the employment of Au seeds; while simultaneously keeping great optical enhancement properties of Ag.

The syntheses of colloidal systems of Au-Ag NPs were undertaken in a similar fashion to Ag-Ag NPs syntheses. The colloidal systems were either prepared from stable 7-months aged seed solution, or the seed solution was freshly prepared prior to the synthesis.

The seed solutions AuNP-Bh-5min-(1) and AuNP-Bh-5min-(I) were prepared preceding the synthesis of the final colloidal systems AuNPBh_Ag+_Asc-(1) and AuNPBh_Ag+_Asc-(I).

UV-Vis spectra of these seed solutions and final colloidal systems are shown in Figure 18. Absorption peaks of seed solutions AuNP-Bh-5min-(1) and AuNP-Bh-5min-(I) (blue and green line, respectively) are beyond the value of 500 nm, and at relatively low intensity, indicating the presence of Au seeds.

UV-Vis spectra of the final colloidal systems AuNPBh_Ag+_Asc-(1) and AuNPBh_Ag+_Asc-(I) (red and purple line, respectively) differ in the intensity of absorption values of SPR peaks which are located at around 400 nm (i.e. the characteristic position of SPR for Ag NPs).

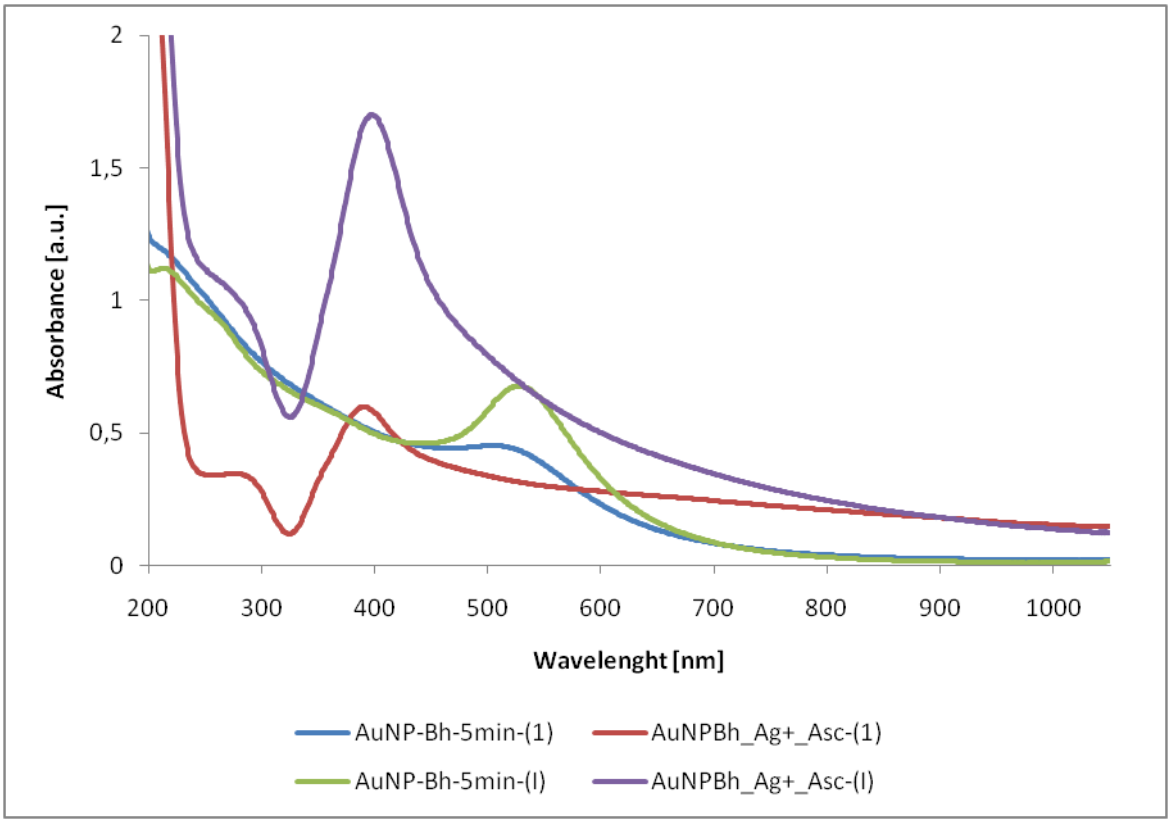

Figure 18 UV-Vis spectra of the seed solutions AuNP-Bh-5min-(1), AuNP-Bh-5min-(1) (blue and green line, respectively) and of the final colloidal systems AuNPBh_Ag+_Asc-(1), AuNPBh_Ag+_Asc-(I) (red and purple line, respectively).

TEM images of the seed solution AuNP-Bh-5min-(1) in Figure 19 show the seeds linked together (Figure 19B) and forming an interconnected net (Figure 19A). The presence of these aggregates is supported by the UV-Vis spectra in Figure 18 (blue line) and the flattened broad absorption peak of the seed solution AuNP-Bh-5min-(1).

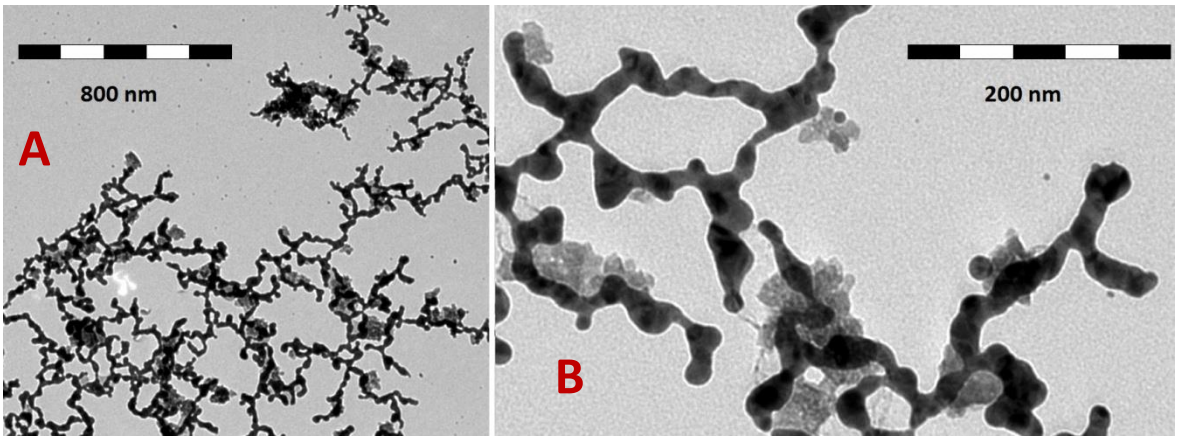

Figure 19 TEM images of the seed solution AuNP-Bh-5min-(1). A) interconnected seeds, B) a close-up view of the connection between the seeds

TEM images of the final colloidal system AuNPBh_Ag+_Asc-(1), synthesized from the seed solution AuNP-Bh-5min-(1), display core-shell Au-Ag NPs (Figure 20). The links between Au seeds (observable in Figure 19) disconnected (however, no solitary seeds were found in the TEM sample), and Ag layer was formed around them. The layer is not continuous and does not have the same thickness around the circumference of the Au core.

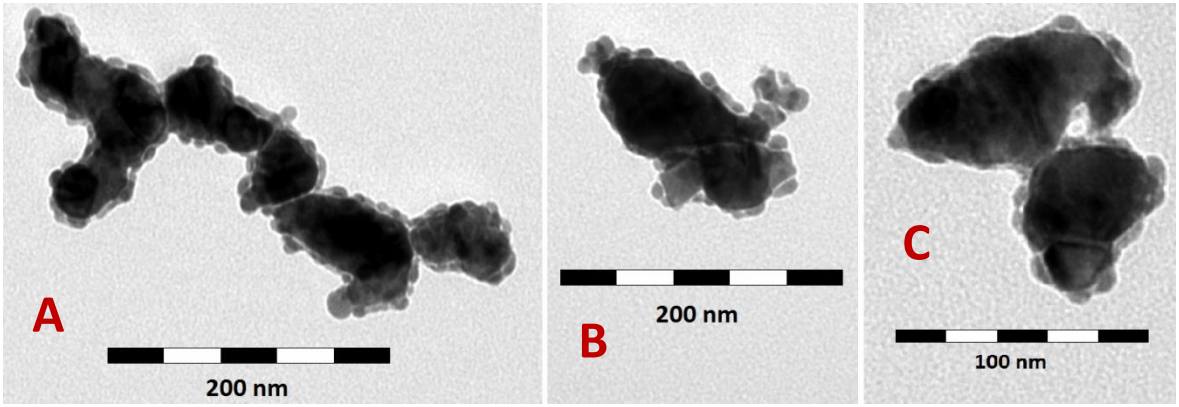

Figure 20 TEM images of the seed solution AuNPBh_Ag+_Asc-(1). A) – C) core shell Au-Ag NPs of the different thickness of the Ag layer.

In contrast, TEM images of the seed solution AuNP-Bh-5min-(I) in Figure 21 show aggregated symmetrical seeds with no direct link between them.

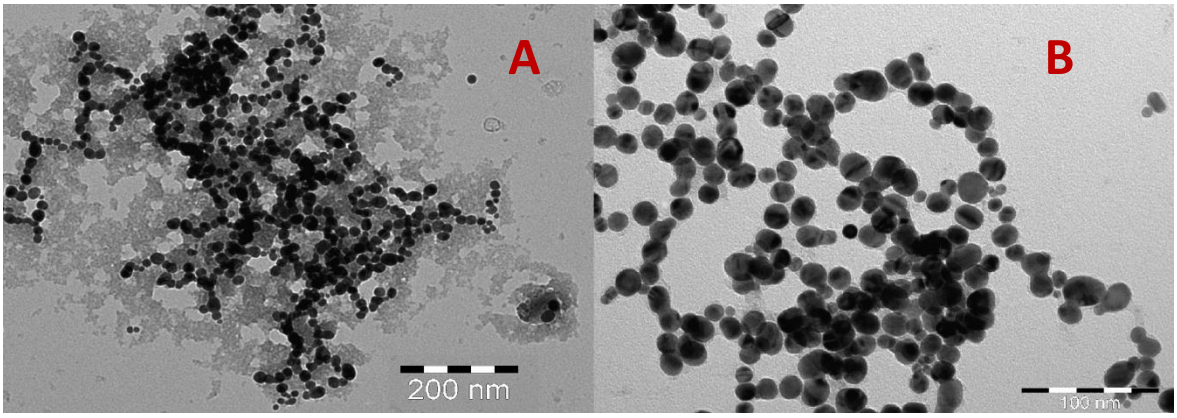

Figure 21 TEM images of the seed solution AuNP-Bh-5min-(I). A) aggregated seeds, B) a close-up view of the aggregate, showing there is no connection between the seeds (the scale bar is 100 nm)

In case of TEM images of the final colloidal system AuNPBh_Ag+_Asc-(I), synthesized from the seed solution AuNP-Bh-5min-(I), there are no complete core-shell Au-Ag NPs. The images in Figure 22 show random agglomerations of Au and Ag fragments, with Ag fragments in the outer eccentric layer. This difference (compared to Figure 20) may be due to the late stage of hydrolysis and simultaneous oxidation of sodium borohydride, which has a strong influence on the formation process of the seeds.

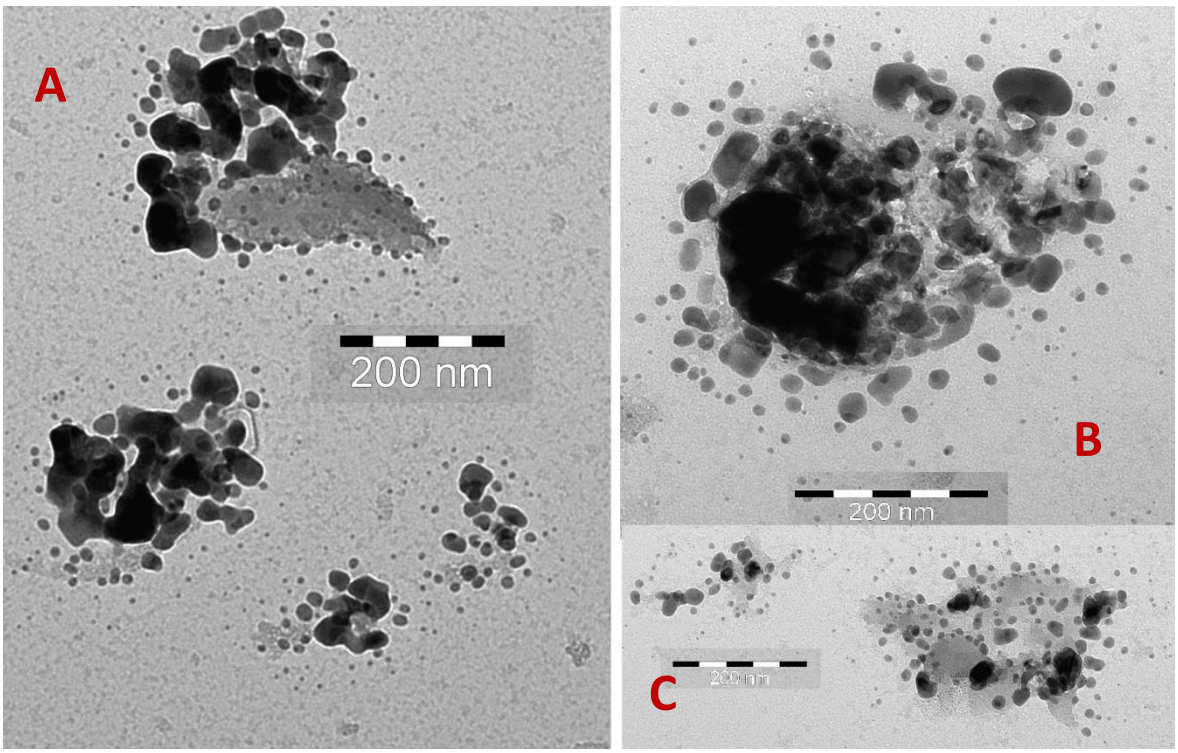

Figure 22 TEM images of the seed solution AuNPBh_Ag+_Asc-(1). A) – C) Agglomeration of Au and Ag fragments (Ag in the outer layer), the scale bar is 200 nm in all three images.

5.1.2.2 Usage of stable seeds

The final colloidal systems AuBhNP-7m_Ag+_Asc-(1) and AuBhNP-7m_Asc_Ag+-(1) (red and green lines, respectively, in Figure 23) were prepared from the seed solution AuBhNP-7m (blue line in Figure 23). The final colloidal system AuBhNP-7m_Ag+_Asc-(1) (red line) differs from the final colloidal system AuBhNP-7m_Asc_Ag+-(1) (green line) in the intensity of SPR absorption peaks at round 400 nm (Figure 23). The final colloidal system AuBhNP-7m_Asc_Ag+-(1) (green line, Figure 23), prepared by the reverse order of reactants addition in the seed-mediated-growth has the sharper absorption peak. It can be caused by a seemingly better formation of EDL.

Indeed, this is not the case in Ag-Ag NPs, more specifically in the final colloidal system AgBhNP-7m_Asc_Ag+ (Figure 15), where the reversed order of reactants addition in the synthesis ensued in an aggregation.

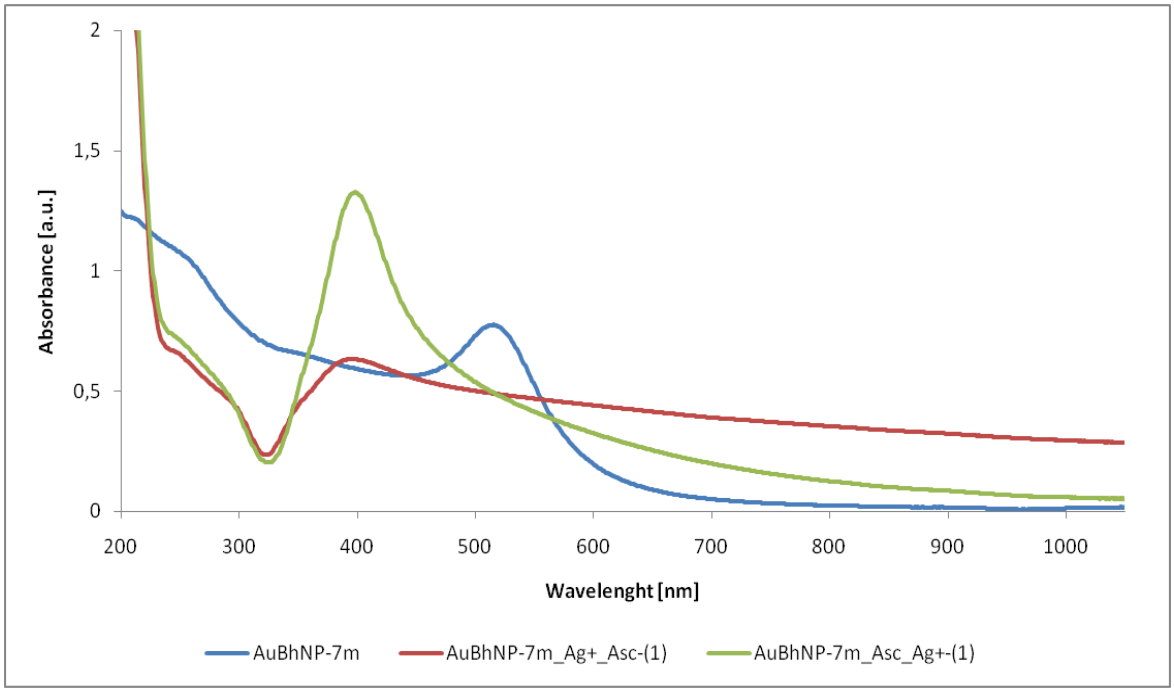

Figure 23 UV-Vis spectra of the seed solution AuBhNP-7m (blue line) and the final colloidal systems: AuBhNP-7m_Ag+_Asc-(1), AuBhNP-7m_Asc_Ag+-(1) (red line and green line, respectively).

TEM images of the final colloidal system AuBhNP-7m_Ag+_Asc-(1) are shown in Figure 24. In all images, the dark central mass represents the Au core (the seed), surrounded by the cloud of Ag particles, which may also serve as a connection among Au seeds. The Ag did not form a fully compact layer around the Au core (although the parts of a formed Ag layer can be seen on several edges of NPs). This could be induced by the fact that the Au seed solution used during the synthesis is stable, presumably discouraging the surface reactivity of the seeds. Therefore, the difference in the distance between the core and the shell layer can be attributed to the age of the seeds as the Ag shell is formed more closely around the freshly prepared Au seeds (Figure 20).

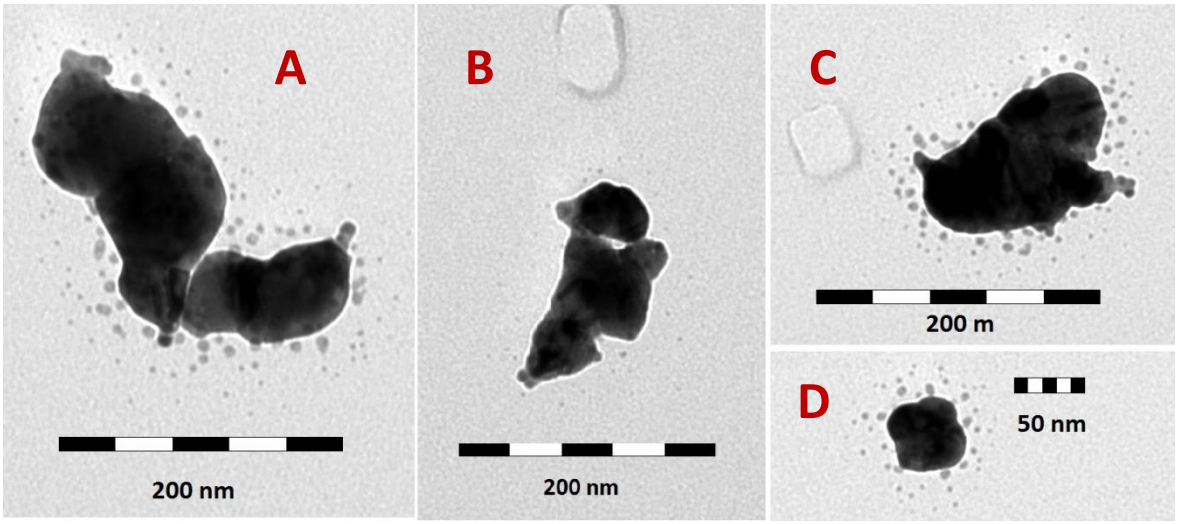

Figure 24 TEM images of the final colloidal system AuBhNP-7m_Ag+_Asc-(1). A)-D) NPs composed of the Au core (the dark central mass) and surrounding non-compact layer of Ag

TEM images of the final colloidal system AuBhNP-7m_Asc_Ag+-(1) in Figure 25 are similar to the TEM images in Figure 24, however, the Ag shell does not surround the Au core as closely. Figure 25A displays small aggregate of seeds, presumably connected by a small Ag layer on their surfaces, with a surrounding cloud of Ag particles (the surrounding amount is apparently smaller than in TEM images in Figure 24).

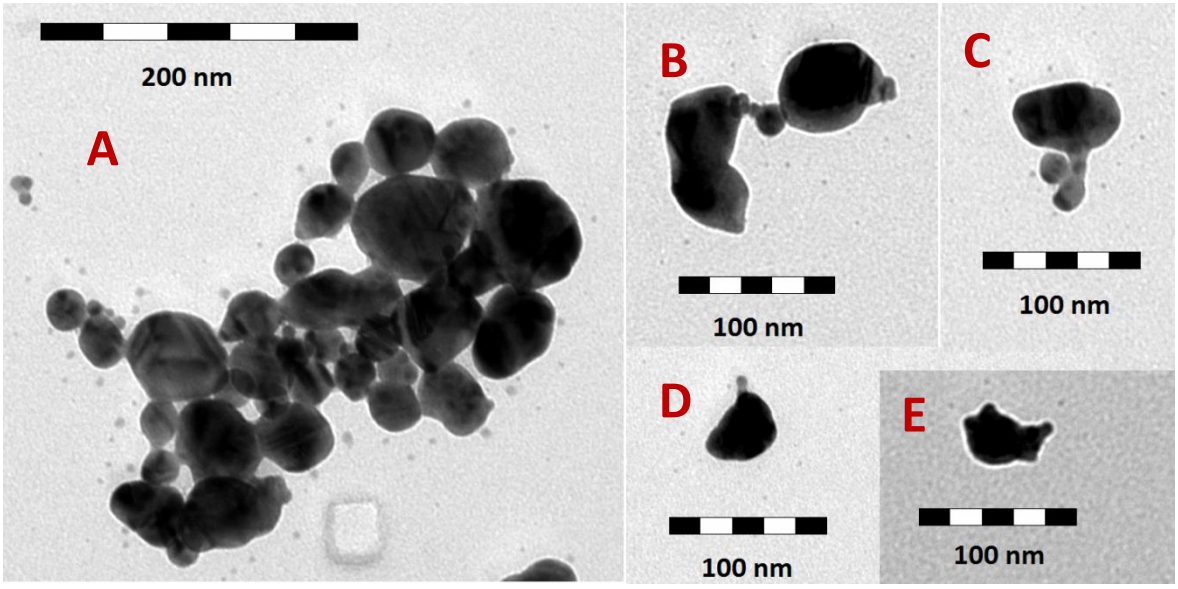

Figure 25 TEM images of the final colloidal system AuBhNP-7m_Asc_Ag+-(1). A) The aggregate of Au seeds connected and surrounded by Ag layer and NPs, B) – E) NPs composed of the Au core (the dark central mass) and surrounded by a small amount of Ag particles.

To further determine the reactivity and subsequent stability of the colloidal system AuBhNP_Ag+_Asc-(1), the measurement of the UV-Vis spectrum was repeated after one week and named AuBhNP_Ag+_Asc-(1)-1w as the final colloidal system was 1 week aged (Figure 26).

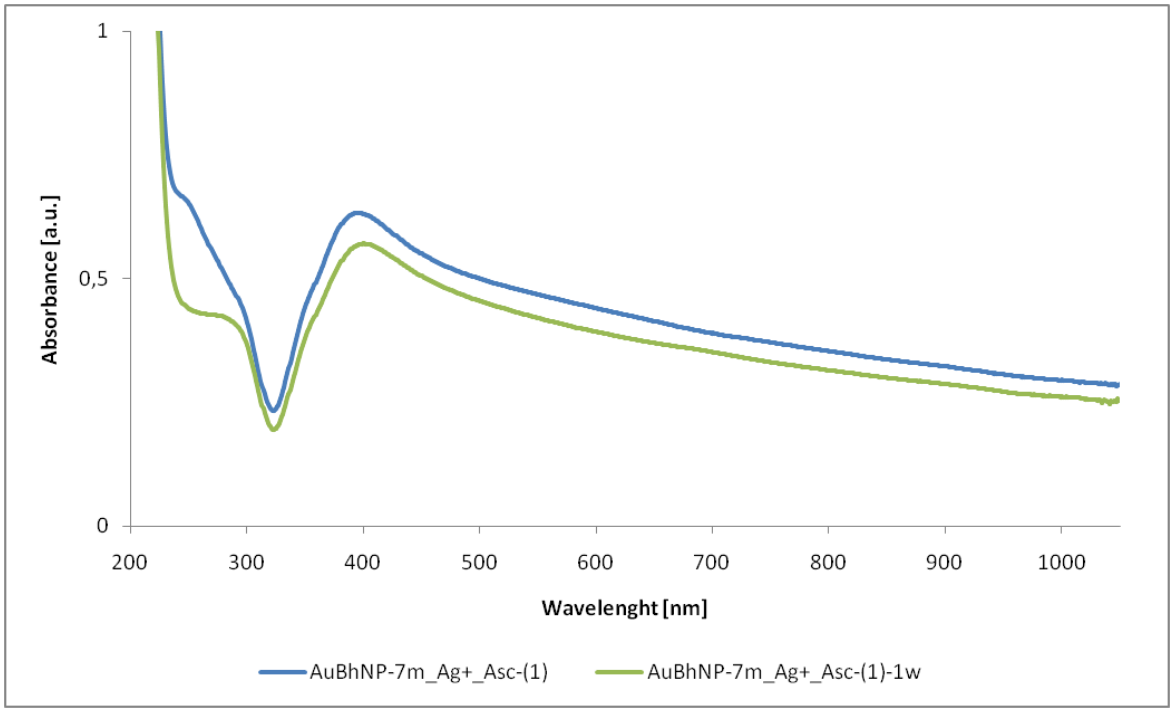

Figure 26 UV-Vis spectral comparison of the final colloidal system AuBhNP_Ag+_Asc-(1) (blue), and the repeated measurement of the same system after 1 week, AuBhNP _Ag+_Asc -(1)-1w (green).

The UV-Vis spectrum recorded after 1 week (green line in Figure 26) shows only a couple of slight changes: (i) bathochromic (red) shift of the absorption maximum and (ii) hypochromic shift above 500 nm. In order to evidence these changes more clearly, the UV-Vis spectra were normalised to their respective maximum of the SPR absorption peak (at around 400 nm) – Figure 27. The changes occurring in the final colloidal systems after a longer time period will be further discussed in the following chapters.

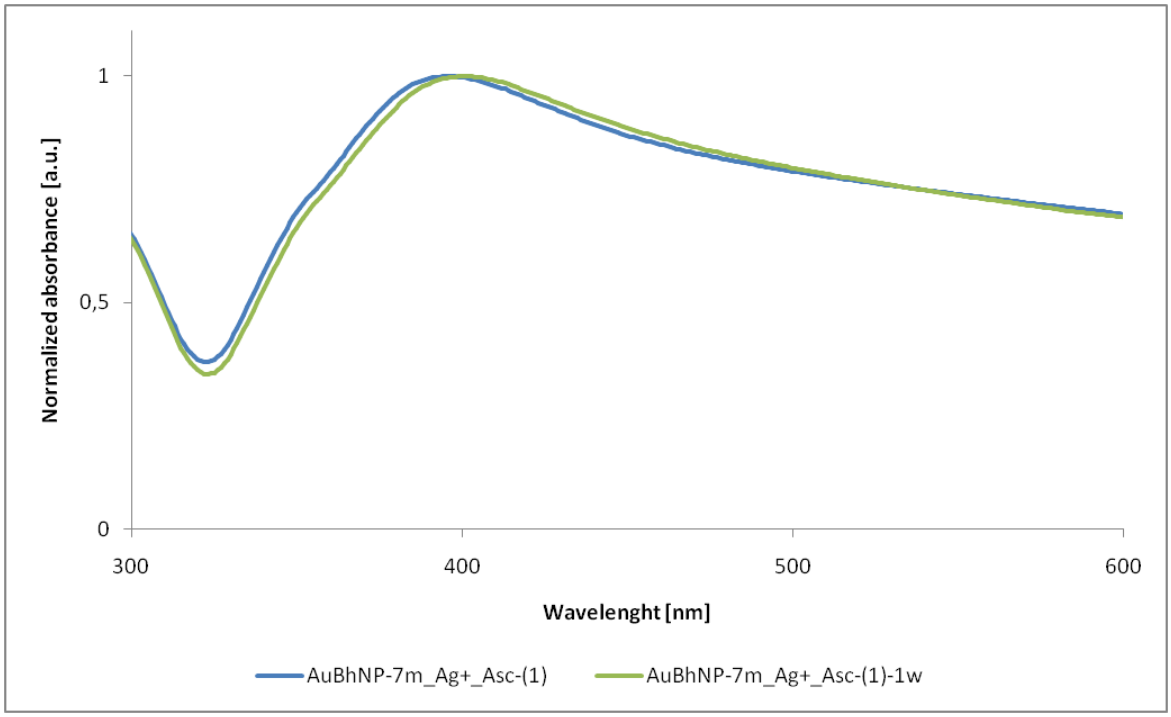

Figure 27 Normalized UV-Vis spectra of the colloidal system AuBhNP-7m_Ag+_Asc-(1) (blue) and AuBhNP-7m_Ag+_Asc-(1)-1w (green), normalized to the SPR maximum. Only a part of UV-Vis spectra is shown for the sake of a better visibility.

The UV-Vis measurement of the colloidal system AuBhNP-7m_Asc_Ag+-(1) was repeated after one week as well. The comparison of UV-Vis spectra in Figure 28 reveals that the absorption spectrum measured 1 week later (purple line) has a broader absorption peak and further aggregation occurred in the colloidal system.

This finding is confirmed after the normalization of UV-Vis spectra to their SPR maximum (as is shown in Figure 29).

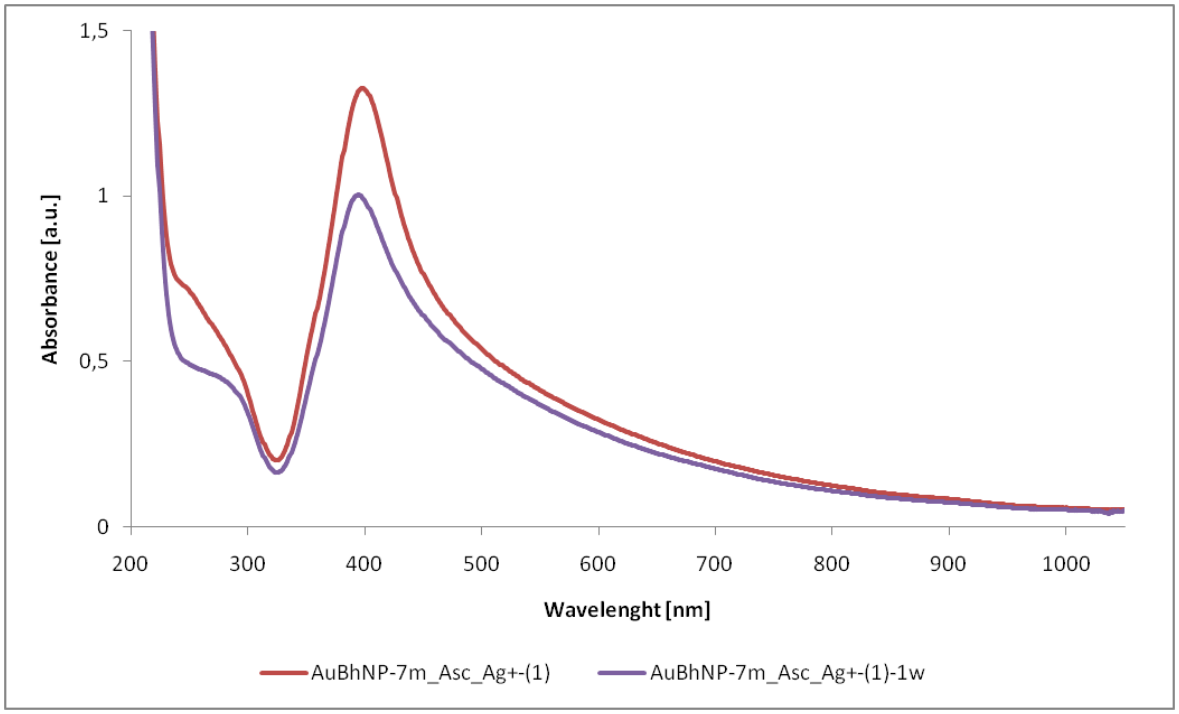

Figure 28 UV-Vis spectra of the colloidal system AuBhNP-7m_Asc_Ag+-(1) (red), and the repeated measurement after 1 week, AuBhNP-7m_Asc_Ag+-(1)-1w (purple).

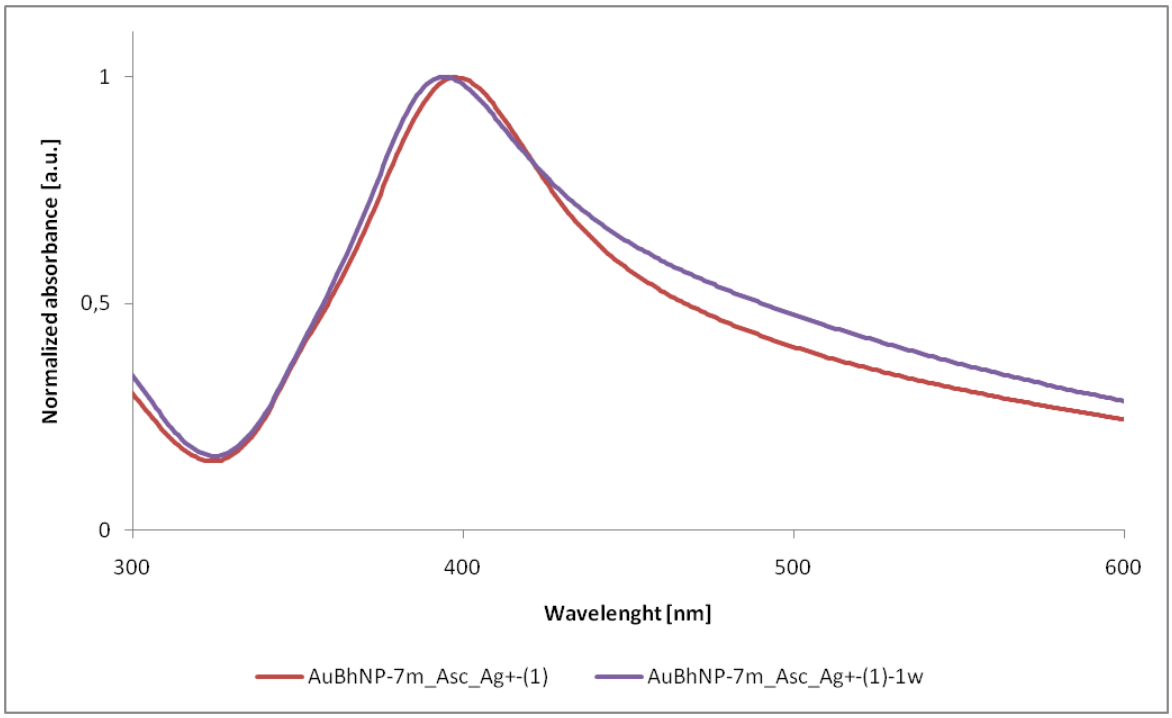

Figure 29 Normalized UV-Vis spectra of the colloidal system AuBhNP-7m_Asc_Ag+-(1) (red), and the repeated measurement after 1 week, AuBhNP-7m_Asc_Ag+-(1)-1w (purple). Normalization performed to SPR maximum. Only a part of UV-Vis spectra is shown for the sake of a better visibility.

5.1.2.3 Effect of citrate-reduced Au seeds on the final colloidal systems

The next approach to seed-mediated growth synthesis is to use the seed solution produced by employing sodium citrate (chapters 4.4.4 and 4.4.5). From the seed solution AuCtrNP-7m the final colloidal systems AuCtrNP-7m_Ag+_Asc-(1) and AuCtrNP-7m_Asc_Ag+-(1) were prepared. UV-Vis spectra of these three NP systems are shown in Figure 30.

From a great resemblance of UV-Vis absorption spectra in Figure 30, it can be deduced that both colloidal systems possess approximately the same reactivity. The similarity of absorption peaks at around 400 nm can be attributed to the presumably dense barrier of citrate molecules around the seeds, which subsequently takes longer time to be disrupted. Ergo, the approach of using the reverse order of the reactants in the final colloidal system synthesis does not provide any distinct difference in this case. This is in contrast to the seed solution and final colloidal systems containing borohydride as the first reducing agent (Figure 23). The intensity of absorbance of the final colloidal system AuCtrNP-7m_Ag+_Asc-(1) (red line in Figure 30) is more than double of the intensity of the final colloidal system AuBhNP-7m_Ag+_Asc-(1) (red line in Figure 23).

Furthermore, the absorption peaks of the ascorbic acid (at around 260 nm) are present in the spectra of the final colloidal systems from citrate seed solution AuCtrNP-7m (when using the borohydride seed solution AuBhNP-7 there are no such absorption peaks, see Figure 23) due to the stabilizing effect of sodium citrate disallowing the complete disintegration of double bond in ascorbic acid during the relatively short time interval of the synthesis.

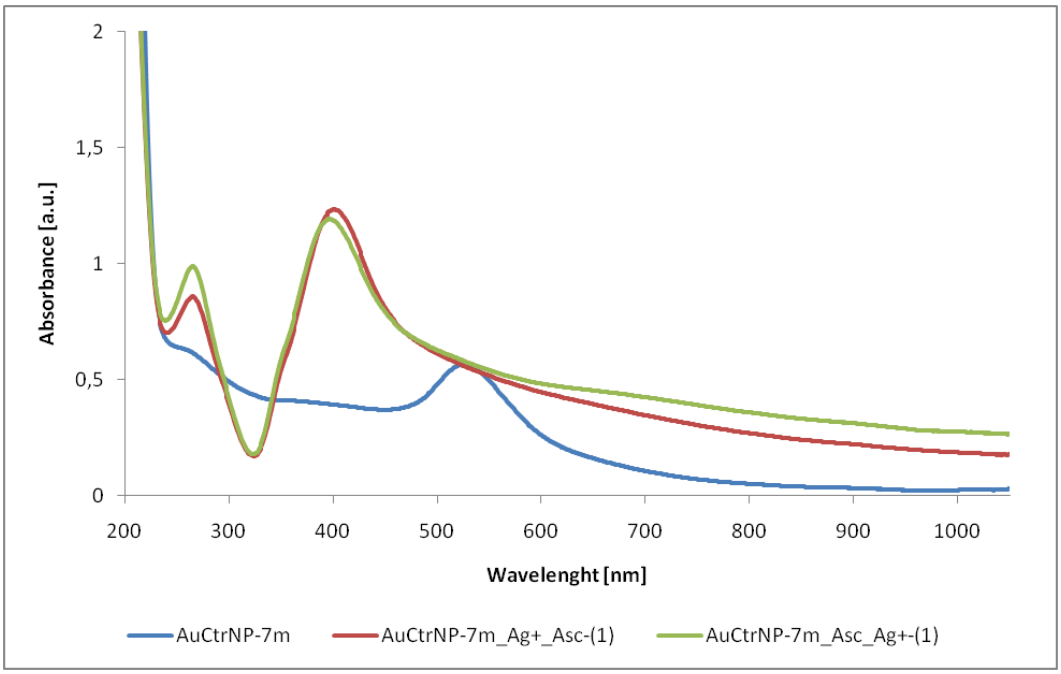

Figure 30 UV-Vis spectra of the seed solution AuCtrNP-7m (blue) and final colloidal systems AuCtrNP-7m_Ag+_Asc-(1) (red) and AuCtrNP-7m_Asc_Ag+-(1) (green).

TEM images of the final colloidal systems, AuCtrNP-7m_Ag+_Asc-(1) and AuCtrNP-7m_Asc_Ag+-(1), differ from each other regardless of the similarity between their UV-Vis spectra.

In the Figure 31B and 31C, the parts of Ag layer can be seen on the edges and sides of dark Au cores, while Figure 31A shows only nondescript agglomeration of particles.

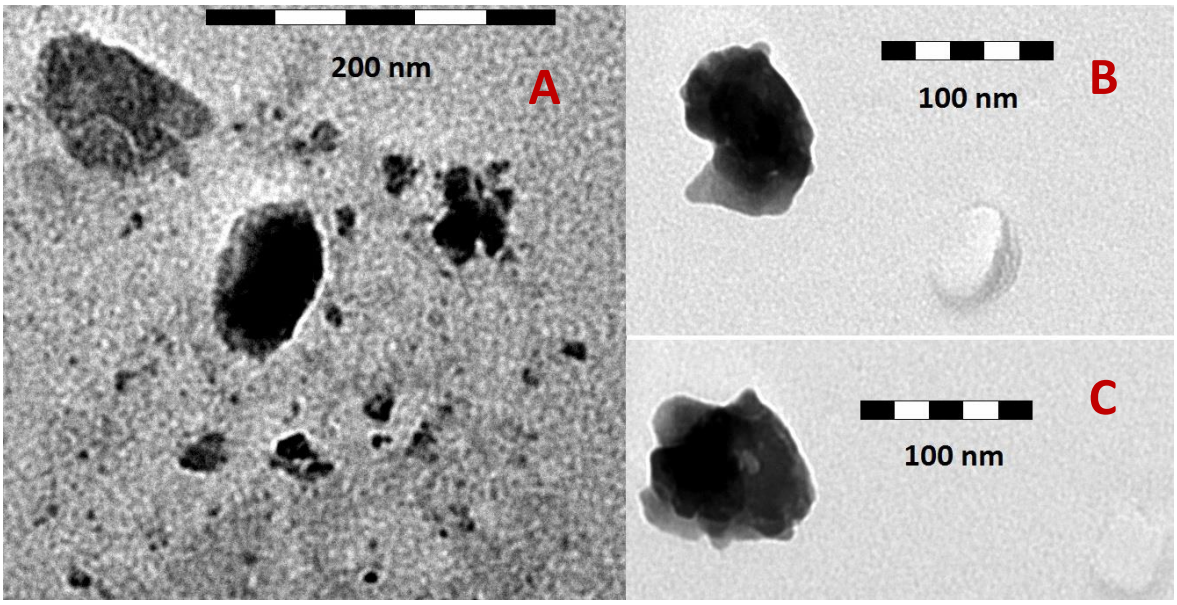

Figure 31 TEM images of the colloidal system AuCtrNP_Ag+_Asc-(1). A) agglomeration of particles, B) – C) NPs with parts of the Ag layer on the edges.

On the other hand, TEM images of the final colloidal system AuCtrNP-7m_Asc_Ag+-(1) show a completely formed Ag shell around the Au core (Figure 32B and 32C), even around the aggregated seeds (Figure 32A).

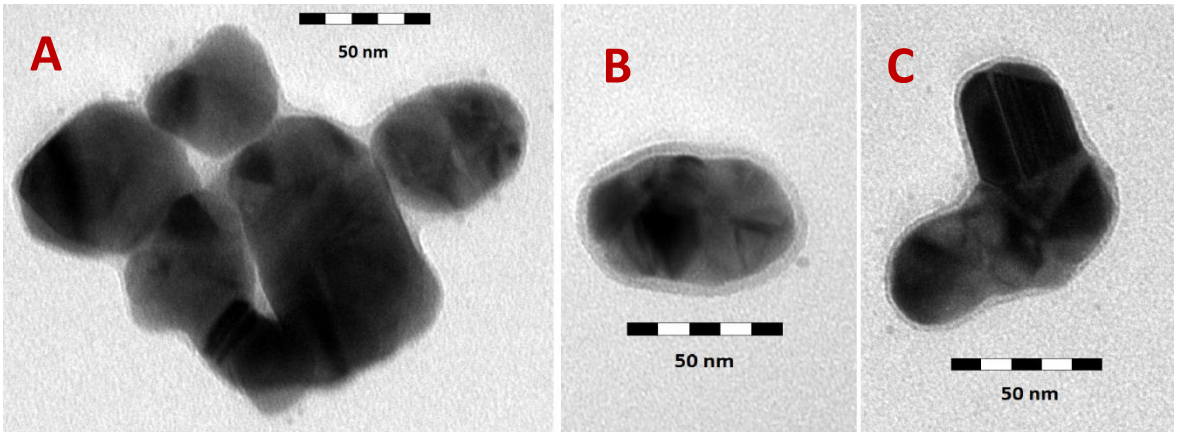

Figure 32 TEM images of the colloidal system AuCtrNP-7m_Asc_Ag+-(1). Core-shell Au-Ag NPs. Completely formed Ag shell around Au core: A) shell around the aggregated seeds, B) – C) shell around the single Au cores

In order to determine the reactivity and stability of the final colloidal systems AuCtrNP-7m_Ag+_Asc-(1) and AuCtrNP-7m_Asc_Ag+-(1), the measurement of UV-Vis spectra was repeated 1 week later, resulting thus in UV-Vis spectra AuCtrNP-7m_Ag+_Asc-(1)-1w and AuCtrNP-7m_Asc_Ag+-(1)-1w.

In Figure 33, AuCtrNP-7m_Ag+_Asc-(1)-1w (green line) reveals that the SPR absorption peak is broader and slightly red-shifted with respect to that of AuCtrNP-7m_Ag+_Asc-(1). This means that the final colloidal system AuCtrNP_Ag+_Asc-(1) still undergoes changes during the first week counted from the moment of its synthesis. Due to the slow reduction process caused by the presence of citrate residues at the NP surfaces of the seeds, the colloidal system has a lot of monomers of ascorbic acid (evidenced by the presence of the peak located at 260 nm – Figure 33, blue curve and/or Figure 30, red curve) and Ag+ ions, meaning that the reduction process is still running during the first week (counted from the moment of the final colloidal system synthesis).

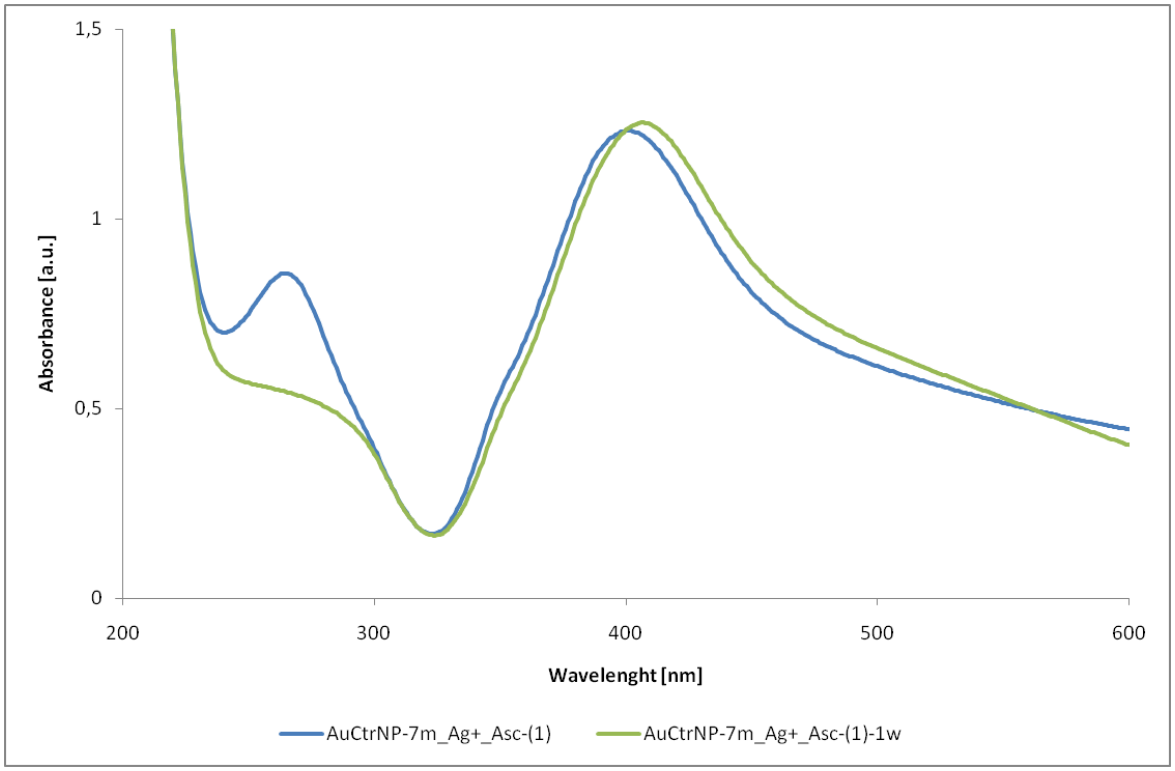

Figure 33 UV-Vis spectra of the final colloidal system AuCtrNP-7m_Ag+_Asc-(1) and the repeated measurement 1 week later, AuCtrNP-7m_Ag+_Asc-(1)-1w.

The same changes of the shape and position of the SPR absorption peak is even more pronounced in the final colloidal system AuCtrNP-7m_Asc _Ag+-(1) and its repeated measurement 1 week later, AuCtrNP-7m_Asc _Ag+-(1)-1w (Figure 34). The reason for such changes has been already discussed in the case of Figure 33.

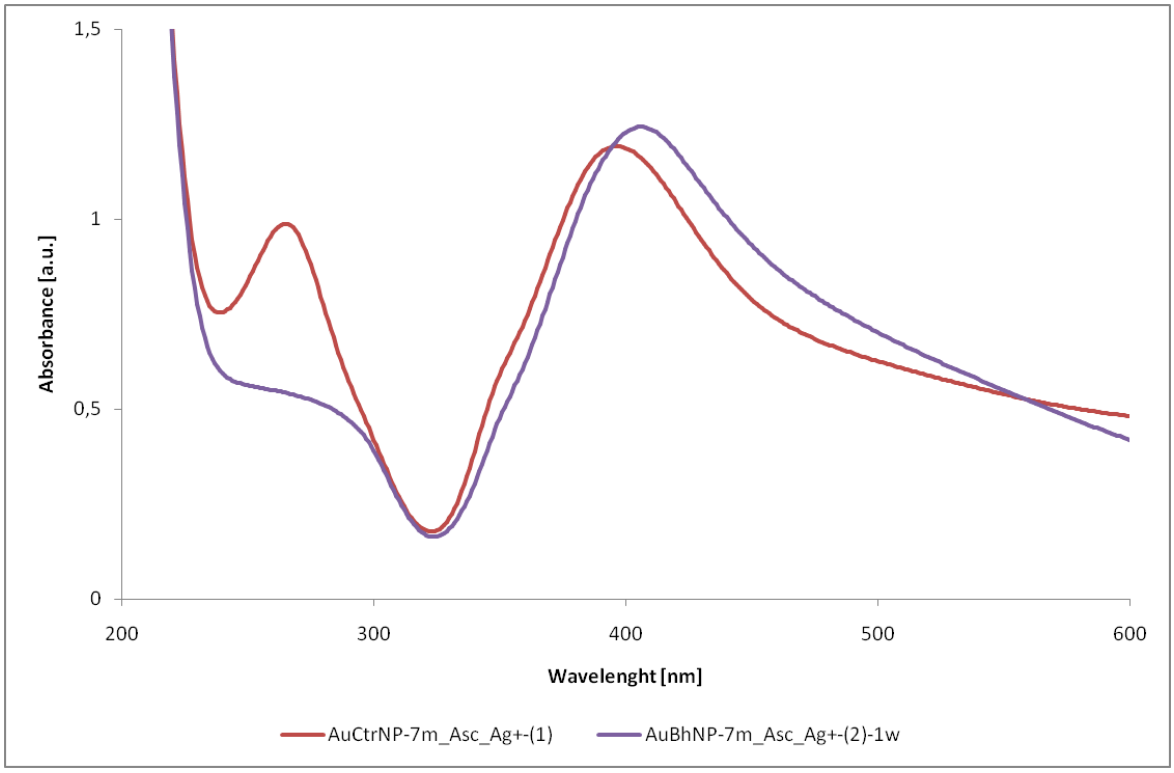

Figure 34 UV-Vis spectra of the final colloidal system AuCtrNP-7m_Asc _Ag+-(1) and the repeated measurement 1 week later, AuCtrNP-7m_Asc _Ag+-(1)-1w.

5.1.3 Additional notes concerning TEM images

In many TEM images of Au-Ag NPs colloidal systems, rectangular transparent formations were found. This is the case for almost all final colloidal Au-Ag systems (and after careful investigation, one such transparent rectangle was found in Ag-Ag colloidal system). The second stage of the synthesis of the final colloidal systems, i.e. the mutual interaction of the reactants in the presence of particular seeds might be a possible cause for such formations. To further verify this hypothesis, the second stage of the synthesis was replicated but this time without the addition of any seeds, i.e. 0.2 mM$AgNO_3$ aqueous solution and 250 μL of 10 mM ascorbic acid aqueous solution were mixed together and characterized by TEM (Figure 35Aand 35B).

In the TEM images are also present aggregates on the edges of the copper grid, most probably indicating an additional interaction between the colloidal sample and the grid possibly during the drying process. (Figure 35C).

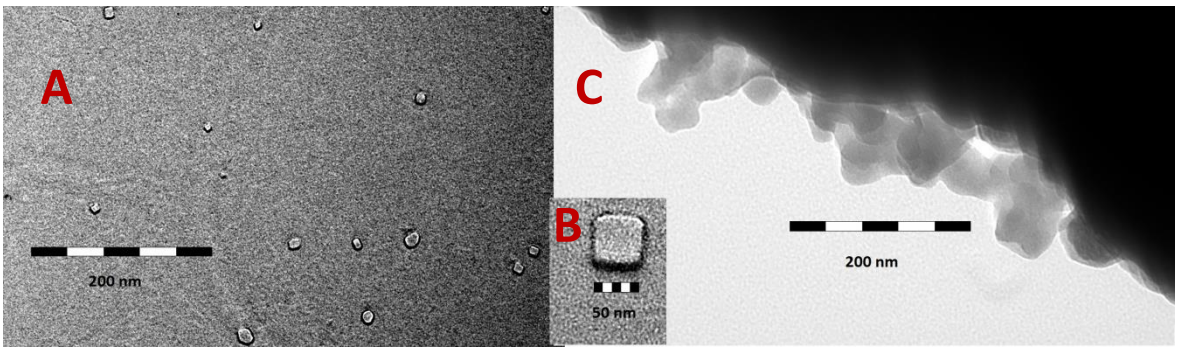

Figure 35 TEM images of aqueous solution containing ascorbic acid and $AgNO_3$ in the same ratio as during the seeded-growth process. A) rectangular transparent crystals/formations (scale bar is 200 nm), B) a close-up image (scale bar is 50 nm), C) aggregates on the edges of the TEM copper grid (scale bar is 200 nm).

5. 2 DLS and zeta-potential values

At the time of DLS measurement and the measurement of the zeta-potential values, the seed solutions and the final colloidal systems were 9 months aged. Visual assessment was conducted to determine the suitability of the seed solutions and final colloidal systems for the following characterization. If no visible micro-particles and aggregates were detected (by the naked eye), the measurement of UV-Vis spectrum followed by DLS measurement and the measurement of the zeta-potential values of particular seed solutions or final colloidal system were carried out.

5.2.1 DLS and zeta-potential of Ag-Ag NPs

The DLS measurement was performed with diluted samples (see chapter 4.5.3) to achieve the best result. Nevertheless, the seed solutions and final colloidal systems did not have required monodispersity. The observed borderline polydispersity might have led to distorting of measured data and ensuing results of the NP sizes. The resulting data will have multiple peaks of size distribution, due to size variety of NPs present in the sample. If the monodispersity is adequate, there will be one resulting type of the size measurement.

The acquired size distribution data (Table 5) shows the intensity of scattered light from particles of various sizes ("DLS Intensity") and two of its most common peaks ("Peak 1, Size", "Peak 2, Size" with standard deviation and approximation in percentages "%"). This intensity-based distribution can be converted to the number-based distribution (in Table 6, "DLS Number"), representing a number of particles that scatter the light with a varying amount of intensity. In general, the bigger particles scatter more light than the smaller ones, leading thus to a very common discrepancy between intensity and number based distributions.

Table 5 Size distribution data of the 9 months-aged Ag Seed solutions and Ag-Ag final colloidal systems showing the distribution based on intensity of scattered light from particles ("DLS Intensity"), and two of most common peaks for each distribution ("Peak 1, Size", "Peak 2, Size" with standard deviation and approximation of content in percentages "%").

No.	Name	DLS Intensity			
		Peak 1		Peak 2	
		Size [nm]	%	Size [nm]	%
1.	AgNP-Bh-5min-(2)-9m	16.6 ± 2.5	48.7	71.2 ± 25.5	41.9
2.	AgNP-Bh-5min-(II)-9m	341.1 ± 14.8	100,0	-	-
3.	AgNPBh_Ag+_Asc-(2)-9m	49.4 ± 5.4	94.8	7.3 ± 6.3	5.2
4.	AgNPBh_Ag+_Asc-(II)-9m	84.5 ± 0.7	89.4	19.5 ± 1.8	10.6
5.	AgBhNP-7m_Ctr -Ag+_Asc-9m	80.4 ± 4.4	84.0	17.2 ± 1.2	16.0
6.	AgBhNP-7m_Asc_Ag+-9m	102.0 ± 2.2	94.6	16.5 ± 14.4	5.4

Table 6 Size distribution data of the 9 months-aged Ag Seed solutions and Ag-Ag final colloidal systems showing the number-based distribution of scattered light from particles ("DLS Number"), and two of most common peaks for each distribution ("Peak 1, Size", "Peak 2, Size" with standard deviation and approximation of content in percentages "%").

No.	Name	DLS Number			
		Peak 1		Peak 2	
		Size [nm]	%	Size [nm]	%
1.	AgNP-Bh-5min-(2)-9m	14.6 ± 2.6	100,0	-	-
2.	AgNP-Bh-5min-(II)-9m	327.3 ± 73.8	100,0	-	-
3.	AgNPBh_Ag+_Asc-(2)-9m	10.7 ± 1.3	99.9	48.0 ± 7.7	0.1
4.	AgNPBh_Ag+_Asc-(II)-9m	17.6 ± 2.9	99.8	68.4 ± 14.7	0.2
5.	AgBhNP-7m_Ctr -Ag+_Asc-9m	13.8 ± 2.9	99.9	55.0 ± 14.3	0.1
6.	AgBhNP-7m_Asc_Ag+-9m	22.8 ± 3.5	99.4	82.2 ± 18.3	0.6

The intensity-based distribution of the final colloidal systems, namely: AgNPBh_Ag+_Asc-(II)-9m, AgBhNP-7m_Ctr-Ag+_Asc-9m, AgBhNP-7m_Asc_Ag+-9m, show that NPs of the size in the interval between 80 nm and 100 nm dominate. On the other hand, the number-based distribution in Table 5 reveals that the majority of NPs present in these samples is of the size in the interval between 10 nm and 20 nm, with sparingly present NPs of a larger size. As above mentioned, the disagreement between the results of intensity and number based distributions is due to the stronger intensity emission from larger NPs which, even in small content, can overlap the smaller NPs.

The only exception is the seed solution AgNP-Bh-5min-(II)-9m, which number-based distribution shows no additional peaks and intensity and number based distributions are mutually in accord (the sizes above 300 nm as the only size of NPs.

Comparing the NP size distribution derived from DLS measurements with that obtained from TEM imaging (Figure 11, 13, 15, 16, e.g. in Figure 11, the displayed NPs of the seed solution are of the size around 200 nm), there are quite huge differences which is due to a different approach of each method. The sample for TEM imaging is prepared by drying the drop of the sample on a TEM grid; subsequently, an unpredictable process takes place as for the uniform distribution of the particles. The drying process can distort the sample, among others with a possible interaction among a copper grid and the metal NPs. On the contrary, the DLS is measured directly in solution (i.e. NP dispersions), leaving the state and distribution of NPs through the sample undisturbed.

Zeta-potential values of the same colloidal samples are evaluated in Table 6. The results show that the Ag seed solution (AgNP-Bh-5min-(2)-9m) can be considered completely stable at the age of 9 months due to an efficient build-up of EDL surrounding NPs (indeed, its zeta potential value exceeds -30 mV. Zeta-potential values of the final colloidal systems with values around -30 mV imply suitable colloidal stability. There is thus the only exception among the otherwise stable final colloidal systems based on zeta potential values: AgNPBh_Ag+_Asc-(2)-9m system.

Table 7 Zeta-potential values (with standard deviations) of the 9 months-aged Ag seed solutions and Ag-Ag final colloidal systems.

No.	Name	Zeta-potential [mV]
1.	AgNP-Bh-5min-(2)-9m	-39.3 ± 3.2
2.	AgNP-Bh-5min-(II)-9m	-26.6 ± 4.2
3.	AgNPBh_Ag+_Asc-(2)-9m	-18.8 ± 2.0
4.	AgNPBh_Ag+_Asc-(II)-9m	-31.8 ± 0.8
5.	AgBhNP-7m_Ctr -Ag+_Asc-9m	-30.9 ± 0.9
6.	AgBhNP-7m_Asc_Ag+-9m	-33.2 ± 5.9

UV-Vis spectra of the 9 months aged seed solutions and final colloidal systems were recorded to determine further changes to the SPR absorption peak and related changes of the NPs properties.

In Figure 36, there are UV-Vis spectra of the final colloidal systems AgNPBh_Ag+_Asc-(2), AgNPBh_Ag+_Asc-(II) measured in the day of their preparation and after 9 months(AgNPBh_Ag+_Asc-(2)-9m, AgNPBh_Ag+_Asc-(II)-9m). Compared to UV-Vis spectra recorded shortly after the syntheses (red and blue lines, respectively), there is a red-shift in the UV-Vis spectra of aged systems and a decrease in the SPR intensity. The shape of SPR absorption peak (Figure 36) and the value of zeta-potential (in Table 6) indicate a better overall stability in the case of AgNPBh_Ag+_Asc-(II)-9m than AgNPBh_Ag+_Asc-(2)-9m. The disappearance of the slight shoulder at around 350 nm with a simultaneous decrease of absorption in the region above 450 nm in AgNPBh_Ag+_Asc-(2)-9m, AgNPBh_Ag+_Asc-(II)-9m (Figure 36, green and purple lines, respectively), compared to AgNPBh_Ag+_Asc-(2), AgNPBh_Ag+_Asc-(II) (Figure 36, blue and red lines, respectively), suggests the disappearance of nanorods.

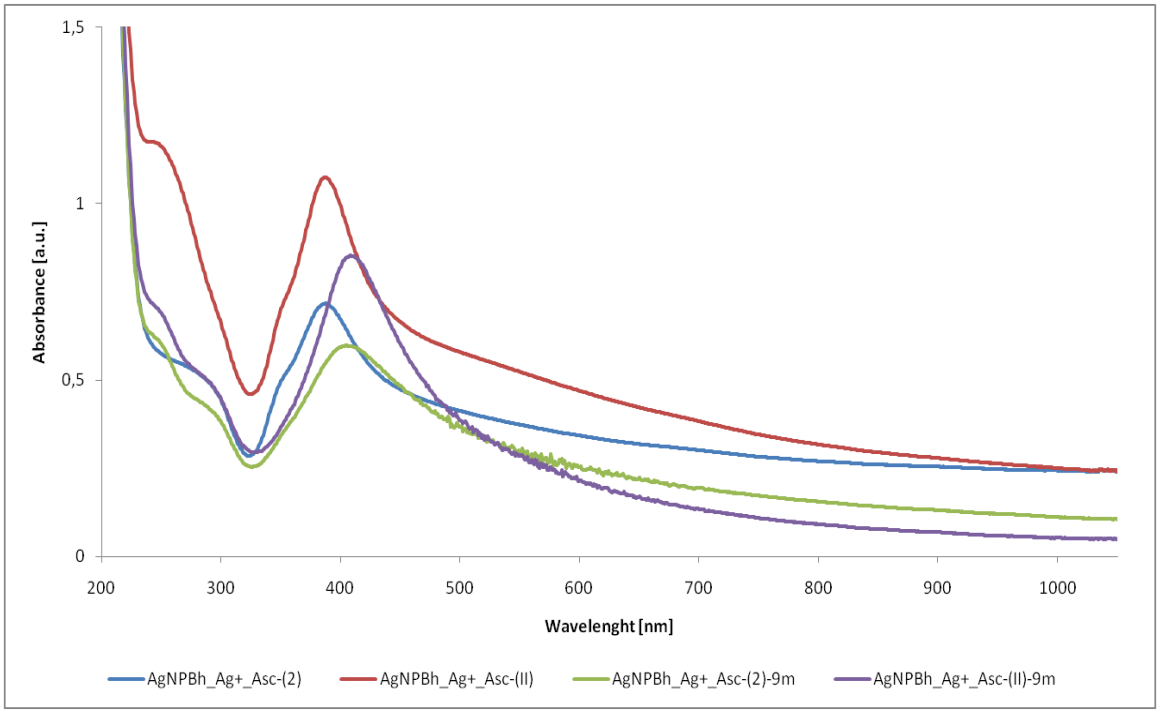

Figure 36 UV-Vis spectra of the freshly prepared final colloidal systems AgNPBh_Ag+_Asc-(2) (blue), AgNPBh_Ag+_Asc-(II) (red) and the same systems re-measured after 9 months (AgNPBh_Ag+_Asc-(2)-9m, AgNPBh_Ag+_Asc-(II)-9m – green and purple, respectively).

Figure 37 shows UV-Vis spectra of the final colloidal systems AgBhNP-7m_Ctr-Ag+_Asc, AgBhNP-7m_Asc_Ag+freshly prepared and after 9-months (AgBhNP-7m_Ctr-Ag+_Asc-9m, AgBhNP-7m_Asc_Ag+-9m). Both pairs of the final colloidal systems (recorded shortly after the syntheses and after 9 months) display an overall similarity of the shape of absorption peak with no noticeable red-shifts (compare blue and purple lines and/or red and green lines, Figure 37). In the case of AgBhNP-7m_Asc_Ag+-9m (green line) there is a decrease of the intensity and a disappearance of the slight shoulder at around 350 nm; it can be plausibly related to the disappearance of nanorods. On the contrary, the shoulder at 350 nm is still present in the case of AgBhNP-7m_Ctr-Ag+_Asc-9m (purple line, Figure 37) pointing towards the continuing presence of nanorods.

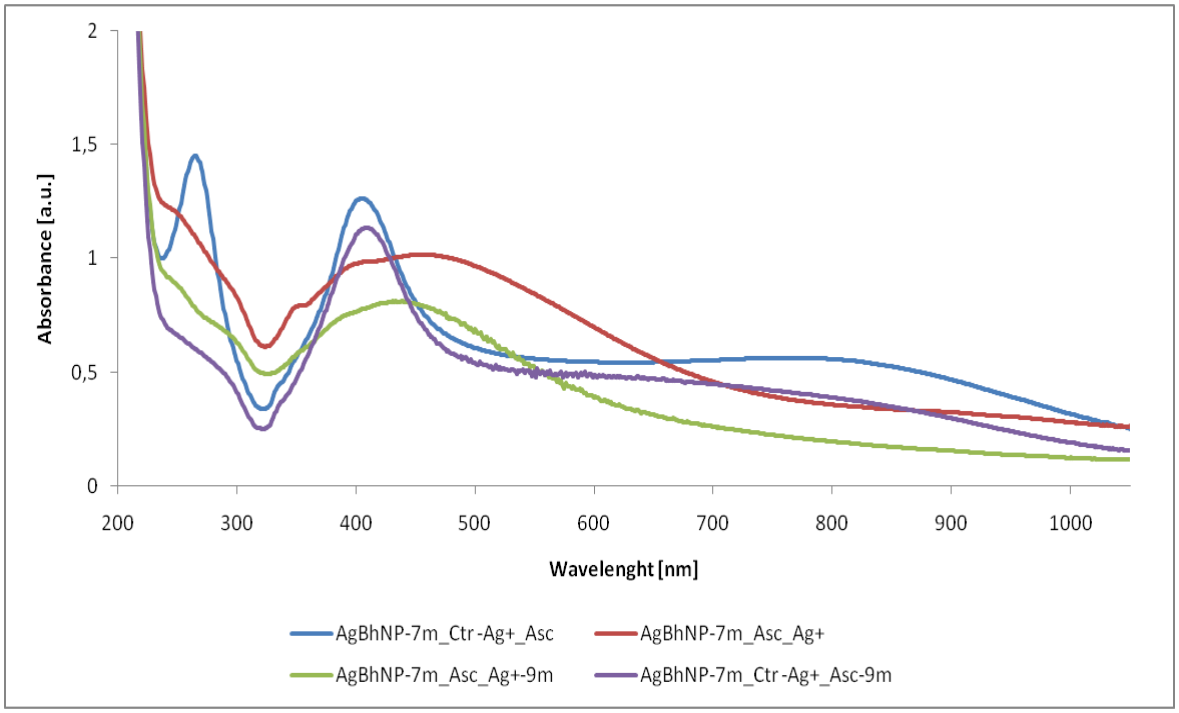

Figure 37 UV-Vis spectra of the freshly prepared final colloidal systems AgBhNP-7m_Ctr-Ag+_Asc (blue), AgBhNP-7m_Asc_Ag+(red)compared with the UV-Vis spectra of the same systems after 9 months (AgBhNP-7m_Ctr-Ag+_Asc-9m (purple), AgBhNP-7m_Asc_Ag+-9m (green).

5.2.2 DLS and zeta-potential of Au-Ag NPs

The DLS measurement of Au-Ag NPs was performed in the same way as the measurement of Ag-Ag NPs. The recurring issue with borderline polydispersity was not as common as in the case of Ag-Ag NPs, but it was still present in a few samples.

As in the previous chapter, the acquired size distribution data (Table 8) shows the intensity of scattered light from particles of various sizes ("DLS Intensity") and its two most common peaks ("Peak 1, Size", "Peak 2, Size" with standard deviation and approximation in percentages "%"). Converting the intensity-based distribution to the number-based distribution (in Table 9, "DLS Number"), yields a representation of a number of particles that scatter the light with a varying amount of intensity.

Table 8 Size distribution data of the 9 months-aged Au Seed solution and Au-Ag final colloidal systems showing the distribution based on intensity of scattered light from particles ("DLS Intensity"), and two most common peaks for each distribution ("Peak 1, Size", "Peak 2, Size" with standard deviation and approximation of content in percentages "%").

.

No.	Name	DLS Intensity			
		Peak 1		Peak 2	
		Size [nm]	%	Size [nm]	%
1.	AuBhNP-7m_Ag+_Asc-(1)-9m	105.8 ± 9.8	87.7	27.6 ± 4.6	12.3
2.	AuBhNP-7m_Asc_Ag+-(1)-9m	68.7 ± 4.3	80.1	17.8 ± 4.3	17.9
3.	AuCtrNP-7m_Ag+_Asc-(1)-9m	43.6 ± 3.0	83.4	6.0 ± 0.8	15.2
4.	AuCtrNP-7m_Asc_Ag+-(1)-9m	58.0 ± 4.7	85.0	10.8 ± 2.1	15.0
5.	AuBhNP-7m_Ag+_Asc-(2)-9m	77.4 ± 5.5	81.7	18.0 ± 1.0	17.7
6.	AuBhNP-7m_Asc_Ag+-(2)-9m	63.6 ± 1.4	68.5	13.1 ± 3.8	24.7
7.	AuCtrNP-7m_Ag+_Asc-(2)-9m	54.9 ± 2.0	85.4	8.1 ± 1.4	14.6
8.	AuCtrNP-7m_Asc_Ag+-(2)-9m	70.3 ± 0.4	79.3	12.9 ± 0.7	20.7
9.	AuNP-Bh-5min-(I)-9m	83.1 ± 6.0	64.0	19.9 ± 6.3	26.9
10.	AuNPBh_Ag+_Asc-(I)-9m	69.2 ± 6.2	74.5	10.5 ± 1.6	25.0

The intensity based distribution in Table 8 shows that the average size of NPs in the final colloidal Au-Ag systems varies, with the dominant size interval between 60 nm and 100 nm (with the exception of the final colloidal system AuCtrNP-7m_Ag+_Asc-(1)-9m, where the measured size is smaller than 60 nm; and the final colloidal system AuBhNP-7m_Ag+_Asc-(1)-9m with slightly larger NPs than 100 nm).

Nonetheless, the number-based distribution in Table 9 reveals that most of NPs in the final colloidal systems are around or under the size of 10 nm. The exception is again the final colloidal system AuBhNP-7m_Ag+_Asc-(1)-9m with the size of the NPs over 20 nm, with the presence of larger NPs of the size over 80 nm (which leads to screening of smaller NPs and the opposite result in Table 8).

The pairs of the final colloidal systems from the same seed solution show a great similarity of results in Table 9. Namely, AuCtrNP-7m_Ag+_Asc-(1)-9m and AuCtrNP-7m_Ag+_Asc-(2)-9m, along with AuCtrNP-7m_Asc_Ag+-(1)-9m and

AuCtrNP-7m_Asc_Ag+-(2)-9m (with no presence of the larger NPs in the later). The final colloidal systems from borohydride seed solutions differ from each other more, however, the final colloidal systems prepared with the reversed order of the synthesis AuBhNP-7m_Asc_Ag+-(1)-9m and AuBhNP-7m_Asc_Ag+-(2)-9m show a smaller size of NPs than the systems prepared in the normal order (AuBhNP-7m_Ag+_Asc-(1)-9m and AuBhNP-7m_Ag+_Asc-(2)-9m). The opposite is true for the final colloidal systems from the citrate seed solution, where the reversed order of the steps in the synthesis results in slightly larger NPs.

The only seed solution AuNP-Bh-5min-(I)-9m in Tables 8 and 9 display the presence of small, presumably non-aggregated Au seeds. In contrast to that Ag seeds prepared with the same process AgNP-Bh-5min-(II)-9m aggregated into larger sizes (Table 5 and 6).

The final colloidal system AuNPBh_Ag+_Asc-(I)-9m from the freshly prepared seed solution shows the presence of Au-Ag NPs of only slightly larger size than in the seed solution. The TEM images in Figure 22 of the same system do not show any completely formed core-shell NPs, instead, only agglomerations with more than 200 nm in diameter are observed. The course of time may have altered the state of the colloidal system and, simultaneously, the same issues of TEM imaging as discussed in previous chapter apply.

Table 9 Size distribution data of the 9 months-aged Au Seed solution and Au-Ag final colloidal systems showing the number-based distribution of scattered light from particles ("DLS Number"), and two most common peaks for each distribution ("Peak 1, Size", "Peak 2, Size" with standard deviation and approximation of content in percentages "%").

No.	Name	DLS Number			
		Peak 1		Peak 2	
		Size [nm]	%	Size [nm]	%
1.	AuBhNP-7m_Ag+_Asc-(1)-9m	22.3 ± 4.0	99.5	81.6 ± 18.4	0.5
2.	AuBhNP-7m_Asc_Ag+-(1)-9m	10.1 ± 2.1	99.9	49.5 ± 11.7	0.1
3.	AuCtrNP-7m_Ag+_Asc-(1)-9m	5.3 ± 0.9	100.0	-	-
4.	AuCtrNP-7m_Asc_Ag+-(1)-9m	10.1 ± 1.6	99.9	47.1 ± 9.3	0.1
5.	AuBhNP-7m_Ag+_Asc-(2)-9m	15.6 ± 2.7	99.8	56.3 ± 13.9	0.2
6.	AuBhNP-7m_Asc_Ag+-(2)-9m	7.6 ± 1.4	100.0	-	-
7.	AuCtrNP-7m_Ag+_Asc-(2)-9m	6.9 ± 1.3	100.0	-	-
8.	AuCtrNP-7m_Asc_Ag+-(2)-9m	10.1 ± 2.2	100.0	-	-
9.	AuNP-Bh-5min-(I)-9m	6.3 ± 1.6	100.0	-	-
10.	AuNPBh_Ag+_Asc-(I)-9m	8.8 ± 1.7	100.0	-	-

Zeta-potential values of the final Au-Ag NPs colloidal systems and Au seed solution are evaluated in Table 10. The final colloidal systems prepared from the aged seed solutions display varying degrees of the zeta-potential values and resulting stability.

As was the case with the Ag seed solutions, the seed solution AuNP-Bh-5min-(I)-9m can be considered completely stable at the age of 9 months.

The zeta-potential value of the final colloidal system AuNPBh_Ag+_Asc-(I)-9m comes closest to the value of -30 mV (Table 10), implying a suitable colloidal stability, which was further verified by UV-Vis measurements (Figure 38).

Table 10 Zeta-potential values (with standard deviations) of the 9 months-aged Au seed solution and Au-Ag final colloidal systems.

No.	Name	Zeta-potential [mV]
1.	AuBhNP-7m_Ag+_Asc-(1)-9m	-13.5 ± 2.9
2.	AuBhNP-7m_Asc_Ag+-(1)-9m	-9.6 ± 0.7
3.	AuCtrNP-7m_Ag+_Asc-(1)-9m	-9.2 ± 0.7
4.	AuCtrNP-7m_Asc_Ag+-(1)-9m	-12.8 ± 0.9
5.	AuBhNP-7m_Ag+_Asc-(2)-9m	-16.2 ± 1.3
6.	AuBhNP-7m_Asc_Ag+-(2)-9m	-23.4 ± 1.7
7.	AuCtrNP-7m_Ag+_Asc-(2)-9m	-11.7 ± 1.6
8.	AuCtrNP-7m_Asc_Ag+-(2)-9m	-10.9 ± 1.2
9.	AuNP-Bh-5min-(I)-9m	-36.2 ± 6.0
10.	AuNPBh_Ag+_Asc-(I)-9m	-27.5 ± 2.9

In Figure 38, there are UV-Vis spectra of the final colloidal system AuNPBh_Ag+_Asc-(I) (blue line), measured in the day of its preparation and after 9 months (AuNPBh_Ag+_Asc-(I)-9m, red line). The UV-Vis spectra recorded after 9 months do not show any bathochromic shift, only the slight broadening of the SPR peak and a significant decrease of intensity.

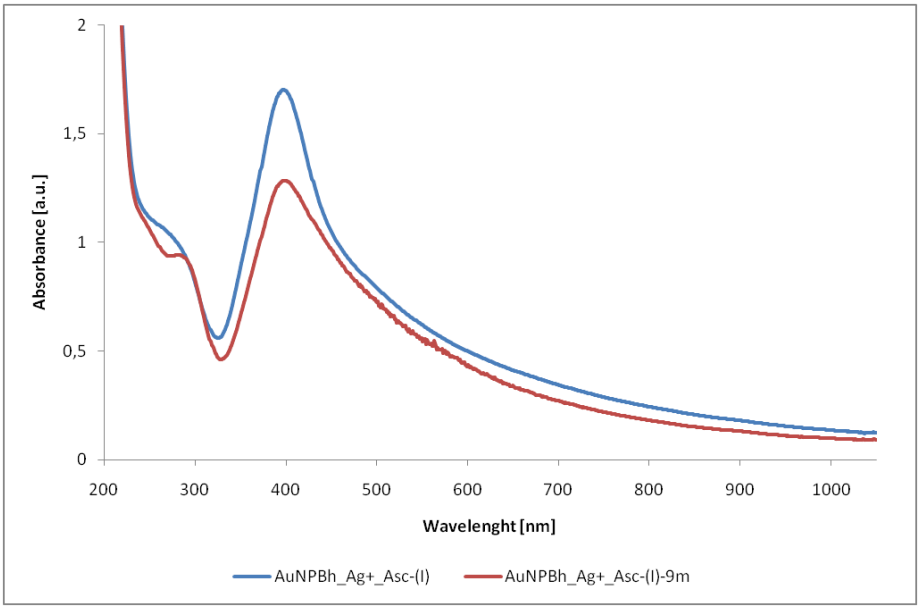

Figure 38 UV-Vis spectra of the freshly prepared final colloidal system AuNPBh_Ag+_Asc-(I) (blue), and the same system re-measured after 9 months AuNPBh_Ag+_Asc-(I)-9m (red).

5. 3 SERS

Several of the final colloidal systems were selected for the SERS measurement. The main criterion for the selection was the stability of a particular system. Each of the selected systems represents a different type of the final colloid: (i) Ag-Ag NPs with freshly prepared seeds used in the second step of the synthesis, (ii) Ag-Ag NPs with the addition of citrate as a surface modifier of the seeds, and (iii) Au-Ag NPs with freshly prepared seeds used in the second step of the synthesis.

The selected systems were then tried to enhance Raman signal of the model protein (BSA). Since BSA reveals a negative overall charge in aqueous solution and the seed-mediated grown NPs are also negatively charged (negative zeta potential values), it is necessary to flip the charge of NPs closer to zero and/or into positive values. This should result in NPs aggregation which can be observed by UV-Vis absorption spectroscopy. Therefore, UV-Vis spectra were measured prior to the SERS measurements.

There are two approaches to NPs aggregation known from the literature, either using chlorides (HCl and/or NaCl) [72, 73] or with L-aspartic acid (D); the latter being developed by our group a few years ago.

UV-Vis and SERS spectra were measured after adding aspartic acid or sodium chloride to the diluted colloidal system to examine bathochromic shift of aggregated NPs and potential SERS signal, respectively. Subsequently, BSA was introduced into the systems and UV-Vis and SERS spectra were recorded again.

5.3.1 SERS of BSA using AgNPBh_Ag+_Asc-(II)-9m

Figure 39 shows the comparison of two approaches to the aggregation of the same colloidal system (AgNPBh_Ag+_Asc-(II)-9m): (i) the aggregation with aspartic acid AgNPBh_Ag+_Asc-(II)-9m_D (green line), with subsequent addition of BSA, AgNPBh_Ag+_Asc-(II)-9m_D_BSA (blue line), and (ii) the aggregation with sodium chloride AgNPBh_Ag+_Asc-(II)-9m_NaCl (red line), with subsequent addition of BSA, AgNPBh_Ag+_Asc-(II)-9m_NaCl_BSA (purple line).

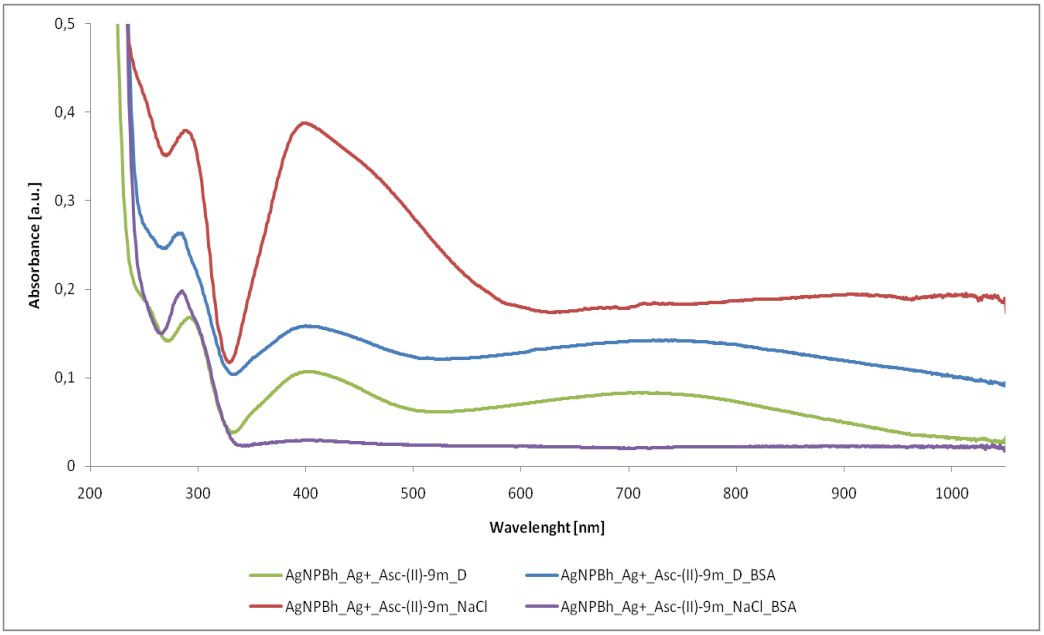

Figure 39 UV-Vis spectra of the 9 months-aged final colloidal system after the addition of aspartic acid AgNPBh_Ag+_Asc-(II)-9m_D (green), with subsequent addition of BSA, AgNPBh_Ag+_Asc-(I)-9m_D_BSA (blue); the same final colloidal system after the addition of sodium chloride AgNPBh_Ag+_Asc-(II)-9m_NaCl (red), with subsequent addition of BSA, AgNPBh_Ag+_Asc-(II)-9m_NaCl_BSA (purple)

The aggregation with sodium chloride (red line, Figure 39) yields noticeably different results with a broadened right side of the still visible SPR peak, compared to the aggregation with aspartic acid (green line, Figure 39) which manifested itself by the appearance of a secondary maximum located at around 710 nm (note: this secondary maximum was not present in the spectrum of AgNPBh_Ag+_Asc-(II)-9m– purple curve in Figure 36).

The addition of BSA to the system pre-aggregated with NaCl (purple line, Figure 39) almost completely reduces any absorbance of the sample beyond the point of 340 nm. Most probably, the system collapsed after the addition of BSA (purple line, Figure 39). On the contrary, all bands retained and only slightly broadened in AgNPBh_Ag+_Asc-(II)-9m_D_BSA in comparison to AgNPBh_Ag+_Asc-(II)-9m_D; the overall background increased and the UV band blue-shifted. It can be directly related to the influence of BSA presence.

Following the measurement of the UV-Vis spectra, SERS measurement was performed with the excitation laser lines of 532 nm and 785 nm.

For the final colloidal system AgNPBh_Ag+_Asc-(II)-9m (without any aggregation), there was no enhancement of Raman scattering of BSA detected as assumed (not shown here). For the measured SERS spectra of this final colloidal system aggregated with both approaches (the excitation laser line of 532 nm) see Appendix 1.While in the system aggregated with NaCl only the Raman signal of water is observed (Appendix 1, black and magenta curves); the system aggregated via aspartic acid (Appendix 1, blue and cyan curves) manifested itself by spectral features of (i) organic acid molecules attached

through carboxylic groups to the surface of AgNPs (e.g. the peak located at 235 nm) and (ii) graphitic carbon characteristic by two intensive peaks situated at around 1350 and 1590 cm^{-1} (stemming most probably from a huge local electromagnetic field leading to organic molecules decomposition). Since there is no difference in the spectrum with and without BSA addition, we conclude that the observed spectral pattern is coming from aspartic acid molecules only. The same result (only the signal of aspartic acid) was obtained by using 785 nm excitation laser line (spectra not shown here).

5.3.2 SERS of BSA using AgBhNP-7m_Ctr-Ag+_Asc-(I)-9m

In Figure 40, there are UV-Vis spectra of the 9 months-aged final colloidal systemAgBhNP-7m_Ctr-Ag+_Asc-(I)-9m (blue line), of the same colloidal system after the addition of aspartic acid AgBhNP-7m_Ctr-Ag+_Asc-(I)-9m_D (red line), and after subsequent addition of BSA, AgBhNP-7m_Ctr-Ag+_Asc-(I)-9m_D_BSA (green line).

Compared to the UV-Vis spectra of the previous Ag-Ag final colloidal system (Figure 39), the addition of aspartic acid to the diluted colloidal system did not change the SPR peak and resulted in a slight widening of the right part of the absorption spectra (red line, Figure 40). The subsequent addition of BSA yielded a fully aggregated system (green line, Figure 40) with a slight absorption enlarged over the whole visible and near infra-red region.

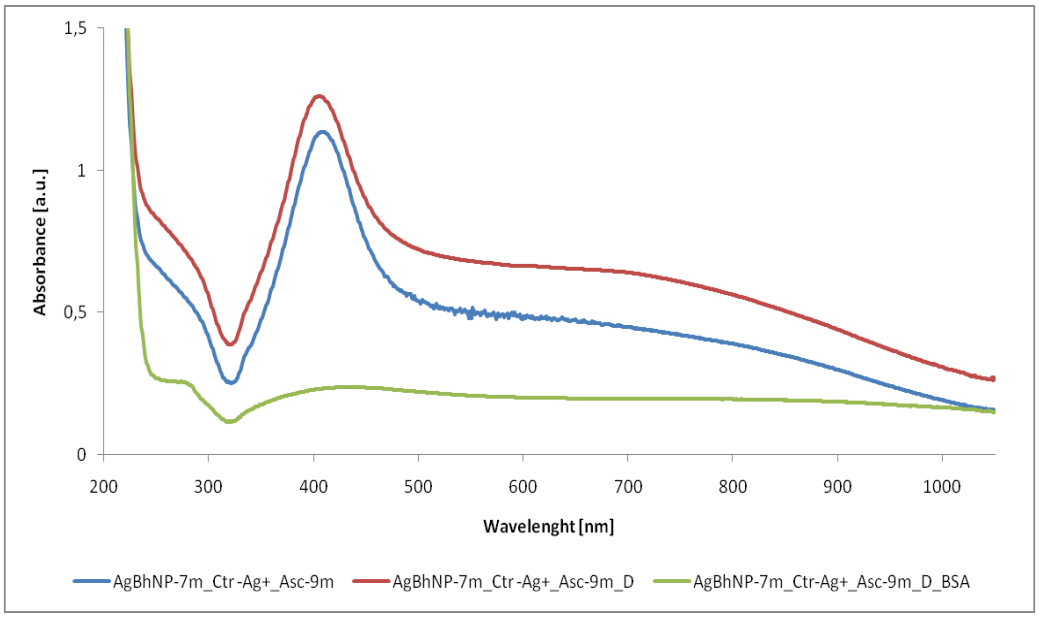

Figure 40 UV-Vis spectra of the 9 months-aged final colloidal system AgBhNP-7m_Ctr-Ag+_Asc-(I)-9m (blue), after the addition of aspartic acid AgBhNP-7m_Ctr-Ag+_Asc-(I)-9m_D (red), and subsequent addition of BSA, AgBhNP-7m_Ctr-Ag+_Asc-(I)-9m_D_BSA (green)

SERS spectra of the final colloidal Ag-Ag system after the addition of aspartic acid AgBhNP-7m_Ctr-Ag+_Asc-(I)-9m_D (red line), and after the subsequent addition of BSA,

AgBhNP-7m_Ctr-Ag+_Asc-(I)-9m_D_BSA (green line) with the excitation line 532 nm are shown in Figure 41.

The SERS spectra were normalized to the band of the carboxylate group positioned at 1395 cm^{-1}. This symmetric stretching vibration of RCOO- typically signifies that the carboxylate of amino acid is adsorbed onto the surface of Ag NPs (Figure 41). [74]

Other bands detected are the ones for amide III (at 1280 cm^{-1}) and amide I (at 1552 cm^{-1}) which are characteristic for the Raman spectrum of the protein [75]. The vibrations of aromatic compounds provide generally more intensive Raman signal than the aliphatic ones, therefore, the signal of several aromatic acid residues present in BSA structure (e.g. tyrosine Y, tryptophan W) is detected (Figure 41, green curve). It can be thus concluded that not only the Raman signal of aspartic acid, but also the signal of BSA is observed due to AgBhNP-7m-Ctr-Ag+_Asc-(I)-9m using 532 nm excitation laser line.

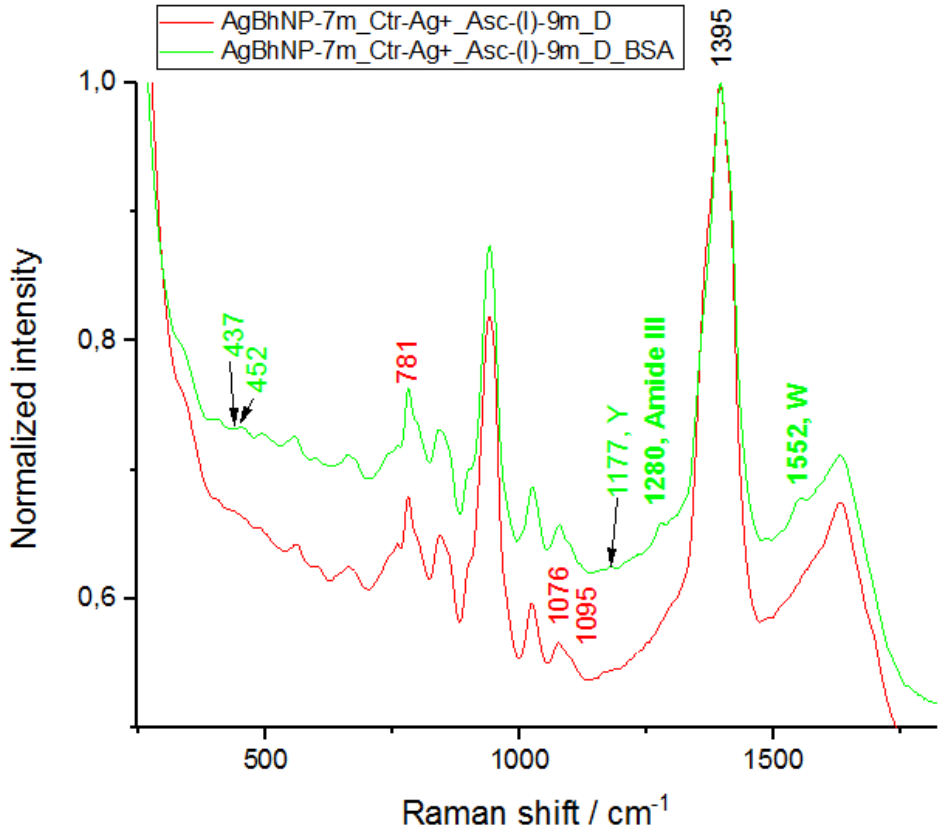

Figure 41 Normalized SERS spectra (excitation laser line of 532 nm) of AgBhNP-7m_Ctr-Ag+_Asc-(I)-9m_D (red), and AgBhNP-7m_Ctr-Ag+_Asc-(I)-9m_D_BSA (green). Normalization is performed with respect to the symmetric stretching of carboxylate molecules (1395 cm^{-1}) being adsorbed on AgNP surface.

Although the aggregation occurred, the decrease of the intensity beyond 700 nm, and mostly flat shape of the absorption spectrum after the addition of BSA (green line, Figure 40) points to the fact that the measurement using the excitation laser line of 785 nm will not yield any interesting result. This was confirmed; the SERS spectrum of AgBhNP-7m_Ctr-Ag+_Asc-(I)-9m_D_BSA copied (with a slightly higher intensity) the

SERS spectrum of AgBhNP-7m_Ctr-Ag+_Asc-(I)-9m_D (not shown here). Ergo, only aspartic acid was detected with the excitation line of 785 nm.

The discrepancy between the SERS results obtained with 532 vs. 785 nm excitations can be explained by the fact that different experimental setups are exploited in the two apparatuses: the signal is collected from almost the whole cuvette in the experiment performed by using 532 nm excitation laser line; while only the upper part of the whole high-volume solution (1,35 mL) is measured when 785 nm excitation exploited. In the latter case, the large aggregates which settle down at the bottom of the cuvette are thus not measured by SERS.

5.3.3 SERS of BSA using AuNPBh_Ag+_Asc-(I)-9m

In Figure 42, there are UV-Vis spectra of the 9 months-aged final colloidal system AuNPBh_Ag+_Asc-(I)-9m (blue line), of the same colloidal system after the addition of aspartic acid AuNPBh_Ag+_Asc-(I)-9m_D (red line), and after the subsequent addition of BSA, AuNPBh_Ag+_Asc-(I)-9m_D_BSA (green line).

The UV-Vis spectrum of AuNPBh_Ag+_Asc-(I)-9m_D (red line) demonstrates the start of NPs aggregation (demonstrated by broadening and slight blue-shifting of the SPR peak), and the UV-Vis spectrum of AuNPBh_Ag+_Asc-(I)-9m_D_BSA (green line)reveals a possible collapse of the system after the addition of BSA (similarly as observed in Figure 40).

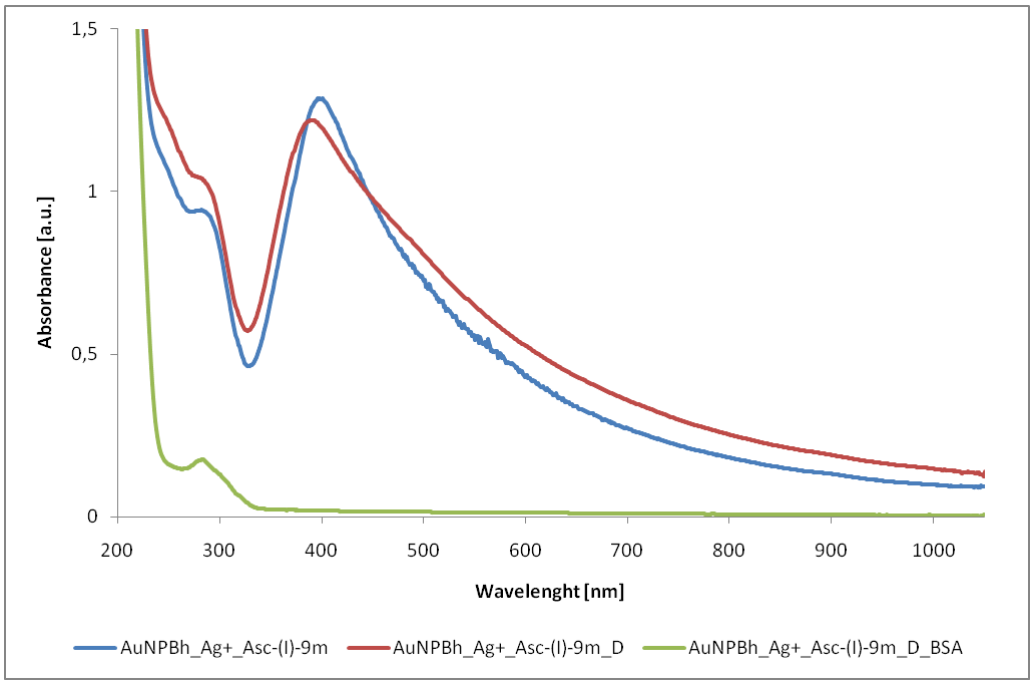

Figure 42 UV-Vis spectra of the 9 months-aged final colloidal system AuNPBh_Ag+_Asc-(I)-9m (blue), after the addition of aspartic acid AuNPBh_Ag+_Asc-(I)-9m_D (red), and subsequent addition of BSA AuNPBh_Ag+_Asc-(I)-9m_D_BSA (green)

In the SERS spectra measured with the excitation laser line of 532 nm (Appendix 2, red and black curves), two characteristic bands of graphitic carbon with a very high intensity dominate. Otherwise, there is no distinct difference between the spectra with and without BSA. The SERS spectra of the final colloidal system after the addition of aspartic acid, AuNPBh_Ag+_Asc-(I)-9m_D (red line), and after subsequent addition of BSA, AuNPBh_Ag+_Asc-(I)-9m_D_BSA (blue line), measured with the excitation laser line of 785 nm are shown in Figure 43.

The SERS spectrum of the colloidal Au-Ag system with BSA (blue curve, Figure 43) differs from the spectrum of the system with aspartic acid (red curve, Figure 43), meaning that the spectral pattern of BSA is most probably observed. Changes in relative intensity are detected, as well as, several characteristic bands appear, for instance: 1413 cm^{-1} (either deformation vibrations of CH_x, or stretching of carboxylic acid –$RCOO^-$), 1640 cm^{-1} (either amide I or deformation vibration of O-H), 3120 cm^{-1} (C-H stretching of aromatic amino acids from BSA adsorbed on NP surfaces) [75].

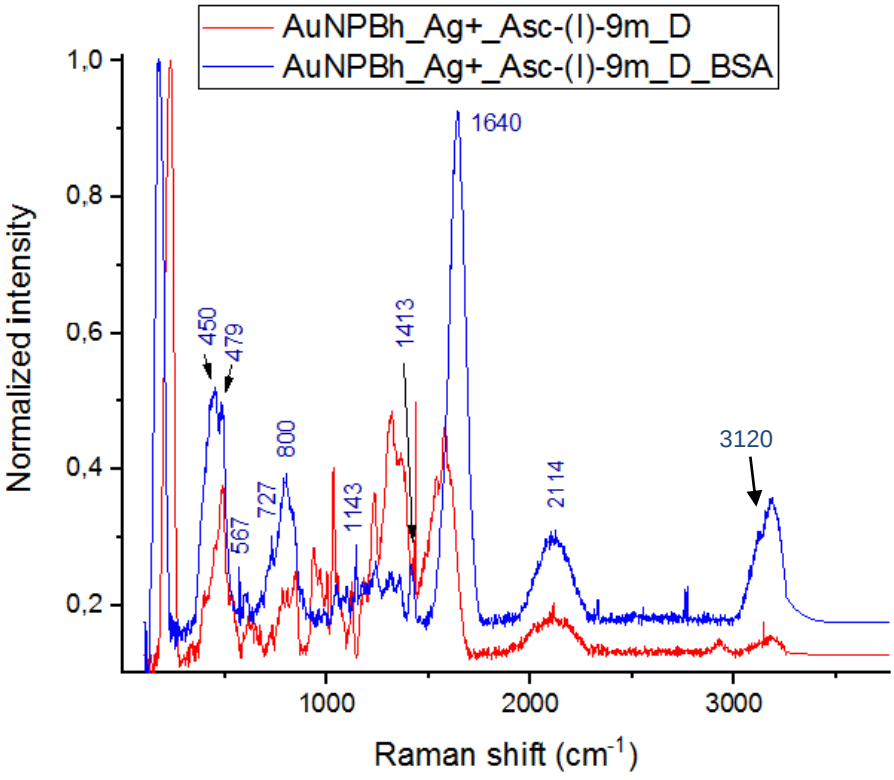

Figure 43 Normalized SERS spectra (excitation laser line of 785 nm) of AuNPBh_Ag+_Asc-(I)-9m_D (red), and AuNPBh_Ag+_Asc-(I)-9m_D_BSA (blue). Normalization is performed with respect to the most intensive peak within a particular spectrum.

It can be summed up that by using 785 nm excitation laser line, the NP system yielded the signal of BSA; while employing 532nm excitation it did not, in the case of the Au-Ag core-shell NPs. This is in a direct contrast to the Ag-Ag core-shell NPs discussed in section 5.3.2 (where the detection of BSA was obtained only by using 532 nm excitation

laser line). It might be related to the differences in the metallic core (Au vs. Ag) and/or the absence/presence of citrate molecules during the second step of the final colloidal system synthesis. This point will be further investigated.

6 Conclusion

The focus of this work was the synthesis and characterization of core-shell Ag-Ag and Au-Ag NPs which were prepared by two-step seed-mediated growth methods.

The final colloidal systems of Ag-Ag and Au-Ag NPs were prepared with four and five types of the syntheses, respectively, and the naming convention was developed. Seed solutions used were both several months aged, as well as, freshly prepared prior the synthesis of the final colloidal systems. The seeds solutions and final colloidal systems were characterized shortly after their synthesis with UV-Vis spectroscopy and TEM.

Based on our experiments, it can be concluded that the synthesis of the final **Ag-Ag NPs** colloidal systems from freshly prepared seed solutions is **affected by a different stage of the hydrolysis and simultaneous oxidation of sodium borohydride**, which has a strong influence on the formation process of the seeds. From the evaluation of UV-Vis spectra (the SPR absorption peak) and TEM images it was determined that the addition of **sodium citrate as a surface modifier to Ag-Ag NPs** synthesis proves to be **beneficia**l for obtaining a relatively narrow size distribution and smaller sizes of NPs.

Similarly, the earlier addition of ascorbate by **reversing the order of the reactants in the second step** of the synthesis **alters** the formation process of Ag-Ag NPs. The **importance of an electrostatic stabilization of the seeds by EDL** is thus demonstrated. It is especially significant for Ag-Ag NPs because of their reactivity, polydispersity and lower reproducibility.

Therefore, the final size of Ag-Ag NPs is strongly influenced by mixing conditions and other experimental parameters.

Au-Ag NPs were synthesised to produce core-shell NPs and to improve reproducibility of the synthesis while attaining enhancement properties of Ag.

In the final Au-Ag colloidal systems prepared from the fresh seed solutions (reduced by using borohydride), either core-shell Au-Ag NPs with relatively well formed (although little irregular) Ag shell, or only agglomerations of Au and Ag fragments were observed.

The usage of stable seeds (reduced by using borohydride) results in Au core being surrounded by a cloud of Ag particles (smaller in the case of the reversed reactants order in the second step of the synthesis), which did not form any compact layer around the Au core. The Au seed solution was considered stable at the time of the synthesis with a presumed lesser surface reactivity of the seeds than the freshly prepared ones.

Therefore, similarly as in the case of Ag-Ag NPs, the **stage of the borohydride hydrolysis and oxidation plays an important role in the process of Au-Ag NPs formation**.

Reversing the order of reactants (ascorbic acid prior to $AgNO_3$) **in the second** step of the Au-Ag synthesis had a similar influence as in the case of Ag-Ag NPs: an improved NPs formation (determined by a higher and narrower SPR absorption peak).

Hence, **the electrostatic stabilization of the seeds** is proved to be **a very important factor in Au-Ag NPs generation as well.**

The final colloidal Au-Ag NPs systems exploiting the **citrate**-reduced Au seeds generally possessed the similar reactivity, regardless the order of the reactants in the second step of the final colloidal system synthesis. It means that citrate residues are creating an efficient EDL which results in a **better stability and, thus, reproducibility of the synthesis.**

TEM images of the final systems from the citrate-reduced Au seeds revealed fully formed core-shell Au-Ag NPs with a compact silver layer around the Au core.

The measurement of DLS and zeta-potential values was performed with the final colloidal systems and seeds solutions aged for 9 months, along with re-measuring of their UV-Vis spectra.

Two dominant size distributions (particles below 20 nm and above 43 nm) were determined **by DLS in** the final colloidal systems and seed solutions in both cases: **Ag-Ag NPs, as well as, Au-Ag NPs**.

According to the zeta-potential values, the 9 months-aged Ag-Ag systems can be **generally considered stable**; nevertheless, the UV-Vis spectra of the 9 months-aged Ag-Ag systems prepared from fresh seeds display a bathochromic shift.

The final Au-Ag systems can be also considered relatively stable based on their zeta potential values and UV-Vis spectra (which show mostly the broadening of the SPR peak with no shifts).

Lastly, the **ability of** the prepared Ag-Ag and Au-Ag NPs to **enhance Raman scattering of BSA** were tested out. The final colloidal systems AgNPBh_Ag+_Asc-(I)-9m, AgBhNP-7m_Ctr-Ag+_Asc-(I)-9mand AuNPBh_Ag+_Asc-(I)-9m were selected for SERS measurements (employing 532 and 785 nm excitation laser lines). Two aggregation agents of the final colloidal systems were tested: NaCl and aspartic acid.

The detection of the BSA with the colloidal system AgNPBh_Ag+_Asc-(I)-9m was unsuccessful with both excitation laser lines and aggregation approaches. On the other hand, several characteristic peaks of BSA were detected by using **AgBhNP-7m_Ctr-Ag+_Asc-(I)-9m aggregated by aspartic acid** and **using** the excitation laser line of **532 nm**. On the contrary, the excitation laser line of **785 nm** enabled the detection of BSA employing the colloidal system **AuNPBh_Ag+_Asc-(I)-9m aggregated by aspartic acid**. The discrepancy between the SERS results obtained with 532 vs. 785 nm excitations was explained by another experimental setup of the two apparatuses.

7 References

1. POLTE, Jörg. Fundamental growth principles of colloidal metal nanoparticles - a new perspective. *CrystEngComm*. 2015. Vol. 17, no. 36, p. 6809–6830. DOI 10.1039/c5ce01014d.

2. JEEVANANDAM, Jaison, BARHOUM, Ahmed, CHAN, Yen S., DUFRESNE, Alain and DANQUAH, Michael K. Review on nanoparticles and nanostructured materials: History, sources, toxicity and regulations. *Beilstein Journal of Nanotechnology*. 2018. Vol. 9, no. 1, p. 1050–1074. DOI 10.3762/bjnano.9.98.

3. KRISHNAMOORTHY, S. *Nanomaterials: A Guide to Fabrication and Applications* [online]. 1. CRC Press, 2016. Devices, Circuits, and Systems. ISBN 9781466591264. Available from: https://books.google.cz/books?id=3Dg0CwAAQBAJ

4. CHAUDHARY, Gulshan and SINGH, Sumit Kumar. *Biotechnology Products in Everyday Life* [online]. Springer International Publishing, 2019. ISBN 978-3-319-92398-7. Available from: http://link.springer.com/10.1007/978-3-319-92399-4

5. KOOL, Lars, BUNSCHOTEN, Anton, VELDERS, Aldrik H and SAGGIOMO, Vittorio. Gold nanoparticles embedded in a polymer as a 3D-printable dichroic nanocomposite material. *Beilstein Journal of Nanotechnology* [online]. 2019. Vol. 10, p. 442–447. DOI 10.3762/bjnano.10.43. Available from: https://www.beilstein-journals.org/bjnano/content/pdf/2190-4286-10-43.pdf

6. MOATS, Kyle A., ASADI, Ebrahim and LARADJI, Mohamed. Phase field crystal simulations of the kinetics of Ostwald ripening in two dimensions. *Physical Review E*. 2019. Vol. 99, no. 1, p. 1–9. DOI 10.1103/PhysRevE.99.012803.

7. Colloids. *The Chemistry LibreTexts* [online]. [Accessed 1 March 2019]. Available from: https://chem.libretexts.org/Bookshelves/Physical_and_Theoretical_Chemistry_Textbook_Maps/Supplemental_Modules_(Physical_and_Theoretical_Chemistry)/Physical_Properties_of_Matter/Solutions_and_Mixtures/Colloid

8. MYERS, Drew. *Surfaces, Interfaces, and Colloids* [online]. 1999. ISBN 0471330604. Available from: http://books.google.com.mx/books?id=UdgsAAAACAAJ%0Ahttp://doi.wiley.com/10.1002/0471234990

9. R. BECKER AND W. DORING. Kinetic treatment of germ formation in supersaturated vapour. In : *Ann. Phys*. 1935. p. 719–752.

10. KINELL, P. O. Colloid Science. *Nature*. 2008. Vol. 164, no. 4158, p. 43–44. DOI 10.1038/164043a0.

11. SHARMA, Virender K., SISKOVA, Karolina M., ZBORIL, Radek and GARDEA-TORRESDEY, Jorge L. Organic-coated silver nanoparticles in biological and environmental conditions: Fate, stability and toxicity. *Advances in Colloid and Interface Science* [online]. 2014. Vol. 204, p. 15–34. DOI 10.1016/j.cis.2013.12.002. Available from: http://dx.doi.org/10.1016/j.cis.2013.12.002

12. HUNASHYAL, Anand M., SHOBA, H., YARADODDI, Jayachandra S., HIREMATH, Gurusiddesh B., SALIMATH, Basavaraja, SHETTAR, Ashok S., GANACHARI, Sharanabasava V., VENKATARAMAN, Abbaraju, BANAPURMATH, Nagaraj R. and PATIL, Parvathi. Synthesis Techniques for Preparation of Nanomaterials. *Handbook of Ecomaterials*. 2017. P. 1–21. DOI 10.1007/978-3-319-48281-1_149-1.

13. JU-NAM, Yon and LEAD, Jamie R. Manufactured nanoparticles: An overview of their chemistry, interactions and potential environmental implications. *Science of the Total Environment* [online]. 2008. Vol. 400, no. 1–3, p. 396–414. DOI 10.1016/j.scitotenv.2008.06.042. Available from: http://dx.doi.org/10.1016/j.scitotenv.2008.06.042

14. PARVEEN, Khadeeja, BANSE, Viktoria and LEDWANI, Lalita. Green synthesis of nanoparticles: Their advantages and disadvantages. *AIP Conference Proceedings*. 2016. Vol. 1724. DOI 10.1063/1.4945168.

15. KHAN, M. Z.H., TAREQ, F. K., HOSSEN, M. A. and ROKI, M. N.A.M. Green synthesis and characterization of silver nanoparticles using Coriandrum sativum leaf extract. *Journal of Engineering Science and Technology*. 2018. Vol. 13, no. 1, p. 158–166.

16. FISCHER, Anna, THUENEMANN, Andreas F., EMMERLING, Franziska, RADEMANN, Klaus, KRAEHNERT, Ralph, POLTE, Jörg, TUAEV, Xenia and WUITHSCHICK, Maria. Formation Mechanism of Colloidal Silver Nanoparticles: Analogies and Differences to the Growth of Gold Nanoparticles. *ACS Nano*. 2012. Vol. 6, no. 7, p. 5791–5802. DOI 10.1021/nn301724z.

17. ABBASI, Elham, MILANI, Morteza, AVAL, Sedigheh Fekri, KOUHI, Mohammad, AKBARZADEH, Abolfazl, NASRABADI, Hamid Tayefi, NIKASA, Parisa, JOO, San Woo, HANIFEHPOUR, Younes, NEJATI-KOSHKI, Kazem and SAMIEI, Mohammad. Silver nanoparticles: Synthesis methods, bio-applications and properties. *Critical Reviews in Microbiology*. 2016. Vol. 42, no. 2, p. 173–180. DOI 10.3109/1040841X.2014.912200.

18. WUITHSCHICK, Maria, BIRNBAUM, Alexander, WITTE, Steffen, SZTUCKI, Michael, VAINIO, Ulla, PINNA, Nicola, RADEMANN, Klaus, EMMERLING, Franziska, KRAEHNERT, Ralph and POLTE, Jörg. Turkevich in New Robes: Key Questions Answered for the Most Common Gold Nanoparticle Synthesis. *ACS Nano*. 2015. Vol. 9, no. 7, p. 7052–7071. DOI 10.1021/acsnano.5b01579.

19. GONZÁLEZ-RUBIO, Guillermo, DE OLIVEIRA, Thais Milagres, ALTANTZIS, Thomas, LA PORTA, Andrea, GUERRERO-MARTÍNEZ, Andrés, BALS, Sara, SCARABELLI, Leonardo and LIZ-MARZÁN, Luis M. Disentangling the effect of seed size and crystal habit on gold nanoparticle seeded growth. *Chemical Communications*. 2017. Vol. 53, no. 82, p. 11360–11363. DOI 10.1039/c7cc06854a.

20. NASRABADI, Hamid Tayefi, ABBASI, Elham, DAVARAN, Soodabeh, KOUHI, Mohammad and AKBARZADEH, Abolfazl. Bimetallic nanoparticles: Preparation, properties, and biomedical applications. *Artificial Cells, Nanomedicine and Biotechnology* [online]. 2016. Vol. 44, no. 1, p. 376–380. DOI 10.3109/21691401.2014.953632. Available from: http://dx.doi.org/10.3109/21691401.2014.953632

21. LU, Lehui, WANG, Haishui, ZHOU, Yonghui, XI, Shiquan and ZHANG, Hongjie. Seed-mediated growth of large , monodisperse core – shell gold – silver nanoparticles with Ag-like optical properties. *Chemical Communications*. 2002. Vol. 2, p. 144–145.

22. SHARMA, Gaurav, KUMAR, Amit, SHARMA, Shweta, NAUSHAD, Mu, PRAKASH DWIVEDI, Ram, ALOTHMAN, Zeid A. and MOLA, Genene Tessema. Novel development of nanoparticles to bimetallic nanoparticles and their composites: A review. *Journal of King Saud University - Science* [online]. 2017. DOI 10.1016/j.jksus.2017.06.012. Available from: http://dx.doi.org/10.1016/j.jksus.2017.06.012

23. KAHRAMAN, Mehmet, MULLEN, Emma R., KORKMAZ, Aysun and WACHSMANN-HOGIU, Sebastian. Fundamentals and applications of SERS-based bioanalytical sensing. *Nanophotonics*. 2017. Vol. 6, no. 5, p. 831–852. DOI 10.1515/nanoph-2016-0174.

24. MOURDIKOUDIS, Stefanos, PALLARES, Roger M. and THANH, Nguyen T.K. Characterization techniques for nanoparticles: Comparison and complementarity upon studying nanoparticle properties. *Nanoscale*. 2018. Vol. 10, no. 27, p. 12871–12934. DOI 10.1039/c8nr02278j.

25. PERKAMPUS, H H, GRINTER, H C and THRELFALL, T L. *UV-VIS Spectroscopy and Its Applications* [online]. Springer Berlin Heidelberg, 2013. Springer Lab Manuals. ISBN 9783642774775. Available from: https://books.google.cz/books?id=6ejwCAAAQBAJ

26. Ultraviolet - Visible Spectroscopy (UV). *Royal Society of Chemistry* [online]. [Accessed 15 March 2019]. Available from: http://www.rsc.org/learn-chemistry/content/filerepository/CMP/00/001/304/UV-Vis_Student resource pack_ENGLISH.pdf

27. WILLETS, Katherine A and DUYNE, Richard P Van. Localized Surface Plasmon Resonance Spectroscopy and Sensing 2007. DOI 10.1146/annurev.physchem.58.032806.104607.

28. TOMASZEWSKA, Emilia, SOLIWODA, Katarzyna, KADZIOLA, Kinga, TKACZ-SZCZESNA, Beata, CELICHOWSKI, Grzegorz, CICHOMSKI, Michal, SZMAJA, Witold and GROBELNY, Jaroslaw. Detection Limits of DLS and UV-Vis Spectroscopy in Characterization of Polydisperse Nanoparticles Colloids. . 2013. Vol. 2013.

29. AMENDOLA, Vincenzo and MENEGHETTI, Moreno. Size Evaluation of Gold Nanoparticles by UV - vis Spectroscopy. . 2009. P. 4277–4285.

30. HAISS, Wolfgang, THANH, Nguyen T K, AVEYARD, Jenny and FERNIG, David G. Determination of Size and Concentration of Gold Nanoparticles from UV - Vis Spectra. . 2007. Vol. 79, no. 11, p. 4215–4221. DOI 10.1021/ac0702084.

31. NAVARRETE, Jose, SIEFE, Chris, ALCANTAR, Samuel, BELT, Michael, STUCKY, Galen D. and MOSKOVITS, Martin. Merely Measuring the UV-Visible Spectrum of Gold Nanoparticles Can Change Their Charge State. *Nano Letters*. 2018. Vol. 18, no. 2, p. 669–674. DOI 10.1021/acs.nanolett.7b02592.

32. KIM, Youngsoo, SMITH, Jeremy G. and JAIN, Prashant K. Harvesting multiple electron-hole pairs generated through plasmonic excitation of Au nanoparticles. *Nature Chemistry* [online]. 2018. Vol. 10, no. 7, p. 763–769. DOI 10.1038/s41557-018-0054-3. Available from: http://dx.doi.org/10.1038/s41557-018-0054-3

33. HSU, Cheng-Liang, WU, Hsin-Yu, FANG, Chung-Cheng and CHANG, Sheng-Po. Solution-Processed UV and Visible Photodetectors Based on Y-Doped ZnO Nanowires with TiO 2 Nanosheets and Au Nanoparticles. *ACS Applied Energy Materials*. 2018. Vol. 1, no. 5, p. 2087–2095. DOI 10.1021/acsaem.8b00180.

34. SIKDER, Mithun, LEAD, Jamie R., CHANDLER, G. Thomas and BAALOUSHA, Mohammed. A rapid approach for measuring silver nanoparticle concentration and dissolution in seawater by UV–Vis. *Science of the Total Environment* [online]. 2018. Vol. 618, p. 597–607. DOI 10.1016/j.scitotenv.2017.04.055. Available from: https://doi.org/10.1016/j.scitotenv.2017.04.055

35. LI, Meng, XING, Zipeng, JIANG, Jiaojiao, LI, Zhenzi, YIN, Junwei, KUANG, Junyan, TAN, Siyu, ZHU, Qi and ZHOU, Wei. Surface plasmon resonance-enhanced visible-light-driven photocatalysis by Ag nanoparticles decorated S-TiO2−x nanorods. *Journal of the Taiwan Institute of Chemical Engineers* [online]. 2018. Vol. 82, p. 198–204. DOI 10.1016/j.jtice.2017.11.023.
Available from: https://doi.org/10.1016/j.jtice.2017.11.023

36. Transmission Electron Microscopy (TEM). *The University of Wawrick* [online]. [Accessed 19 March 2019]. Available from: https://warwick.ac.uk/fac/sci/physics/current/postgraduate/regs/mpagswarwick/ex5/techniques/structural/tem/

37. REIMER, Ludwig. *Transmission Electron Microscopy: Physics of Image Formation and Microanalysis* [online]. 1. Springer, 2013. ISBN 3662135531, 9783662135532. Available from: https://books.google.cz/books?id=CUfsCAAAQBAJ&dq=transmission+electron+microscopy&lr=&hl=cs&source=gbs_navlinks_s

38. BRENT FULTZ, James M. Howe. *Transmission Electron Microscopy and Diffractometry of Materials* [online]. 4. Springer Science & Business Media, 2012. ISBN 3642297609, 9783642297601. Available from: https://books.google.cz/books?id=tgOC3vlEY0sC&dq=transmission+electron+microscopy&lr=&hl=cs&source=gbs_navlinks_s

39. SONG, Boao, HE, Kun, YUAN, Yifei, SHARIFI-ASL, Soroosh, CHENG, Meng, LU, Jun, SAIDI, Wissam A. and SHAHBAZIAN-YASSAR, Reza. In situ study of nucleation and growth dynamics of Au nanoparticles on MoS 2 nanoflakes. *Nanoscale*. 2018. Vol. 10, no. 33, p. 15809–15818. DOI 10.1039/c8nr03519a.

40. KIM, Byung Hyo, YANG, Jiwoong, LEE, Donghoon, CHOI, Back Kyu, HYEON, Taeghwan and PARK, Jungwon. Liquid-Phase Transmission Electron Microscopy for Studying Colloidal Inorganic Nanoparticles. *Advanced Materials*. 2018. Vol. 30, no. 4, p. 1–20. DOI 10.1002/adma.201703316.

41. ZHU, Chao, LIANG, Suxia, SONG, Erhong, ZHOU, Yuanjun, WANG, Wen, SHAN, Feng, SHI, Yantao, HAO, Ce, YIN, Kuibo, ZHANG, Tong, LIU, Jianjun, ZHENG, Haimei and SUN, Litao. In-situ liquid cell transmission electron microscopy investigation on oriented attachment of gold nanoparticles. *Nature Communications* [online]. 2018. Vol. 9, no. 1, p. 1–7. DOI 10.1038/s41467-018-02925-6.
Available from: http://dx.doi.org/10.1038/s41467-018-02925-6

42. PANÁČEK, Aleš, KVÍTEK, Libor, SMÉKALOVÁ, Monika, VEČEŘOVÁ, Renata, KOLÁŘ, Milan, RÖDEROVÁ, Magdalena, DYČKA, Filip, ŠEBELA, Marek, PRUCEK, Robert, TOMANEC, Ondřej and ZBOŘIL, Radek. Bacterial resistance to silver nanoparticles and how to overcome it. *Nature Nanotechnology* [online]. 2018. Vol. 13, no. 1, p. 65–71. DOI 10.1038/s41565-017-0013-y.
Available from: http://dx.doi.org/10.1038/s41565-017-0013-y

43. BUSZEWSKI, Bogusław, RAILEAN-PLUGARU, Viorica, POMASTOWSKI, Paweł, RAFIŃSKA, Katarzyna, SZULTKA-MLYNSKA, Malgorzata, GOLINSKA, Patrycja, WYPIJ, Magdalena, LASKOWSKI, Dariusz and DAHM, Hanna. Antimicrobial activity of biosilver nanoparticles produced by a novel Streptacidiphilus durhamensis strain. *Journal of Microbiology, Immunology and Infection*. 2018. Vol. 51, no. 1, p. 45–54. DOI 10.1016/j.jmii.2016.03.002.

44. LI, Haoze, SHEN, Liyan, ZHANG, Kaifu, SUN, Bojing, REN, Liping, QIAO, Panzhe, PAN, Kai, WANG, Lei and ZHOU, Wei. Surface plasmon resonance-enhanced solar-driven photocatalytic performance from Ag nanoparticle-decorated self-floating porous black TiO2foams. *Applied Catalysis B: Environmental* [online]. 2018. Vol. 220, p. 111–117. DOI 10.1016/j.apcatb.2017.08.023.
Available from: http://dx.doi.org/10.1016/j.apcatb.2017.08.023

45. LANGEVIN, D., LOZANO, O., SALVATI, A., KESTENS, V., MONOPOLI, M., RASPAUD, E., MARIOT, S., SALONEN, A., THOMAS, S., DRIESSEN, M., HAASE, A., NELISSEN, I., SMISDOM, N., POMPA, P. P., MAIORANO, G., PUNTES, V., PUCHOWICZ, D., STĘPNIK, M., SUÁREZ, G., RIEDIKER, M., BENETTI, F., MIČETIĆ, I., VENTURINI, M., KREYLING, W. G., VAN DER ZANDE, M., BOUWMEESTER, H., MILANI, S., RÄDLER, J. O., MÜLHOPT, S., LYNCH, I. and DAWSON, K. Inter-laboratory comparison of nanoparticle size measurements using dynamic light scattering and differential centrifugal sedimentation. *NanoImpact* [online]. 2018. Vol. 10, p. 97–107. DOI 10.1016/j.impact.2017.12.004. Available from: https://doi.org/10.1016/j.impact.2017.12.004

46. WAGHMARE, Manik, KHADE, Bipin, CHAUDHARI, Pradip and DONGRE, Prabhakar. Multiple layer formation of bovine serum albumin on silver nanoparticles revealed by dynamic light scattering and spectroscopic techniques. *Journal of Nanoparticle Research* [online]. 2018. Vol. 20, no. 7. DOI 10.1007/s11051-018-4286-3. Available from: http://dx.doi.org/10.1007/s11051-018-4286-3

47. MARASSI, Valentina, RODA, Barbara, CASOLARI, Sonia, ORTELLI, Simona, BLOSI, Magda, ZATTONI, Andrea, COSTA, Anna Luisa and RESCHIGLIAN, Pierluigi. Hollow-fiber flow field-flow fractionation and multi-angle light scattering as a new analytical solution for quality control in pharmaceutical nanotechnology. *Microchemical Journal* [online]. 2018. Vol. 136, p. 149–156. DOI 10.1016/j.microc.2016.12.015. Available from: https://doi.org/10.1016/j.microc.2016.12.015

48. URBAN, Dominic A., MILOSEVIC, Ana M., BOSSERT, David, CRIPPA, Federica, MOORE, Thomas L., GEERS, Christoph, BALOG, Sandor, ROTHEN-RUTISHAUSER, Barbara and PETRI-FINK, Alke. Taylor Dispersion of Inorganic Nanoparticles and Comparison to Dynamic Light Scattering and Transmission Electron Microscopy. *Colloids and Interface Science Communications* [online]. 2018. Vol. 22, no. August 2017, p. 29–33. DOI 10.1016/j.colcom.2017.12.001.
Available from: https://doi.org/10.1016/j.colcom.2017.12.001

49. LANGEVIN, D., RASPAUD, E., MARIOT, S., KNYAZEV, A., STOCCO, A., SALONEN, A., LUCH, A., HAASE, A., TROUILLER, B., RELIER, C., LOZANO, O., THOMAS, S., SALVATI, A. and DAWSON, K. Towards reproducible measurement of nanoparticle size using dynamic light scattering: Important controls and considerations. *NanoImpact* [online]. 2018. Vol. 10, no. 2017, p. 161–167. DOI 10.1016/j.impact.2018.04.002.
Available from: https://doi.org/10.1016/j.impact.2018.04.002

50. PECORA, R. *Dynamic Light Scattering: Applications of Photon Correlation Spectroscopy* [online]. 1. Springer Science & Business Media, 2013. ISBN 1461323894, 9781461323891. Available from: https://books.google.cz/books?id=jBEGCAAAQBAJ&dq=dynamic+light+scattering&lr=&hl=cs&source=gbs_navlinks_s

51. Dynamic Light Scattering: An Introduction in 30 Minutes. *Malvern Instruments* [online]. [Accessed 20 March 2019]. Available from: https://warwick.ac.uk/fac/cross_fac/sciencecity/programmes/internal/themes/am2/booking/particlesize/intro_to_dls.pdf

52. STETEFELD, Jörg, MCKENNA, Sean A and PATEL, Trushar R. Dynamic light scattering: a practical guide and applications in biomedical sciences. *Biophysical reviews* [online]. 6 October 2016. Vol. 8, no. 4, p. 409–427. DOI 10.1007/s12551-016-0218-6. Available from: https://www.ncbi.nlm.nih.gov/pubmed/28510011

53. HUNTER, R J, OTTEWILL, R H and ROWELL, R L. *Zeta Potential in Colloid Science: Principles and Applications* [online]. Elsevier Science, 2013. Colloid science. ISBN 9781483214085.
Available from: https://books.google.cz/books?id=9I3-BAAAQBAJ

54. GABOR, F. "Characterization of Nanoparticles Intended for Drug Delivery." *Scientia Pharmaceutica* [online]. 2011. Vol. 79, no. 3, p. 701–702. DOI 10.3797/scipharm.br-11-01. Available from: http://www.mdpi.com/2218-0532/79/3/701

55. AFSHINNIA, Kamelia, MARRONE, Brandon and BAALOUSHA, Mohammed. Potential impact of natural organic ligands on the colloidal stability of silver nanoparticles. *Science of the Total Environment* [online]. 2018. Vol. 625, p. 1518–1526. DOI 10.1016/j.scitotenv.2017.12.299.
Available from: https://doi.org/10.1016/j.scitotenv.2017.12.299

56. TSENG, Kuo Hsiung, LIN, Yu Hung, TIEN, Der Chi, WU, Tong chi and STOBINSKI, Leszek. Preparation of Ag Nanoparticles in Ammonia by Using EDM and a Study of the Relationships Between Ammonia and Silver Nanoparticles. *Journal of Cluster Science* [online]. 2018. Vol. 29, no. 6, p. 1115–1122. DOI 10.1007/s10876-018-1425-z. Available from: https://doi.org/10.1007/s10876-018-1425-z

57. ROSTEK, Alexander, BREISCH, Marina, LOZA, Kateryna, GARCIA, Paulo R.A.F., OLIVEIRA, Cristiano L.P., PRYMAK, Oleg, HEGGEN, Marc, KÖLLER, Manfred, SENGSTOCK, Christina and EPPLE, Matthias. Wet-Chemical Synthesis of Pd-Au Core-Shell Nanoparticles (8 nm): From Nanostructure to Biological Properties. *ChemistrySelect*. 2018. Vol. 3, no. 17, p. 4994–5001. DOI 10.1002/slct.201800638.

58. SENDRA, M., VOLLAND, M., BALBI, T., FABBRI, R., YESTE, M. P., GATICA, J. M., CANESI, L. and BLASCO, J. Cytotoxicity of CeO2 nanoparticles using in vitro assay with Mytilus galloprovincialis hemocytes: Relevance of zeta potential, shape and biocorona formation. *Aquatic Toxicology* [online]. 2018. Vol. 200, no. March, p. 13–20. DOI 10.1016/j.aquatox.2018.04.011. Available from: https://doi.org/10.1016/j.aquatox.2018.04.011

59. RU, E L and ETCHEGOIN, P. *Principles of Surface-Enhanced Raman Spectroscopy: and Related Plasmonic Effects* [online]. Elsevier Science, 2008. ISBN 9780080931555. Available from: https://books.google.cz/books?id=dp9qw_sFZ9EC

60. COLTHUP, N. *Introduction to Infrared and Raman Spectroscopy* [online]. 2. Elsevier Science, 2012. ISBN 9780323161602. Available from: https://books.google.cz/books?id=RZSJ_5mkH-YC

61. SUR, Ujjal Kumar. Surface-enhanced Raman spectroscopy. *Resonance*. 2010. Vol. 15, no. 2, p. 154–164. DOI 10.1007/s12045-010-0016-6.

62. LANE, Lucas A., QIAN, Ximei and NIE, Shuming. SERS Nanoparticles in Medicine: From Label-Free Detection to Spectroscopic Tagging. *Chemical Reviews*. 2015. Vol. 115, no. 19, p. 10489–10529. DOI 10.1021/acs.chemrev.5b00265.

63. ABALDE-CELA, Sara, CARREGAL-ROMERO, Susana, COELHO, João Paulo and GUERRERO-MARTÍNEZ, Andrés. Recent progress on colloidal metal nanoparticles as signal enhancers in nanosensing. *Advances in Colloid and Interface Science* [online]. 2016. Vol. 233, p. 255–270. DOI 10.1016/j.cis.2015.05.002. Available from: http://dx.doi.org/10.1016/j.cis.2015.05.002

64. REGUERA, Javier, LANGER, Judith, JIMÉNEZ DE ABERASTURI, Dorleta and LIZ-MARZÁN, Luis M. Anisotropic metal nanoparticles for surface enhanced Raman scattering. *Chemical Society Reviews*. 2017. Vol. 46, no. 13, p. 3866–3885. DOI 10.1039/c7cs00158d.

65. ATANASOV, P. A., NEDYALKOV, N. N., FUKATA, N., JEVASUWAN, W., SUBRAMANI, T., HIRSCH, D. and RAUSCHENBACH, B. Au and Ag films and nanostructures for detection of fungicide mancozeb: SERS analyses. *AIP Conference Proceedings*. 2019. Vol. 2075, no. February. DOI 10.1063/1.5091145.

66. PAZOS-PEREZ, Nicolas, FITZGERALD, Jamie M., GIANNINI, Vincenzo, GUERRINI, Luca and ALVAREZ-PUEBLA, Ramon A. Modular assembly of plasmonic core–satellite structures as highly brilliant SERS-encoded nanoparticles. *Nanoscale Advances*. 2018. Vol. 1, no. 1, p. 122–131. DOI 10.1039/c8na00257f.

67. TANG, Shiwei, LIU, Hongmei, WANG, Mengqi, WANG, Songfan, WANG, Chuanyan, GU, Chenjie, ZHAO, Ziqi, JIANG, Tao and ZHOU, Jun. Further enhancement of SERS signals from Au@Ag@PSPAA core–shell nanoparticles surrounded by Ag nanoplates. *Materials Chemistry and Physics* [online]. 2019. Vol. 225, p. 60–63. DOI 10.1016/j.matchemphys.2018.12.040. Available from: https://doi.org/10.1016/j.matchemphys.2018.12.040

68. YANG, Wen, LI, Zhen, LU, Zhengyi, YU, Jing, HUO, Yanyan, MAN, Baoyuan, PAN, Jie, SI, Haipeng, JIANG, Shouzhen and ZHANG, Chao. Graphene-Ag nanoparticles-cicada wings hybrid system for obvious SERS performance and DNA molecular detection. *Optics Express*. 2019. Vol. 27, no. 3, p. 3000. DOI 10.1364/oe.27.003000.

69. YASEEN, Tehseen, PU, Hongbin and SUN, Da Wen. Fabrication of silver-coated gold nanoparticles to simultaneously detect multi-class insecticide residues in peach with SERS technique. *Talanta* [online]. 2019. Vol. 196, p. 537–545. DOI 10.1016/j.talanta.2018.12.030. Available from: https://doi.org/10.1016/j.talanta.2018.12.030

70. DE MARCHI, Sarah, BODELÓN, Gustavo, VÁZQUEZ-IGLESIAS, Lorena, LIZ-MARZÁN, Luis M., PÉREZ-JUSTE, Jorge and PASTORIZA-SANTOS, Isabel. Surface-enhanced Raman scattering (SERS) imaging of bioactive metabolites in mixed bacterial populations. *Applied Materials Today* [online]. 2019. Vol. 14, p. 207–215. DOI 10.1016/j.apmt.2018.12.005. Available from: https://doi.org/10.1016/j.apmt.2018.12.005

71. CABELLO, Gema, NWOKO, Kenneth C., MARCO, José F., SÁNCHEZ-ARENILLAS, María, MÉNDEZ-TORRES, Ana María, FELDMANN, Jorg, YÁÑEZ, Claudia and SMITH, Tim A.D. Cu@Au self-assembled nanoparticles as SERS-active substrates for (bio)molecular sensing. *Journal of Alloys and Compounds* [online]. 2019. Vol. 791, p. 184–192. DOI 10.1016/j.jallcom.2019.03.279. Available from: https://linkinghub.elsevier.com/retrieve/pii/S0925838819311053

72. ŠLOUFOVÁ, Ivana, ŠIŠKOVÁ, Karolína, VLČKOVÁ, Blanka and ŠTĚPÁNEK, Josef. SERS-activating effect of chlorides on borate-stabilized silver nanoparticles: Formation of new reduced adsorption sites and induced nanoparticle fusion. *Physical Chemistry Chemical Physics*. 2008. Vol. 10, no. 16, p. 2233–2242. DOI 10.1039/b718178g.

73. SISKOVA, Karolina, BECICKA, Ondrej, SAFAROVA, Klara and ZBORIL, Radek. HCl Effect on Two Types of Ag Nanoparticles Utilizable in Detection of Low Concentrations of Organic Species. In : *Sustainable Nanotechnology and the Environment: Advances and Achievements* [online]. American Chemical Society, 2013. p. 151-163 SE–9. ACS Symposium Series. ISBN 0-8412-2784-5. Available from: https://doi.org/10.1021/bk-2013-1124.ch009

74. BOTTA, Raju, RAJANIKANTH, A. and BANSAL, C. Surface Enhanced Raman Scattering studies of l-amino acids adsorbed on silver nanoclusters. *Chemical Physics Letters* [online]. 2015. Vol. 618, p. 14–19. DOI 10.1016/j.cplett.2014.10.052. Available from: http://dx.doi.org/10.1016/j.cplett.2014.10.052

75. FAZIO, Barbara, D'ANDREA, Cristiano, FOTI, Antonino, MESSINA, Elena, IRRERA, Alessia, DONATO, Maria Grazia, VILLARI, Valentina, MICALI, Norberto, MARAGÒ, Onofrio M. and GUCCIARDI, Pietro G. SERS detection of Biomolecules at Physiological pH via aggregation of Gold Nanorods mediated by Optical Forces and Plasmonic Heating. *Scientific Reports* [online]. 2016. Vol. 6, no. July. DOI 10.1038/srep26952. Available from: http://dx.doi.org/10.1038/srep26952

Abbreviations and symbols

Ag	...silver
Ag NPs	...silver nanoparticles
Ag-Ag NPs	...silver nanoparticles prepared with two-step synthesis
Au	...gold
Au NPs	...gold nanoparticles
Au-Ag NPs	...core-shell gold-silver nanoparticles
Cu	...copper
CNT	...classical nucleation theory
DLS	...Dynamic light scattering
EDL	...electrical double layer
λ	...Debye length
$NaBH_4$	...sodium borohydride
NPs	...nanoparticles
$\psi(x)$	...electric surface potential
SERS	...Surface-enhanced Raman spectroscopy
SPR	...Surface plasmon resonance
TEM	...Transmission electron microscopy
UV-Vis	...UV-Vis spectroscopy
$W_{total}(D)$	...total interaction potential

Abbreviations of the naming convention:

(1), (2)	...repetition of the synthesis with freshly prepared $NaBH_4$
(I), (II)	...repetition of synthesis using a later stage of hydrolysis of $NaBH_4$
5min	...5 minutes aged
7m	...7 months aged
9m	...9 months aged
Ag+	...silver nitrate $AgNO_3$
Asc	...L-ascorbic acid
Bh	...sodium borohydride
BSA	...Bovine serum albumin

Ctr	...sodium citrate
D	...L-aspartic acid
NaCl	...sodium chloride
"-"	...divider between abbreviations in the naming order (i.e. AgNP-Bh-5min-(1))
"_"	...progress of the synthesis, i.e. addition of reactants (e.g. "_Asc" means addition of L-ascorbic acid)

Appendices

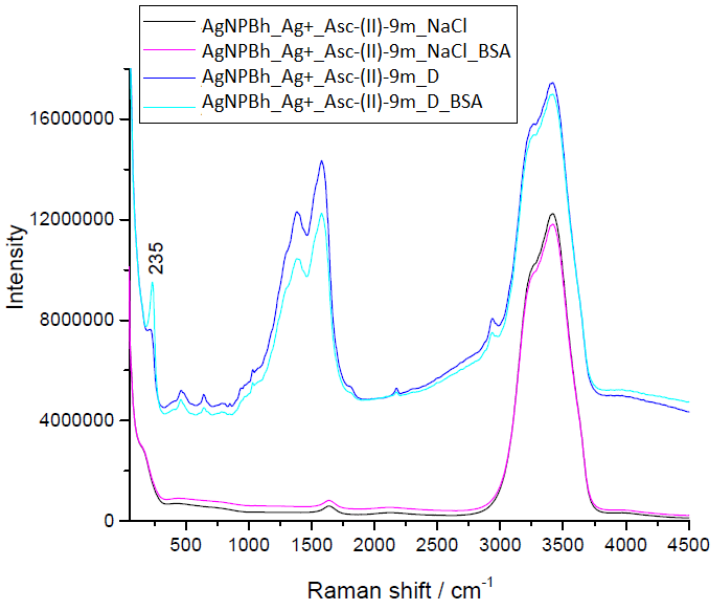

Appendix 1 SERS spectra (excitation laser line of 532 nm) of the 9 months-aged final colloidal system after the addition of sodium chloride AgNPBh_Ag+_Asc-(II)-9m_NaCl (black), with subsequent addition of BSA, AgNPBh_Ag+_Asc-(II)-9m_NaCl_BSA (magenta); the same final colloidal system after the after the addition of aspartic acid AgNPBh_Ag+_Asc-(II)-9m_D (blue), with subsequent addition of BSA, AgNPBh_Ag+_Asc-(I)-9m_D_BSA (cyan)

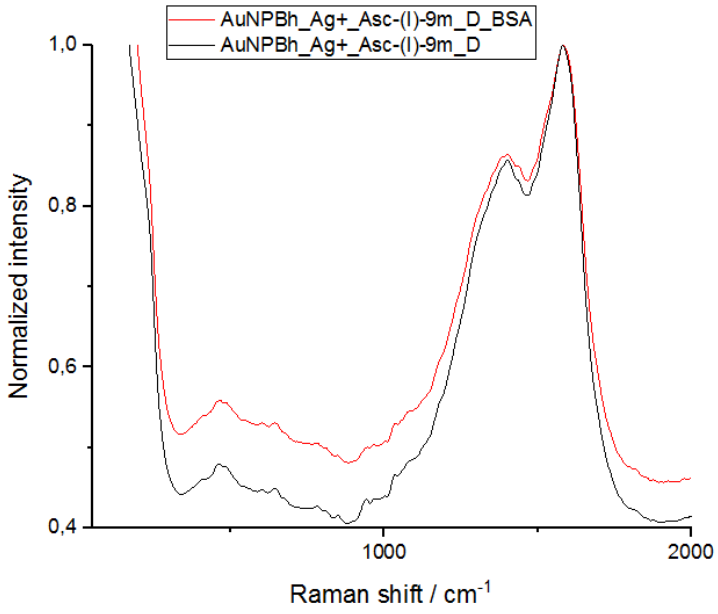

Appendix 2 SERS spectra (excitation laser line of 532 nm) of AuNPBh_Ag+_Asc-(I)-9m_D (black), and AuNPBh_Ag+_Asc-(I)-9m_D_BSA (red).